COMPUTATION AND DISPLAY OF EEG SPECTRAL AND EVENT-RELATED DESYNCHRONIZATION TOPOGRAPHIC MAPS

Colin Murray Andrew

Submitted to the Faculty of Medicine at the University of Cape Town in partial fulfilment of the requirements for the degree of Master of Science in Medicine in the field of Biomedical Engineering.

Cape Town, 1992

DECLARATION

I, ..., hereby declare that this dissertation is my own, unaided work. It is being submitted for the degree of Master of Science at the University of Cape Town. It has not been submitted before for any degree or examination at any other University.

Signed: .....

Date: .....

ABSTRACT

A quantitative EEG system which performs spectral and event-related desynchronization (ERD) mapping was developed. The design and implementation of the system was based on a detailed literature survey of these three quantitative techniques, i.e spectral analysis, ERD analysis and topographical mapping.

The system is PC-based and interfaces to a conventional 18-channel EEG recorder. Two modes of data capture are provided: continuous (1-2 minutes) for spectral analysis and event-related repetitive-period (4-10 seconds) for ERD analysis. Quantification of the EEG waveforms from the multi-channel recording and computation and display of the quantified data in the form of topographical maps, is performed off-line.

A pilot study involving both spectral and ERD tests was performed for system verification.

ACKNOWLEDGEMENTS

The help of the following people is acknowledged with gratitude:

Mladen Poluta, Department Biomedical Engineering, UCT, for his continued assistance and guidance as thesis supervisor, and for the many hours spent proof-reading my thesis write-up.

Professor P.M. Leary from the Department of Neurology, Red Cross War Memorial Children's Hospital, for his help and encouragement as clinical supervisor.

Professor Gert Pfurtscheller from the Institute of Biomedical Engineering, Graz University of Technology, for his assistance and valuable tutorial sessions which provided a solid foundation for the thesis.

Kevin Marcus, who laid the foundations for the topographical mapping aspects.

The staff of the EEG Laboratory for their time and friendly help. Special thanks to Brett Burton for the time spent assisting in the scanning of the recorded EEG data for artifacts.

Victor Moisey and Peter van den Berg, from the Electronic Workshop, Department of Biomedical Engineering, for technical support.

The staff of the UCT Computer Centre, especially Jane Froggat for her many hours spent in producing the colour printouts.

My parents, for their interest, encouragement and support.

TABLE OF CONTENTS

LIST OF FIGURES

LIST OF TABLES

LIST OF ABBREVIATIONS AND SYMBOLS

AC	alternating current
A/D	analoque-to-digital
ADC	analogue-to-digital convertor
AR	autoregressive
ARMA	autoregressive moving average
BAEP	brainstem auditory evoked potential
EEG	electroencephalogram
EOG	electro-oculogram
ERD	event-related desynchronization
D/A	digital-to-analoque
DAC	digital-to-analogue convertor
DMA	direct memory access
DFT	discrete Fourier transform
FFT	fast Fourier transform
IBM	International Business Machines
IRQ	interrupt request
MS-DOS	Microsoft Disk Operating System
PET	positron emission tomography
rCBF	regional cerebral blood flow
RCWMCH	Red Cross War Memorial Children's Hospital
RP	readiness potential
SEP	somatosensory evoked potential
TTL	transistor-transistor logic
VEP	visual evoked potential

dB	decibels
Hz	hertz (cycles per second)
V	volts
μV	micro-volts

CHAPTER 1

INTRODUCTION

Potentials that originate within the brain can be detected with electrodes placed on the surface of the scalp. The record of these potentials is called the electroencephalogram (EEG) and was first measured in humans by Hans Berger in 1929. Classically, the EEG is plotted as multichannel, polygraphic traces onto moving paper. The clinical electroencephalographer correlates brain functions as well as dysfunctions and disease with certain patterns of these EEG traces on an empirical basis.

Quantitative EEG arose from the need to support electroencephalographers' evaluations with EEG data in simplified numerical or graphical form. Various quantitative analytic techniques were applied to the EEG shortly after Berger's first recordings. These have been replaced by modern digital computer techniques. Modern quantitative EEG analysis and display techniques includes frequency (spectral) analysis, topographical mapping, compressed spectral arrays, significance probability mapping, and other complex analytic techniques.

Three quantitative EEG techniques were investigated, viz. spectral analysis, event-related desynchronization (ERD) analysis and topographical mapping. A PC-based system, which performs spectral and ERD topographical mapping, was designed and implemented. The system will be used by the EEG Laboratory at Red Cross War Memorial Children's Hospital (RCWMCH) for research and evaluation of children with learning disabilities. A pilot study involving spectral and ERD tests was performed for system verification.

Chapter 2 provides some background material on quantitative EEG. This includes a brief history of quantitative EEG and a review of quantitative EEG techniques. Also presented in this chapter is the background to quantitative EEG measurements at RCWMCH. A review of the literature pertinent to the thesis is given in Chapter 3. This review is divided into three sections, viz. spectral analysis, event-related desynchronization analysis, and topographical mapping. Chapter 4 begins with an overview of the system and then deals with the design and implementation of the system. Clinical tests form a pilot study for verification of the system. Chapter 5 describes the different tests undertaken and presents the results of these tests. Chapter 6 contains an evaluation of the implemented system, highlighting some of the difficulties encountered with the design and implementation and discusses ways to improve the performance of the system. Also presented is a discussion of the results obtained from the tests performed. Finally, Chapter 7 provides conclusions and recommendations for further

development and improvements to the system.

CHAPTER 2

BACKGROUND

2.1 Quantitative EEG Analysis

2.1.1 History

Frequency analysis of EEG began shortly after Berger's first description of human EEG. As early as 1932, Dietch reported on Fourier analysis of short sections of EEG. This initial frequency analysis was extremely tedious, requiring the optical magnification of the EEG traces and manual measurement and calculation. Using this early Fourier analysis method, normal and abnormal EEG's showed significant differences in their frequency contents. Berger himself made use of these and similar techniques for objective quantitative EEG analysis (1932, 1934, 1936).

Electronic automation of this process began with the development of the "frequency analyzer" by Walter (Walter, 1934; Baldock and Walter, 1946). This electromechanical device averaged the EEG across 10 second epochs. Data were displayed in 24 frequency bands, ranging from 0.5 to 30 Hz. The frequency analysis device allowed a printout of the frequency content from each 10 second epoch, displayed as pen deflections on an EEG machine. This method represented the first practical automated EEG signal processing, allowing discrimination of frequency activity to as narrow as 1 Hz frequency bands.

Investigations into topographical displays of EEG characteristics also began in the early years of quantitative EEG analysis (Cohn, 1942; Goldman et al, 1948). The toposcope developed by Walter and Shipton (1951) was the most popular of these early topographic display devices. EEG characteristics were displayed topographically on a collection of small cathode-ray tubes. Each screen was able to display not only frequency but also phase information.

In the 1950's, work on topographic displays and frequency analysis continued using the technology of that day. Alternative approaches were implemented for arriving at similar results with less effort. Many new techniques were introduced to mimic the results of frequency analysis with much less calculation time. These included auto and cross-correlation functions for EEG analysis (Barlow and Brazier, 1954; Brazier and Casby, 1956), period analysis, and zero crossing analysis (Saltzberg et al, 1957).

The next decade saw the development of a computer algorithm, the fast Fourier transform (FFT) (Cooley and Tukey, 1965), for efficient calculation of the Fourier transform and this quickly came to be applied to the EEG. Together with the increasing availability of digital computer time, the FFT algorithm undercut the need to use quicker alternatives to traditional Fourier frequency analysis. From this time forward, frequency analysis using the traditional Fourier approach came to dominate the automated EEG analysis methodology. Power spectral analysis became the standard for automated EEG processing techniques, along with many variations on these techniques.

In the 1980's, topographical mapping came of age with the widespread availability of fast and relatively cheap digital computers, associated with colour video technology (Duffy et al, 1979) and the last decade has seen widespread research in this area.

2.1.2 Techniques

The features found in most modern quantitative EEG representations can be divided into three broad categories: the stimulation modality, the analysis domain, and the display type. These may be used in various combinations to give a particular quantitative EEG representation (Nuwer, 1988a). An example of a quantitative EEG representation could be recording of raw EEG with patient at rest, eyes closed (stimulus modality). The spectral power in each of the delta, theta, alpha and beta bands could then be calculated (analysis domain) and the spectral power displayed in topographical form (display type).

a) Stimulus Modalities

Stimulus modalities for quantitative EEG recording include no stimulus, continuous stimulation, "evoked potential" stimulation and tasks (See Table 2-1). The stimulus for a particular EEG study is chosen according to the goals of the study and is often dictated by the particular analysis domain used. If one is trying to locate an anatomical lesion (tumour) by location of a focus of abnormal slow activity (delta activity), stimulation is not necessary and the EEG recording can be taken with the patient at rest with eyes closed or open. If, however, the goal of the study is to extract functional information about cognitive processes, then the patient needs to be given a task to perform during the recording of the EEG. This allows the EEG recording to be correlated with the task being performed and allows one to acquire functional information.

Table 2-1 : Options for quantitative techniques. (Adapted from Nuwer, 1988a).

Stimulus modalities

- No stimulus
  - Awake (eyes open or eyes closed), drowsy, asleep
- Continuous stimulation
  - Strobe, text/graphics, music/audio
- Evoked potentials stimulation
  - Visual (Strobe, checkerboard), auditory (click, tones), somatosensory (peripheral nerve stimulation)
- Tasks
  - Button press, read, remember, count, etc

Analysis Domains and Scores

- Time domain
- Frequency domain
  - Power or amplitude, continuous or in bands
  - Coefficient of variation
- Spatial domain
- Coherence
  - Interhemispheric or intrahemispheric coherence
  - Phase
- Significance scores
- Ratios
  - Relative power
  - Ratios between specified bands
  - log [x/(1-x)]
- Slope descriptors
  - Activity, mobility, complexity
- Period, amplitude and zero crossing analysis
- Cognitive-related parameters
  - Event-related desynchronization (ERD)
  - Event-related covariances (ERC)
- Autoregressive modelling
  - Spectral parameter analysis
- Discriminant analysis

Display Formats

- Traditional line format
- Coloured bar format
- Compressed spectral array
- Topographic maps
- Cartooning
- Numerical tables

b) Analysis Domains

Once acquired, the data can be manipulated in a variety of ways, including time domain analysis, frequency domain analysis (spectral analysis), various statistical scores and cognition-related scores. Although these domains and scores might all be carried out successively on the same data, in most cases the EEG is presented primarily in one of these analysis domains or scores (See Table 2-1).

c) Display Formats

Raw or quantified EEG data can be displayed in a variety of ways. Display formats include traditional line format, coloured bar format, compressed spectral arrays, topographic maps, cartoons (animated series of topographical maps) and numerical tables. The line format display is the familiar way in which routine EEG or EP data are usually presented. Line format displays are useful because they are so familiar. A great volume of literature has evolved, and a great deal of training has centred on these displays.

2.2 Quantitative EEG Analysis at Red Cross Children's Hospital

The EEG Laboratory at RCWMCH is interested in investigating abnormalities of the brain which manifest as autism, mental handicap, specific learning disability, paroxysmal behaviour disorders, attention deficit disorders and delay in language development. Results of studies by Duffy involving brain electrical activity mapping (BEAM) of boys with reading retardation (dyslexia) (Duffy et al, 1980), prompted the EEG laboratory to acquire a topographical mapping system which could be used for such research.

A topographical mapping system was developed by Kevin Marcus in the Department of Biomedical Engineering at UCT. This PC-based system, acquired sixteen channels of data from the recorder in the EEG Laboratory and stored the data for off-line processing. The raw EEG data was then transformed into a series of topographical maps displaying the EEG amplitude at different time intervals with a temporal resolution of 10 milliseconds between successive maps. This type of topographical mapping system, although useful in recognising discontinuities such as epileptic spikes and for observing the spatio-temporal relationship of these spikes (Duffy, 1986; van der Meij et al, 1992), is not very useful when studying cognitive functioning and abnormalities of cognitive function. This system was therefore inadequate for the research for which it was intended.

Duffy's studies of dyslexia involved performing spectral analysis of the background EEG activity recorded during different testing conditions or states. These studies were designed to permit recording during simple resting brain activity (with eyes open or closed), and during tests designed to activate the left hemisphere (speech and reading), the right hemisphere (music and geometric figures), and both hemispheres together (paired visual-verbal associations). By producing spectral maps in each of the delta, theta, alpha and beta bands for a group of normal controls and for a group of children classified as dyslexic for each of the different states discussed, Duffy was able to statistically show regional differences between the two groups in the different frequency bands (Duffy et al, 1980). Many other researchers have used spectral analysis in studies of children with dyslexia and learning disabilities (Byring et al, 1991; Colon et al, 1979; Fein et al, 1986; Galin et al, 1992; Leisman and Ashkenazi, 1980; Pinkerton et al, 1989; Sklar et al, 1972,1973). Spectral analysis of the background EEG during rest (eyes open or closed) or during specified tests designed to maintain a particular state of the brain, thus seems to provide a good quantitative EEG tool for studying abnormalities in cognitive functioning.

Professor Gert Pfurtscheller from the Institute of Biomedical Engineering at the Graz University of Technology, visited the Biomedical Engineering Department at UCT in 1991 and introduced his quantitative EEG technique called Event-Related Desynchronization (ERD) Mapping. This technique allows the study of cortical activation patterns during the performance of a specific task by the patient. This task could include motor, sensory and cognitive processes and one could correlate the specific cortical area activated, with the specific process being performed. Pfurtscheller has used this technique for studying cortical activation patterns during a visual-verbal task, where the time course and topographical pattern of cortical activation during visual encoding, cognition, and speech could be seen (Pfurtscheller and Klimesch, 1990). This technique holds great promise for studying abnormalities in cognitive functioning, where differences in patterns of cortical activation for a specific task might be found between a group of normal controls and a group of patients suffering from one of the abnormalities of interest.

Thus it would seem that a topographical mapping system employing both spectral analysis and ERD analysis would provide an adequate quantitative EEG tools which the EEG laboratory could use for their research purposes. A literature review of spectral analysis, ERD analysis and topographical mapping was therefore performed to investigate these techniques in order to formulate a proposal for the design and implementation of such a system.

CHAPTER 3

LITERATURE SURVEY

3.1 Spectral Analysis

3.1.1 Introduction

In contrast to its usefulness in recognising transients and discontinuities, the human eye has proved less successful at analysing the background EEG activity. Many significant clinical neuropathologies fail to generate obvious and easily recognisable discontinuities, but they do alter background spectral content. Fortunately, spectral analysis has been available for many years and has been used for both clinical and research purposes. Detailed spectral analysis has been applied to the automatic classification of sleep states (Brunet et al, 1988; Kuwahara et al, 1988), monitoring of the depth of anaesthesia (Bankman and Gath, 1987; Donegan, 1985) as well as to the classification of a variety of neurological disorders such as epilepsy (Coppola, 1986; Harner, 1986; Kowell et al, 1987), mass lesions (Gotman et al, 1973; Nagata et al, 1985), dyslexia (Byring et al, 1991; Colon et al, 1979; Duffy et al, 1980) and dementia (Coben et al, 1983, 1985; Penttila et al, 1985).

3.1.2 Frequency Bands

In order to obtain a quantitative measure of the contribution of spectral components, the power spectrum is often divided into frequency bands according to customary conventions. The classical frequency bands are delta (0 - 4 Hz), theta (5 - 7 Hz), alpha (8 - 13 Hz) and beta (> 14 Hz) (Nuwer, 1988a). These divisions into classical frequency bands are not always followed in quantitative EEG techniques. Instead of defining theta as 5-7 Hz, it is common to consider it as 4-8 Hz activity. It is also common to consider that beta activity begins at 12 Hz instead of at 14 Hz. These changes allow breaks between bands to occur at 4 Hz intervals (4,8,12 Hz). In addition, the beta and alpha bands may be further subdivided, eg. alpha-1 (8 - 10 Hz) and alpha-2 (10 - 12 Hz).

In the normal awake, relaxed adult, the dominant cerebral activity is the alpha rhythm. This activity does not arise from the whole cortex but rather predominantly from the parieto-occipital and to some extent the temporal regions (See Figure 3-1). The rhythm is interrupted (blocked) by peripheral stimulation (opening the eyes) or mental activity (mental arithmetic). The mean peak alpha frequency is normally between 10 and 10.9 Hz and an interhemispheric

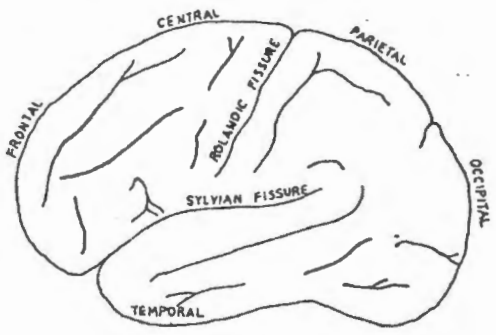

Figure 3-1 : Lateral view of the left hemisphere identifying regions referred to in the text.

difference between peak alpha frequencies of greater than 1 Hz is considered abnormal. Approximately 10 percent of normal individuals have little or no demonstratable alpha activity. A small amount of slower activity in the theta range is seen in the normal alert adults, but on-going delta activity is considered abnormal. Both theta and delta waves are seen during normal sleep. Beta rhythms occur most frequently in the frontal and central regions of the cortex and can be seen in posterior regions when it is not masked by the alpha rhythm (Donegan, 1985).

In the normal child, alpha components begin to appear at about 18 months of age. The frequency of the basic posterior rhythm is about 6 to 7 Hz, increasing to between 7 and 8 Hz in the 3rd year of life. The mean adult frequency ($\approx$ 10 Hz) is reached between 10 and 15 years of age. There are no further striking changes in the EEG throughout adolescence although the admixture of slow activity seen in the posterior cerebral regions of older children gradually diminishes and beta activity over the frontal regions becomes more pronounced (Donegan, 1985).

3.1.3 Spectral Parameters

EEG spectra may be quantified in many ways. The **average intensity** or **amplitude** of EEG activity in each frequency band can be measured (Etevenon et al, 1988; Fisch et al, 1988; Rumsey et al, 1989; Tatsuno, 1988) or the **amplitude** (intensity) **spectrum** displayed along a continuous frequency axis and expressed in microvolts/hertz (μV/Hz). Often, the power present in the EEG signal is measured, either as square-microvolts (μV^2) within a frequency band, or square-microvolts/hertz (μV^2/Hz) (Larsen, 1992) when measured along a continuous frequency axis, in which case it is referred to as the **power spectrum**. The power of a signal

is important as a measure of its ability to deliver energy and therefore cause desired effects. Much early theory of signal processing was developed for engineering applications. Adaption of these methods to EEG analysis has led to the popularity of power spectral measurements for the investigation of EEG signals (Nuwer, 1988a).

The power measurements within a frequency band can either be **absolute** in μV^2 (Duffy et al, 1979; Jackel et al, 1987; Jonkeman and Lelieveld, 1981; Nuwer et al, 1987a, 1987b; Sainio et al, 1983; Salinsky et al, 1991), or **relative**, where the power in a specific frequency band is given as a percentage of the total power within the EEG signal (Cohen et al, 1983, 1985; Corsi-Cabrera et al, 1989; Kopruner and Pfurtscheller, 1984; Penttila et al, 1985; Salinsky et al, 1991; Sainio et al, 1983; Soininen et al, 1988; van der Rijt et al, 1984). Often **power ratios** between the different frequency bands are used, such as (delta power + theta power) / (alpha power + beta power) (Gotman et al, 1973; Kopruner and Pfurtscheller, 1984; Nagata et al, 1985; Sainio et al, 1983; Salinsky et al, 1991; Soininen et al, 1988).

Other spectral parameters include **peak frequency** (Balzar et al, 1986; Ehlers et al, 1989; Jonkeman and Lelieveld, 1981; Kopruner and Pfurtscheller, 1984; Salinsky et al, 1991; Soininen et al, 1988; van der Rijt et al, 1984) and **median** (mean centroid) **frequency** (Cohen et al, 1983, 1985; Etevenon et al, 1988; Penttila et al, 1985; Sainio et al, 1983; Salinsky et al, 1991). For a frequency band, the median frequency is the centre of gravity, computed by summing the spectral amplitudes multiplied by their respective frequencies, normalized by dividing by the sum of the spectral amplitudes.

3.1.4 Spectral Estimation Methods

Spectral estimation methods can be divided into **non-parametric** (classical) and **parametric** (modern) methods. Both have been applied to spectral analysis of the EEG.

a) Non-parametric Spectral Estimation

Non-parametric spectral estimation methods are based on the Fourier transform. A summary of Fourier analysis theory is given in Appendix A. There are two methods which fall under this category, namely the **Blackman-Tukey method** and the **Periodogram** method; both are described in Appendix B.

The periodogram is the method most frequently applied to spectral estimation of the EEG. The periodogram can be implemented without windowing and averaging (as discussed in Appendix B) to give a crude estimation of the EEG spectrum (Ehlers et al, 1989). However, windowing and averaging of the periodogram are usually used to improve the estimation of the EEG spectrum. Fisch et al (1988), Hilfiker and Egli (1992) and Larsen et al (1992) have used the periodogram with a Hanning (cosine) window and with no averaging in their calculations of EEG spectra. The Bartlett periodogram (averaging of segmented periodograms with no window function) has been used by many researchers (Duffy et al, 1979; Ivanova, 1988; Mathis et al, 1980, Nakamura et al, 1985; Petsche et al, 1988). Others have used the Welch modified periodogram with a Hanning window (Autret et al, 1985; Coppola, 1979; Duckrow and Spencer, 1992; Fisch et al, 1988; Rumsey et al, 1989; Salinsky et al, 1991), while Soininen et al (1989) used the Welsh method with a Hanning window but with overlapping of adjacent segments.

b) Parametric Spectral Estimation

The parametric approach is based on the assumption that the measured data evolves from a process that can be represented, or approximately represented, by a model. The spectral estimation is a three step procedure: (1) a specific model is selected, (2) the model parameters are estimated from the measured data, and (3) the spectral estimate is obtained from the model parameters. Appendix C describes the parametric approach and discusses some of the models used for spectral estimation.

For EEG spectral analysis, the **autoregressive** (AR) model is the most widely used with the Yule-Walker algorithm providing estimates of the system parameters (Allen et al, 1992; Blinowska, 1988; Hilfiker and Egli, 1992; Jansen et al, 1981; Pfurtscheller and Haring, 1972; Sauter et al, 1990; Smith et al, 1986). The order of these models varies from 4 to 20. Jansen et al (1981) have shown, using Akaike's final prediction error (FPE) criterion, that a fifth-order model is sufficient to estimate EEG characteristics in 90 percent of the cases. **Autoregressive moving average** (ARMA) models are not as popular for EEG spectral analysis but have been used; Smith et al (1986) used an ARMA model of tenth-order for spectral estimation of the EEG.

3.1.5 Recording Interval and Epoch Length

Recording interval refers to the total recording time. Recording interval can vary from a few

seconds to a few hours for sleep analysis. The interval is normally divided up into shorter length **epochs**, and it is over these epochs that quantification (i.e. spectral estimation) is performed. Epoch lengths in the range from 1 to 30 seconds are typical.

Stationarity and stability (ergodicity) are measures of change (or lack of change) over time in the power spectrum. As used in the EEG literature, **stationarity** has referred to data segments with little or no change in spectra over short periods of time (seconds), whereas **stability** has been applied to change over longer time periods, including between separate test sittings (Nuwer, 1988b). The EEG is not a stable signal in that its power spectrum usually will vary over long periods of time and between different test sittings. However, it is possible to divide the recording interval into shorter epochs which are stationary, and spectral analysis can then be performed on each of these stationary epochs. The length of the epoch determines the lowest frequency which can be resolved (as discussed in Appendix A). Thus it is important to chose an epoch length which is short enough to avoid nonstationary segments, but long enough to obtain the desired frequency resolution. Unless very narrow frequency components are of interest (this might be the case if peak frequency is the spectral parameter of interest), a resolution sufficient to define the edges of the frequency bands to be analyzed is adequate (Coppola, 1986).

Often of interest is how the spectrum changes with time over the recording interval. One can study these changes by plotting the compressed spectral array which is a 3-dimensional plot of frequency content as a function of time as shown in Figure 3-2. The recording interval is divided into stationary epochs, and by studying the spectra of successive epochs in the spectral array plot, one can observe the temporal variation of spectral content.

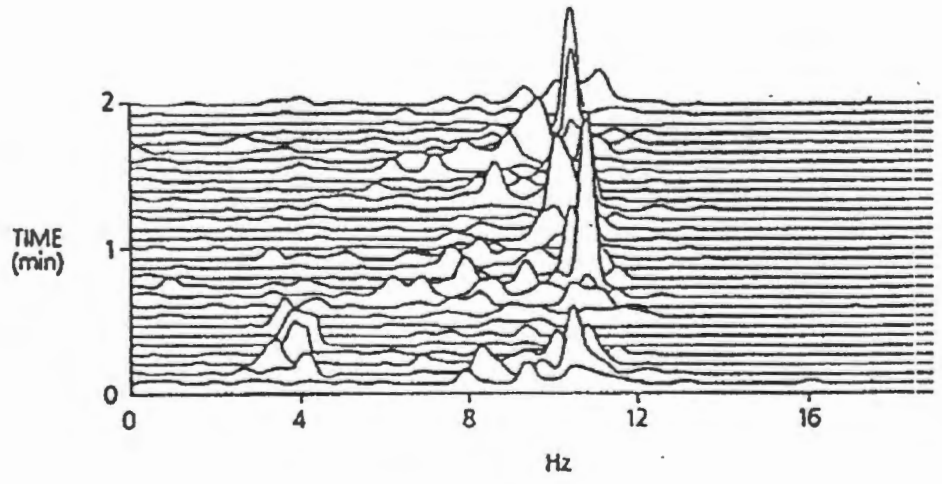

Figure 3-2 : Compressed spectral array.

Sometimes it is of interest to look at the average spectrum; the short-time spectra calculated from sequential epochs being averaged over the recording interval. If parametric methods are being used for the spectral estimation of these spectra, then the model system parameters would be estimated for each epoch.

Often, the non-parametric Fourier-based periodogram method is used for calculation of the short-time spectra. The periodogram is calculated for each epoch, and then the set of short-time periodograms are averaged to produce the average spectrum for the recording interval. If an improved periodogram estimate is required for each epoch, then the method of subdividing each epoch into smaller segments and averaging these segments (Bartlett periodogram), or windowing and averaging these segments (Welsh periodogram) can be applied. The literature often refers to the averaging of the set of short-time spectra over an unstable record as the Bartlett periodogram method. Often the epochs are windowed prior to the computation and averaging of the short-time spectra and the method is then referred to as the Welch periodogram method.

When the average spectrum is calculated, it is possible to obtain an estimate of the constancy or variability of the spectral content with time. This estimate is achieved by calculating the standard deviation and related coefficient of variance during the averaging of the set of short-time spectra. This results in a direct measure of the spectral stability (Duffy, 1986).

3.1.6 Spectral Mapping

The spectral parameters of a multichannel recording are often displayed in the form of topographical maps. The most frequently mapped parameters are the **amplitude or intensity** of EEG activity in a specific frequency band (Breslav et al, 1989; Buchsbaum et al, 1986; Etevenon, 1986; Etevenon et al, 1988; Fisch et al, 1984, Lemos and Fisch, 1991), the **absolute power** in a specific frequency band (Harner, 1986; Nagata et al, 1984; Nagata et al, 1986; Pfurtscheller, 1989b; Samson-Dollfus et al, 1986), and the **relative power** in a specific frequency band (Etevenon, 1986). Gotman (1973) displayed the ratio of (delta + theta) / (alpha + beta) power as a topographical map which he referred to as a canonogram. Figure 3-3 shows 3-D spectral maps of absolute power in each of the delta, theta, alpha and beta bands.

The number and placement of electrodes, the type of derivation, the artifact rejection algorithm and the type of interpolation are all important considerations, and are discussed in

detail in Section 3.3.

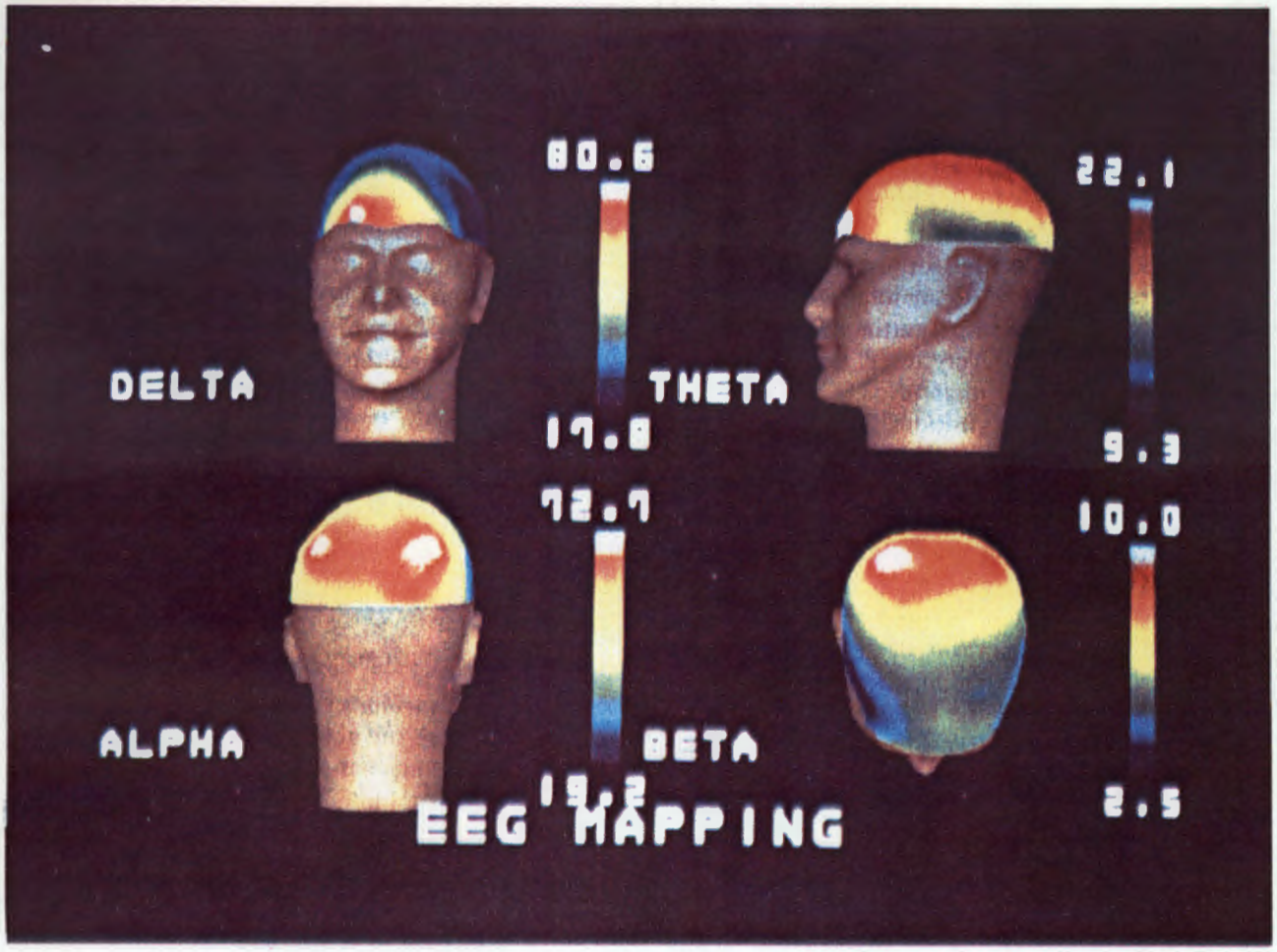

Figure 3-3 : 3-D spectral maps in the 4 bands (delta, theta, alpha, beta) for different positions (frontal, occipital, lateral, vertex) expressed in absolute power. (Reproduced from Soufflet et al, 1991).

3.2 Event Related Desynchronization

3.2.1 Introduction

Event-related desynchronization (ERD) is the name given to the amplitude attenuation or blocking of rhythmic components within the alpha and beta bands (Pfurtscheller and Aranibar, 1977). ERD is a neuronal phenomenon occurring with all types of event-related potentials, such as visual evoked potentials, auditory evoked potentials, contingent negative variation and Bereitschaftpotential (Pfurtscheller, 1989a). ERD analysis is a quantitative method which measures this attenuation and thereby allows the study of the activation of different cortical structures in relation to a specific event or task.

Activation of different cortical and subcortical structures can be studied by measuring the

regional metabolism and blood flow (rCBF) with positron emission tomography (PET) (Nagata et al, 1988; Roland and Widen, 1988). These methods have an excellent spatial resolution in the order of millimetres, but because of the use of radioactive trace substances, they have a poor time resolution. Thus with PET, it is possible to study which cortical areas of the brain are activated during a specific event or task, but it is not possible to study the temporal relationship between these activated cortical areas and the event or task.

Activation of a cortical field is not only accompanied by an increase of metabolism and rCBF, but also by changes in the electric potential and magnetic field of the neuronal mass involved in information processing. Event-related desynchronization analysis is a means of measuring these changes in the electric potential recorded at the scalp to ascertain which cortical structures are activated, and has the advantage of good time resolution when compared with PET techniques. Thus one is able to closely correlate the different cortical activation patterns with the event presented or task being performed.

3.2.2 Physiological Base for ERD

The first reports on blocking or desynchronization of occipital alpha rhythm during visual information processing and mental arithmetic stem from Berger (1930) and Adrian and Matthews (1934). Jasper and Penfield (1949) reported that special cortical areas generate their own rhythmic activity (intrinsic rhythm) which is attenuated (blocked, desynchronized) when the underlying cortical generator structure is activated. Later, Gastaut (1952) and Chatrian et al (1959) described changes of central alpha band rhythms (mu rhythm) in relation to movement. Gastaut also found a blocking of pre-central beta rhythm during sensorimotor activation. It has been shown that speech centres (Broca's area, Wernicke's area) also generate their own intrinsic rhythms that are desynchronized during speech (Pfurtscheller and Klimesch, 1990). These and many other similar observations led to the concept of the alpha and beta band rhythms as "idling" rhythms of the brain, characteristic for inactive cortical fields (Kuhlman, 1978), and alpha or beta desynchronization as characteristic of active cortical fields (Pfurtscheller et al, 1988).

The generation of these intrinsic alpha rhythms involves the thalamic networks including the nucleus reticularis thalami (Pfurtscheller and Klimesch, 1990). The basic element of synchronized alpha waves is inhibition in the neural network. The alpha waves desynchronize when this inhibition is suppressed (disinhibition), either by thalamic afferents or by influx from the brain stem reticular systems, basal ganglia or forebrain areas. It is speculated that multiple thalamocortical systems exist, each characterized by its own cortical epicentre of

alpha band rhythm and each desynchronized when this specific system becomes activated (Lopes da Silva et al, 1973). Because of the involvement of thalamic relay nuclei in nearly all afferent and efferent information flows and its close interactions with various cortical fields, alpha desynchronization can be a highly specific, very localized and circumscribed phenomenon in scalp EEG and characteristic of cortical field activation (Pfurtscheller and Klimesch, 1990).

The desynchronization or blocking of the occipital alpha rhythm after short light stimulation is normally easily seen in the raw EEG data in the occipital and parietal areas (see Figure 3-4).

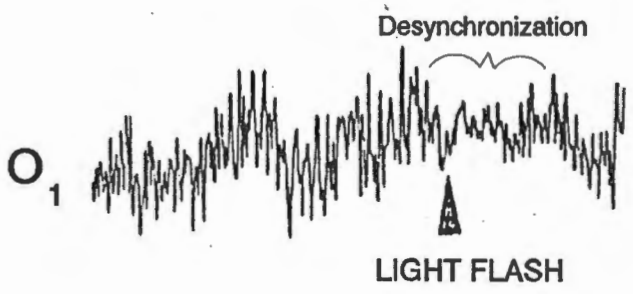

Figure 3-4 : Desynchronization of the EEG recorded from electrode O_1 after light stimulation.

In contrast, blocking of the central mu and beta rhythm during sensorimotor activity is rarely seen in raw EEG. Studies on large groups reported a blocking in only 0-30% of subjects (Chatrian, 1976). Using quantitative EEG, this percentage is increased; Storm van Leeuwen et al (1978) found a blocking of central mu rhythm in 60% of their subjects and Schoppenhorst et al (1980) 57% during repetitive opening and closing of the hand. Pfurtscheller and Aranibar (1979) found a blocking of mu rhythm with voluntary, self-paced movements in 90% of volunteers. This demonstrates that the reactivity of intrinsic rhythms to specific sensory stimulation, sensorimotor activation or higher cognitive processes, is a physiological phenomenon found in nearly every subject, when an appropriate experimental setup and a special recording and analysis technique is used (Pfurtscheller, 1986). ERD analysis is a quantitative EEG technique which allows one to measure this blocking of intrinsic rhythms.

3.2.3 Experimental Setup for ERD Analysis

The ERD is based on the analysis of EEG data recorded during an event or task. Such an event can either be an exogenous stimulus (externally paced) or of endogenous nature

(internally paced, self-paced, self-initiated) and has to be repeated a number of times, with a minimum period of a few seconds between events (Pfurtscheller, 1989a).

a) Exogenous or Externally Paced Events

An example of an exogenous event is median nerve stimulation. The median nerve is stimulated at the wrist, slightly above motor threshold. Each wrist is stimulated separately 60 times with interstimulus intervals of 10 seconds. Sixty trials of 6 seconds each, including 3 or 4 seconds before the stimulation, are used for the processing (Pfurtscheller, 1980). Another example of an externally paced event is visual stimulation. The stimulus could be a flashing strobe light (Aranibar and Pfurtscheller, 1978), or a picture displayed on a computer screen or words displayed on a screen (Pfurtscheller and Klimesch, 1990).

Each conscious sensation of an exogen stimulus is accomplished by at least 2 different neuronal reactions, namely the generation of an evoked potential (EP) and the desynchronisation of the spontaneous EEG. Thus, for example, median nerve stimulation does not only result in desynchronisation of rhythmic activity over the contralateral sensory cortex, but also results in a somatosensory evoked potential (SEP). Similarly, a visual stimulus results in desynchronization of occipital alpha activity as well as the generation of a visual evoked potential (VEP).

b) Endogenous or Internally Paced Events

An endogenous event is an event which is self-paced or self-initiated by the patient. Examples include voluntary movement, speech and mental arithmetic. In a study of patterns of cortical activation during planning of voluntary movement using ERD analysis, volunteers were given the task of performing 60 completely voluntary, self-paced, abrupt movements at intervals not shorter than 10 seconds. The movements required the pressing of a microswitch with the right (left) thumb (Pfurtscheller, 1988).

Planning of motor behaviour is also accompanied by 2 different bioelectric phenomena (Pfurtscheller et al, 1992). One is the desynchronization of sensorimotor rhythms (Pfurtscheller and Berghold, 1989), the other is the Bereitschaftpotential or readiness potential (RP) (Deeke et al, 1976, Vaughan et al, 1968).

An example of a more complex task including both exogenous and endogenous events is given by Pfurtscheller in his study of cortical activation patterns during a visual-verbal task

(Pfurtscheller and Klimesch, 1990). In this example, the event was a visual stimulus, either a word belonging to the category of tools or animals, or a two-digit number. The stimuli were exposed for 250 milliseconds on a screen in intervals of 8 seconds. Forty-eight words and 48 numbers were presented in random order (N=96). Subjects had to perform a semantic classification task and were instructed to respond with "yes" if a word denoted an animal or an odd number, and "no" if a word denoted a tool or an even number.

3.2.4 Data Acquisition for ERD Analysis

Data are acquired from multichannel EEG recordings while the patient is performing a specific task. The patient repeats the task a number of times (usually between 40 to 80 times), resulting in an ensemble of data for each channel. Each trial is an epoch of data (usually between 6 - 10 seconds) consisting of a pre-event and post-event period. Typically, for voluntary, self-paced events, the pre-event period is about 4 seconds in duration, while for exogenous events, the pre-event stimulus is of shorter duration, typically between 1 to 4 seconds (Pfurtscheller et al, 1988). The data are digitized at a sampling rate of between 64 to 128 Hertz using an analogue-to-digital converter and stored. The quantification of the ERD is performed off-line.

In his study of cortical activation patterns during planning of voluntary movement, Pfurstcheller used a sampling rate of 64 Hz. Volunteers were asked to perform 60 voluntary, self-paced movements (movement required the pressing of a microswitch with the right (left) thumb). A 6 second epoch of data was recorded for each movement consisting of a 4 second pre-event period and a 2 second post-event period (the event being the pressing of the microswitch). At a sampling rate of 64 samples/sec, each epoch consisted of 384 samples: 256 pre-event samples and 128 post-event samples. Thus for each channel, an ensemble of 60 trials each consisting of 6 second epochs, are recorded and stored.

3.2.5 Quantification of ERD

Quantification of the ERD can be carried out in either the time domain or the frequency domain. The time domain quantification allows for the calculation of the exact time course of the phasic blocking reaction and ERD measurements in time intervals at least equal to the sample interval (eg. 12 milliseconds at 64 Hz). A disadvantage of this technique is the large amount of computation. For faster computation of the ERD, frequency domain quantification can be used at the expense of losing temporal information (Pfurtscheller, 1986).

a) Time Domain Quantification

A flow chart for computation of ERD is shown in Figure 3-5. This procedure is repeated for each channel :

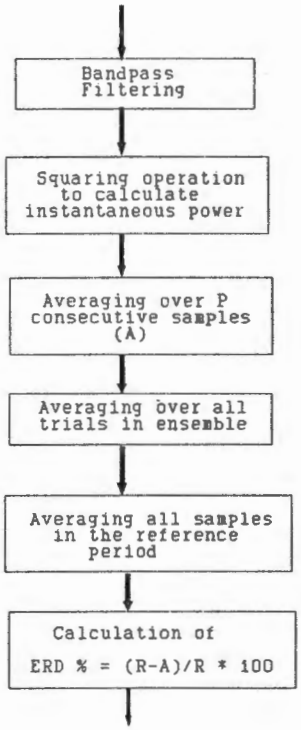

Figure 3-5 : Flow chart for ERD computation. (Adapted from Pfurtscheller, 1989a).

Each epoch of EEG data from the ensemble of trials is bandpassed filtered to the required frequency band. The instantaneous power of the filtered EEG signal in each epoch is then calculated by squaring the signal. To reduce the variance, a number of consecutive power samples are averaged, thereby reducing the time resolution of the original sampled data. Typically between 8 to 16 consecutive values are averaged to reduce the variance (Pfurtscheller, 1977; Pfurtscheller et al, 1988; Pfurtscheller and Klimesch, 1990). The variance-reduced instantaneous power is then averaged over all the trials (the reason for the event being repeated a number of times and then averaged is to improve the statistical reliability of the ERD). The result is one epoch of ensemble-averaged variance-reduced band-limited instantaneous power. The first 1 second of this epoch is assigned as a reference period and the average power in this reference period is calculated (R). The instantaneous power at each sample point in the epoch is then calculated as a percentage power change (increase or decrease) relative to this reference average power. The resultant time curve of percentage power change relative to the average reference power is the ERD and represents the percentage of intrinsic rhythm blocking. An ERD of 100% indicates complete blocking of rhythmic activity, an ERD of 0% indicates no blocking, and a negative ERD indicates an

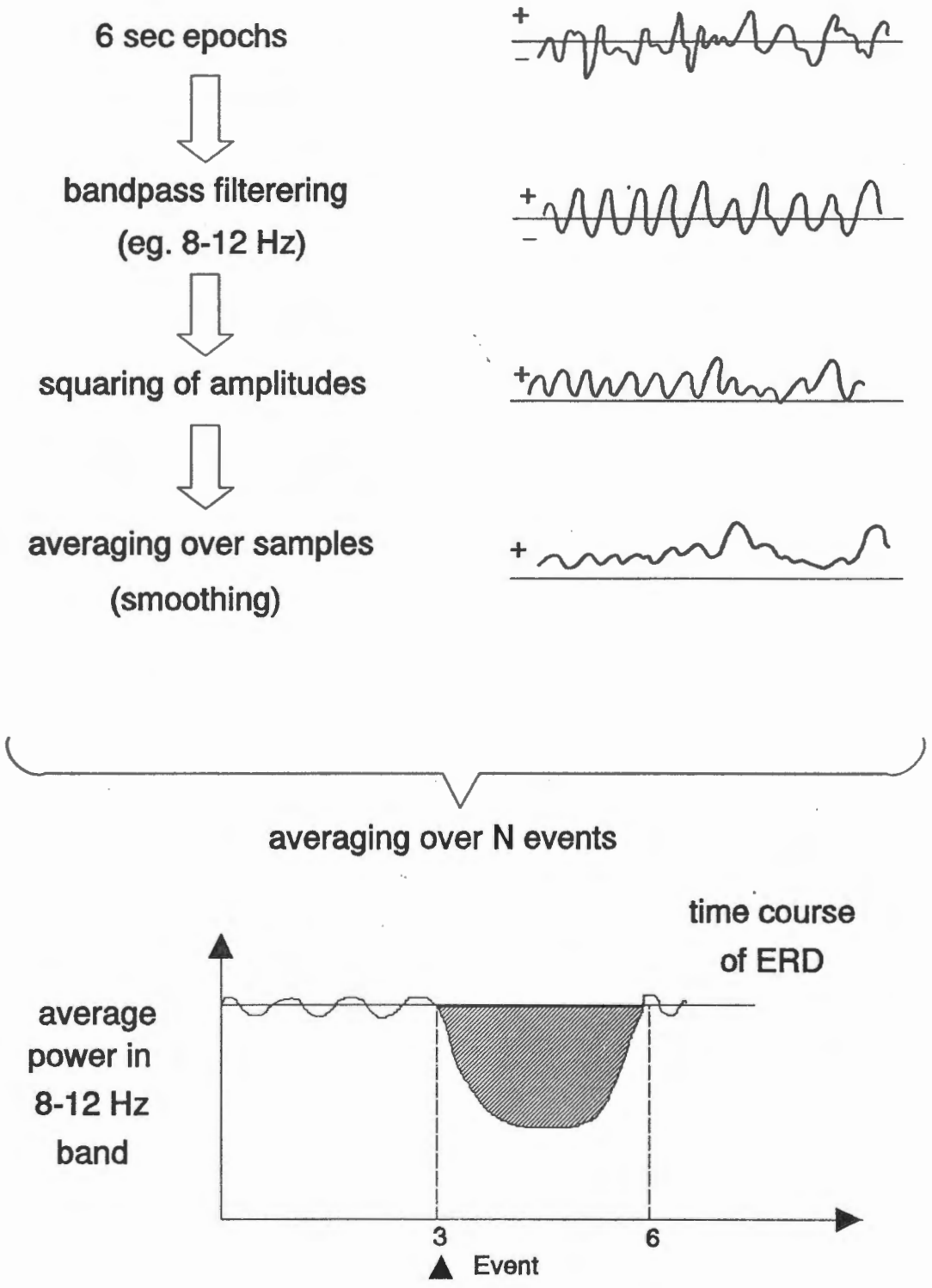

Figure 3-6 : ERD processing in the time domain

enhancement of rhythmic activity. Figure 3-6 shows a diagrammatic summary of ERD computation in the time domain.

b) Frequency Domain Quantification

This method is based on two short-time spectra (1 or 2 seconds), one calculated in the activity period close to the event (post-event period) and the other in the reference period before the event (first second of pre-event period). The exact choice of the activity period depends on whether the events are self-paced (endogenous) or externally paced (exogenous). The logarithmic spectra calculated in both periods can differ significantly in the alpha and beta bands. These differences are measurements for ERD and are equivalent to ERD values obtained in the time domain (Pfurtscheller, 1986).

Figure 3-7 shows resultant ERD from A) calculation in the frequency domain and B) calculation in the time domain.

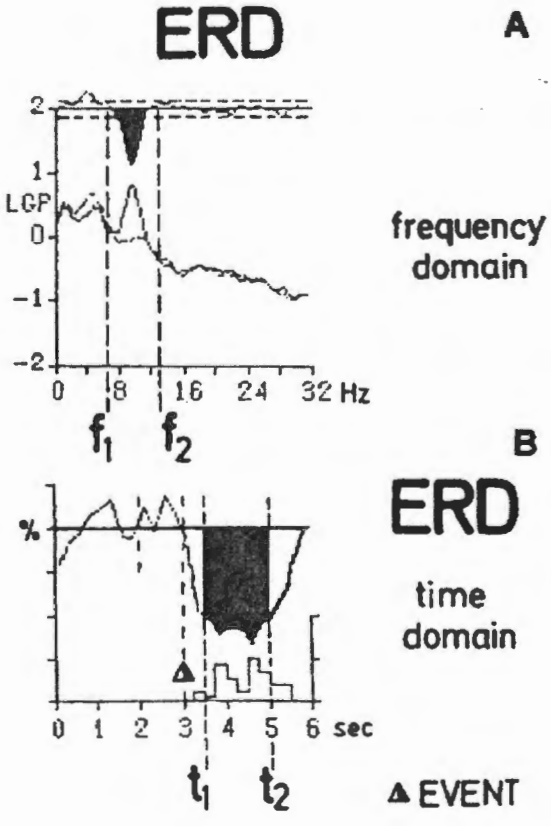

Figure 3-7 : A) Power spectra calculated in the reference period (full-line) and the activity period (stippled-line). The black area indicates the integral over the difference of the two spectra in the frequency band limited by f_1 and f_2 used as ERD parameter for topographical presentation. B) Power versus time curve calculated for the frequency band f_2 - f_1. The black area within the time window t_1 and t_2 can be used as a measurement of ERD. (Reproduced from Pfurtscheller , 1986).

3.2.6 ERD Mapping

Since ERD analysis is used to study cortical activation patterns, the display type normally used is the topographical map. If quantification of the ERD is performed in the time domain, a series of ERD maps can be produced, each corresponding to an instant in time during the task being performed.

By studying the spatial distribution of the ERD, it is possible to locate where blocking of the intrinsic rhythm occurs, and this then indicates the particular cortical areas that are activated. By studying a series of ERD maps produced at sequential time instances during the task, it is possible to follow the changes in the cortical activation patterns and correlate each pattern at a specific time with the specific part of the task being performed at that time. This can be seen in the series of ERD maps shown in Figure 3-8 produced during the visual-verbal task described in Section 3.2.3. The maps indicate the various cortical areas activated during different parts of the task, such as visual encoding, semantic processing and verbal response.

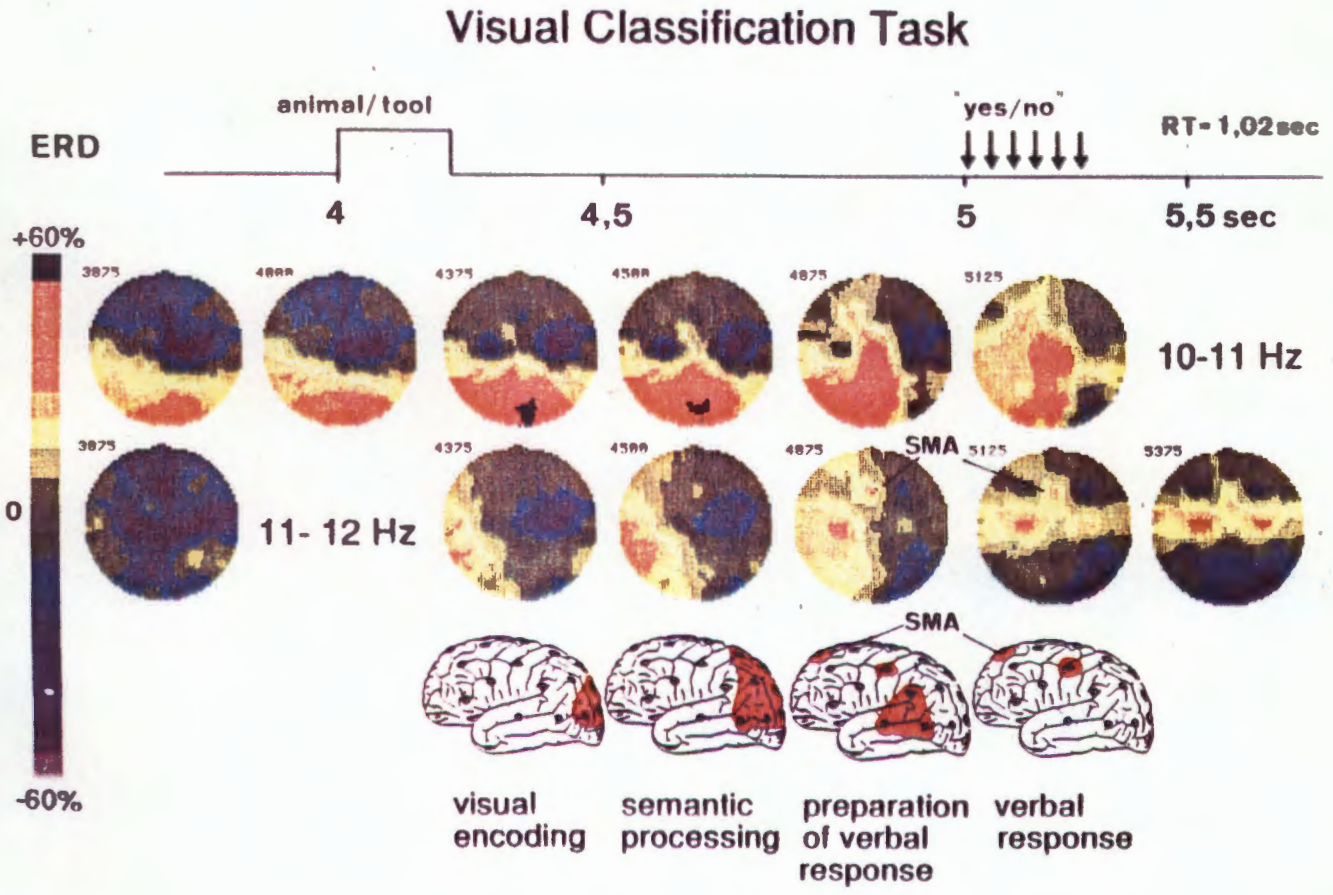

Figure 3-8 : Series of ERD maps computed during a visual-verbal task showing activation of different cortical areas. (Reproduced from Pfurtscheller and Klimesch, 1990).

Again, the number and placement of electrodes, the derivation, artifact rejection and the interpolation are all important considerations and these issues are discussed in detail in Section 3.3.

3.2.7 Local and Temporal ERD Criteria

a) Visual ERD

The visual ERD is strongly localized to occipital and parietal areas. The ERD reaches its maximum amplitude about 200 milliseconds after stimulus and has a duration of some seconds. This latency of the visual ERD was confirmed by studies of alpha blocking after single flash stimulation (Aranibar and Pfurtscheller, 1978). The upper frequency components within the alpha band of the visual ERD are related to the activation of primary and secondary visual areas, while the lower frequency components are more related to the activation of visual association cortex and extrastriate cortical areas as demonstrated in Figure 3-9. The ERD of the upper alpha components starts before the ERD of lower alpha components.

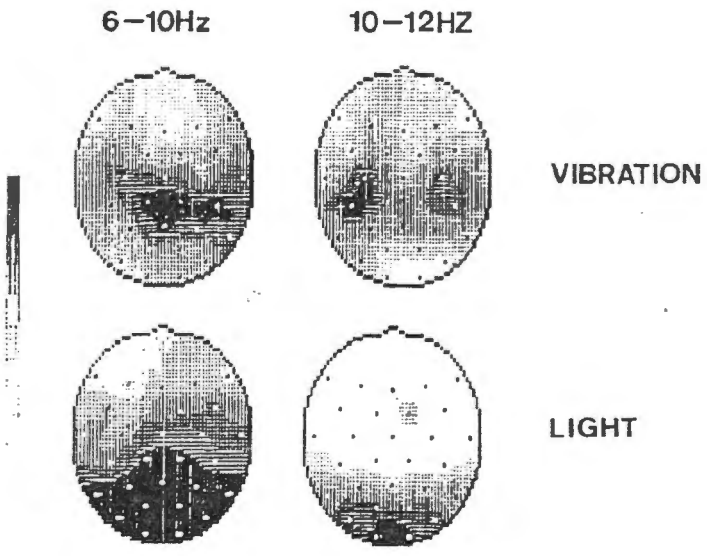

Figure 3-9 : ERD maps calculated during 1 sec mechanical vibration and 1 sec light stimulation using the 6-10 and 10-12 Hz bands. Note that the ERD is more localized to the primary sensory area within the upper alpha components. (Reproduced from Pfurtscheller et al, 1988).

Processing of visual information depends not only on the physical properties of the stimulus and its information content, but also on the initial state of the brain, that is, the degree of activation, arousal, attention, interest and engagement of the subject.

b) Movement-related ERD

Localization, magnitude and distribution of movement-related desynchronization depends on the frequency band analyzed and the type of derivation used. In general, the ERD is more widespread and of larger magnitude in the lower alpha band, similar to the results found during visual stimulation. In the upper alpha band the ERD is less widespread and more localized to the central region, and depends very much on the type of derivation used.

Figure 3-10 shows a series of ERD maps computed during the planning and initiation of left-thumb movements and from these one is able to observe both the spatial and temporal ERD patterns. The ERD is calculated using a local average derivation in the 10 - 12 Hz frequency band. The ERD is maximal at electrode C_4, which overlies the primary sensorimotor hand area, and T_{CP2}, overlying the secondary somatosensory area (Brodmann's area 40 - see Figure 3-13). In addition, an ERD is found at electrode T_{CP1} on the ipsilateral side. This type of ERD pattern, predominantly involving the contralateral right hemisphere, was already present 1750 milliseconds (map 2250) prior to movement onset. Thus the primary sensorimotor hand areas are activated more than 1 second before the movement is made, indicating that some type of planning of movement is taking place. A similar ERD pattern with left hemisphere dominance is observed for right finger movements.

c) Tactile Stimulation

Repetitive mechanical vibration of the first digit of the right index finger demonstrates an ERD pattern similar to that of voluntary movement. The upper alpha band ERD is very localized to primary sensorimotor areas (electrodes C_3 and C_4), and is already present contralaterally in the first hundreds of milliseconds before application of the stimulus (Figure 3-11, lower row, first map). After stimulation, the ERD pattern is bilaterally symmetrical, but still localized to the electrodes C_3 and C_4. The lower alpha components demonstrate a completely different time course. There is no ERD prior to stimulation, and the ERD increases gradually in the first hundreds of milliseconds after stimulation and is more widespread and maximal over parietal areas (Figure 3-11, upper row). Figure 3-9 also demonstrates that upper alpha components are more localized to the primary sensory areas while the lower alpha components are more widespread. The early contralateral ERD before stimulation is presumed to be part of a specific, selective, preparatory process.

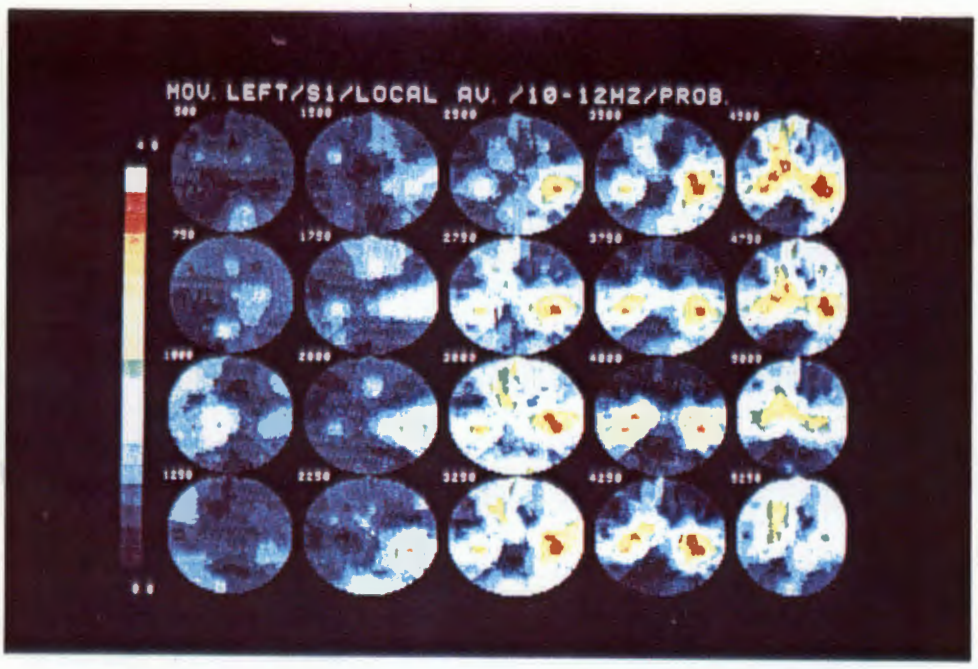

Figure 3-10 : Serial ERD maps from a time period of 3500 msec before (maps 500 - 3750) to 1250 msec after movement (maps 4000 - 5250). EEG data recorded during left finger movement with right ear reference, maps computed with local average reference. (Reproduced from Pfurtscheller et al, 1988).

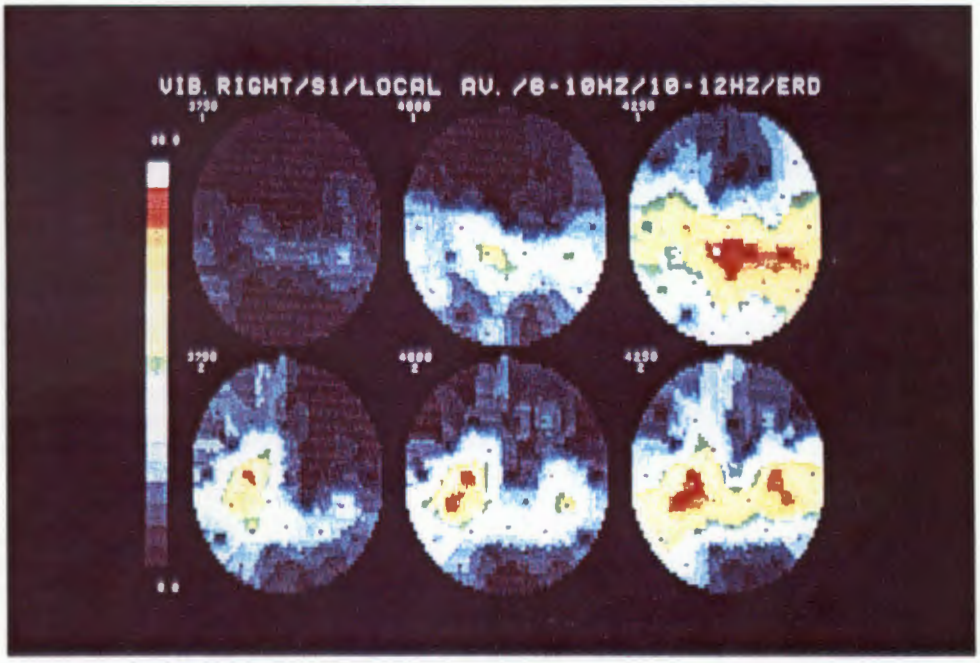

Figure 3-11 : ERD maps computed 250 msec before (map 3750) and during 1 sec vibration of the right index finger (maps 4000 and 4250). Data recorded with right ear reference, maps computed with local average reference. ERD is displayed for the 6-10 Hz (upper row) and 10-12 Hz band (lower row). (Reproduced from Pfurtscheller et al, 1988).

3.3 Topographical Mapping

3.3.1 Introduction

EEG mapping is the topographical display of parameters derived from multichannel EEG recordings, eg. spectral parameters such as alpha power and delta power, evoked potential parameters and ERD percentages. Statistical parameters obtained as a result of comparisons with 'normal' control groups can also be displayed in topographical form.

For the transformation of multiple EEG parameters into a reliable topographic map, some problems have to be addressed. These include the number and placement of electrodes, the type of derivation to be used (i.e. the type of reference used), the interpolation method used, artifact detection and elimination, and the statistical treatment of maps.

3.3.2 Number and Placement of Electrodes

The appropriate number and placement of electrodes is both a theoretical and a practical issue. If it were technically feasible, 1024 scalp electrodes might be employed in a 32 by 32 grid. In such circumstances, minimal or no interpolation would be required for imaging and no scalp region would be left unexplored (Duffy, 1986).

A spatial frequency analysis would dictate electrode density on the basis of a two-dimensional extension of the Nyquist theorem. To prevent spatial aliasing, an inter-electrode distance of less than 2 centimeters is required. Thus for adequate spatial sampling over the adult scalp, at least 128 electrodes are required (Nunez, 1988).

Typically between 12 and 64 electrodes are used, although some systems are now based on 128 electrodes (Gevins and Bressler, 1988). Pfurtscheller et al. (1988) have reported that for studies of functional topography, 30 electrodes are sufficient. Thus electrode placement and interpolation algorithms assume great importance.

The international 10-20 electrode placement system is typically used (19 electrodes) with additional electrodes placed to fill in the gaps between the standard 10-20 electrode positions. Figure 3-12 shows the standard 10-20 electrode positions, while Figure 3-13 shows the electrode positions used by Pfurtscheller in the study of functional topography and their relation to a number of cerebral regions.

However, in some studies a much denser electrode array over the area of interest is used. An example of this is a study of spatial patterns of SEP's obtained by stimulating different digits on the hand, where an electrode array of 81 electrodes was placed overlying the somatomotor area (Duff, 1980).

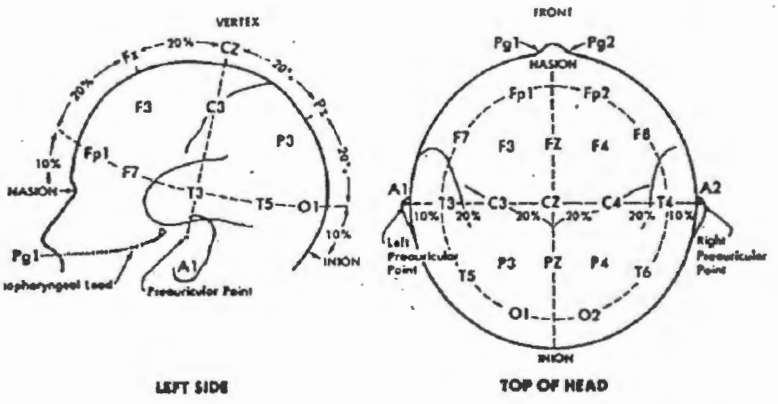

Figure 3-12 : Diagrammatic representation of the International 10-20 system for electrode placement.

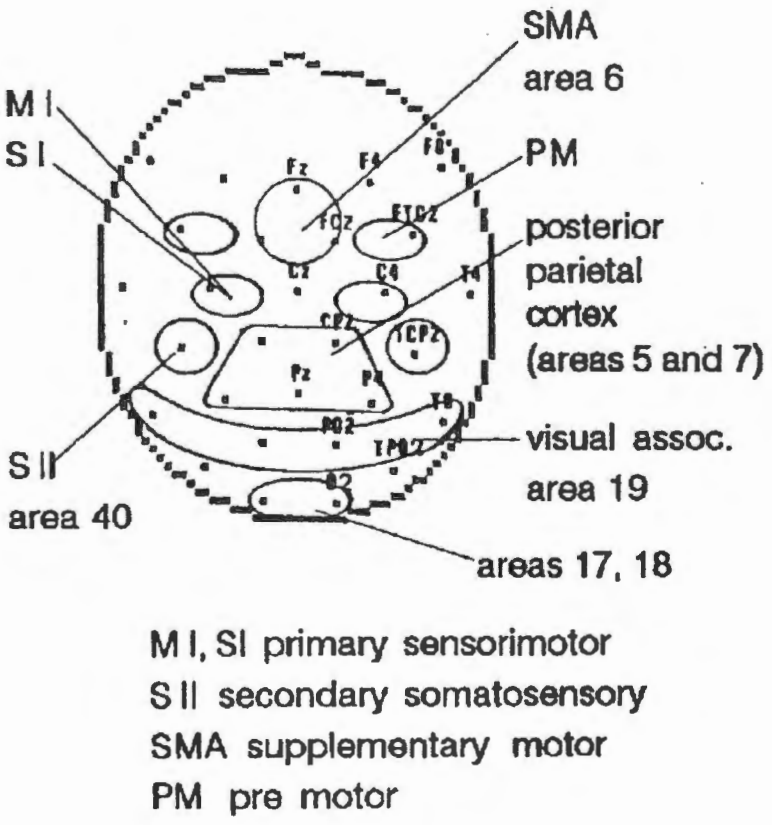

Figure 3-13 : Top-down map showing electrode positions and projections of a number of cerebral regions. (Reproduced from Pfurtscheller, 1989a).

Additional electrodes should be used for detection of artifact. Duffy recommends at least four

additional artifact electrodes placed so as to monitor vertical eye movement, horizontal eye movement, and muscle activity in the temporal and occipital areas (Duffy, 1988).

3.3.3 Interpolation Between Electrodes

EEG parameters are quantified at a limited number of electrode sites placed over the scalp. To obtain a topographical map composed of thousands of pixels (eg. 64 X 64 matrix), spatial interpolation between the discrete electrode positions is necessary. Different types of algorithms exist for this interpolation. The two most common are the N-nearest electrode algorithm and the spline approximation.

a) N-nearest Neighbour Interpolation

The N-nearest neighbour algorithm calculates the values between the discrete electrode positions as being a weighted sum of the values at the nearest surrounding electrodes. The weights are calculated by an inverse relationship of the distance between the point being interpolated and the electrodes used in the interpolation. Normally, the nearest 3 or 4 surrounding electrodes are used for the calculation.

The interpolated value V_{xy} with co-ordinates (x,y) is calculated from the values U_i at the N nearest electrodes of distance

$$d_i = \sqrt{(x-x_i)^2 + (y-y_i)^2}$$

d_i = distance from interpolated value (x,y) to i th electrode position (x_i, y_i)

by the following formula

$$V_{xy} = \left(\sum U_i * d_i^{-m}\right) / \left(\sum d_i^{-m}\right)$$

where m can be 1,2 or of higher order. The linear interpolation (m=1) with 3-nearest neighbours (N=3) or 4-nearest neighbours (N=4) is frequently used (Buchsbaum et al, 1982; Duffy et al, 1979; Pfurtscheller and Berghold, 1989). This method has its advantage in ease of computation and arbitrary location of the recording electrodes, but has some disadvantages in map discontinuities and that extrema are always localized at the electrode sites.

b) Surface Spline Interpolation

Surface spline interpolation is more commonly used in fluid dynamics where a surface spline is the surface obtained by minimizing the bending energy of an infinite plate constrained to pass through known points. Perin et al. (1987) have successfully applied this method for the mapping of scalp potentials, and found that it gives continuous surfaces and better approximates the locations of extrema, these advantages being at the expense of lengthier computation time.

3.3.4 Type of Reference

Two different types of EEG recordings can be made : the reference-dependent and the reference-independent or reference-free recording.

a) Reference-dependent Recording

With the reference-dependent or monopolar recording, each active electrode potential is measured relative to a common reference placed such that it minimizes the possibility of picking up potentials from the brain. Many different common reference sites are used and these include linked mandibles, left or right ear, linked ears, nose and neck. However, because there is no reference point with zero potential, each map depends on the choice of reference and if this reference becomes contaminated with EEG activity, serious ambiguities may arise in the topographical display of the data recorded during.

One solution is to use a technique called referential reconstruction. With this technique, several reference sites are recorded simultaneously. For example, the 19 active sites are recorded using a linked ear reference while simultaneous recording is made from linked ear to the nose, chin and noncephalic site. On playback, a computer could subtract one reference channel from all the main recording channels, yielding data as if they were originally recorded using the second choice of reference. The formula for switching from a linked ear to a chin reference for one of the 19 channels would be :
$(F_{p1} - A_1A_2) - (A_1A_2 - \text{chin}) = (F_{p1} - \text{chin})$ (Nuwer, 1988a).

b) Reference-independent Recording

Another approach to the reference problem is to use reference- free recordings; these include bipolar derivation, common average reference and source derivation.

There is no optimal or universally accepted reference. The choice of reference type depends on the application. Multichannel EEG data should ideally be recorded with one common reference if possible, and then the various reference-independent derivations can be calculated from this data as required. Duffy states (1988) that "only experience will clarify their (reference-independent methods) value relative to more conventional reference electrode placements. Until this is established, most mapping systems used for clinical work should allow many or all of these reference (independent) options" (Duffy, 1988).

i) Bipolar Derivation

Electroencephalographers have long enjoyed bipolar chain montages. Bipolar measurements are made between two, usually adjacent electrodes by taking the difference between the potentials at these electrodes and are equivalent to the first spatial derivative or the potential gradient (μV / cm) (Pfurtscheller, 1989b). There are two types of bipolar derivations, viz transverse and longitudinal.

Bipolar channels can localize some changes better, but they may also cancel out EEG activity with a spatial field wide enough to encompass both of the recording sites (Nuwer, 1988a). This cancellation effect can be advantageous in eye movement artifact during transverse bipolar recordings, where artifactual potentials generated by eye movement are common to both electrode sites in the transverse plane and are therefore cancelled out by the bipolar calculation.

Bipolar reconstruction can be done using the computer to subtract referentially recorded data channels in a manner analogous to that described above for referential reconstruction. The user might directly record the data in bipolar format, but that sacrifices the flexibility of allowing subsequent arbitrary referential or bipolar reconstruction as desired to fit the clinical situation.

The interelectrode distance in the bipolar derivation affects power and ERD measurements. With increasing interelectrode distance, the power (amplitude) increases and the ERD decreases. Bipolar derivations with closely spaced electrodes are more appropriate to measure ERD than widespread montages.

Considering ERD mapping, the transverse bipolar derivation can enhance and localize the ERD better during voluntary movement than earlobe-referenced recordings. Recordings over the sensorimotor cortex with reference to the earlobe may result in the masking of event-

related changes of centrally recorded potentials by large potentials at the reference electrode. Therefore, monopolar recording with an earlobe reference can even demonstrate that there is no blocking reaction due to voluntary movement; bipolar derivations, however, can display a significant ERD in the central region (Figure 3-14).

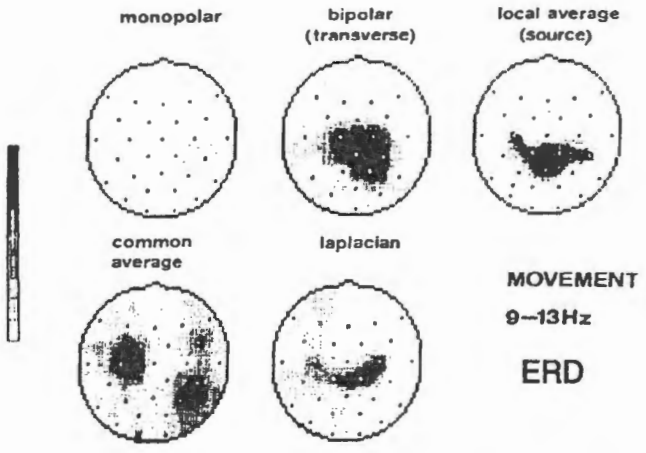

Figure 3-14 : Influence on the type of derivation on the topographical display of ERD during voluntary finger movement. (Adapted from Pfurtscheller et al, 1988).

The difference in ERD maps between monopolar and bipolar derivations during visual stimulation is less pronounced but also evident, as can be seen in Figure 3-15. The bilaterally symmetric representation of the ERD over the occipital region with the bipolar montage is more realistic than the lateralized ERD with monopolar recording (Pfurtscheller et al, 1988).

ii) Common Average Derivation

The common average reference was first introduced by Goldman (1950). With this method the potentials recorded from all electrodes are averaged to produce an average reference and each active electrode is then measured relative to this average reference.

The common average reference system is liable to serious ambiguities if a large population of electrodes pick up similar signals (Pfurtscheller, 1988). In this case when the average reference becomes contaminated, occipital alpha rhythms may appear in frontal derivations and eye movement artifacts may affect posterior electrodes. This can often lead to misinterpretation of foci in topographical maps. Duffy (1986) has reported that the common average derivation shows merit for physiological investigations in normal subjects when electrodes are densely placed over a limited scalp region. However, when the whole scalp is studied and pathological discontinuities exist, reference averaging may artifactually affect nonpathological regions.

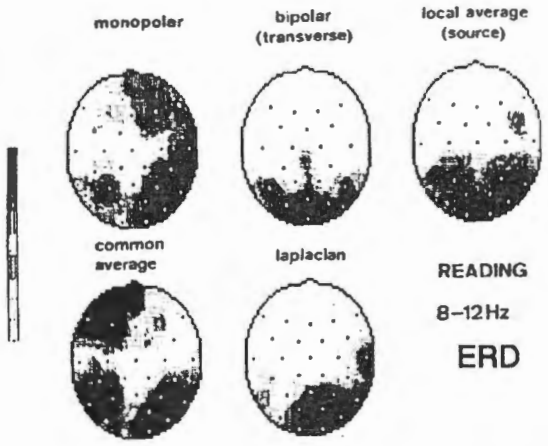

Figure 3-15 : The same as for Figure 3-14, but data recorded during a reading task. (Adapted from Pfurtscheller et al, 1988).

The ERD can also be enhanced with a common average reference, but the localization is very often different from the bipolar derivation. In contrast to the bipolar derivation, the ERD is more widespread and can also be evident over frontal areas with a common average reference (Figures 3-14 and 3-15). Care must be taken in interpreting maps obtained using common average reference (Pfurtscheller et al, 1988).

iii) Source Derivation

Applying a Laplacian operator to the recorded data is another method of solving the reference problem (Pfurtscheller, 1989b). The Laplacian technique is sensitive to field curvature and may be thought of as a "two-dimensional bipolar" recording (Duffy, 1986). The Laplacian method replaces the data by their second spatial derivative (uV/cm^2), increasing the spatial resolution and improving localization of foci in the topographical map. The local average reference or source derivation was introduced by Hjorth and is an approximation of the Laplacian operator (Hjorth, 1975; Hjorth, 1986).

The source derivation is similar to the common average reference except that it uses only the four nearest electrodes to each active electrode instead of all the electrodes to form the average reference. The active electrode is then measured relative to this local average. A detailed mathematical formulation of how the source derivation method approximates the Laplacian operator is given in Appendix D.

The source derivation approach yields good results for electrodes near the vertex, but the quality of the results deteriorates at the periphery, since 3-point operators instead of 5-point operators have to be used in the local average calculation (as explained in Appendix D). The

technique is best applied when there is a very large number of electrodes (Nuwer, 1988a).

3.3.5 Artifacts

Clinical EEG is full of artifacts and these must be excluded before analysis of background EEG can be performed quantitatively. Artifact in EEG data can introduce erroneous foci into topographic maps leading to incorrect interpretations (Nuwer, 1988a).

The most reliable means of artifact detection and elimination is examination of raw EEG data by the technologist or electroencephalographer. This examination can take place on-line or off-line. Oken and Chiapa (1988) used a system that allowed both on-line and off-line examination. EEG with excessive eye movement, muscle or other artifact was rejected on-line by pressing a button which halted the digitizing and backed up the data storage location to the end of the last complete 4 second epoch. In addition, the 4 second epochs were edited off-line, and epochs which contained excessive artifact that had been missed on-line were excluded from further analysis. Automated artifact detection and elimination is helpful, but it should be supplemented by a trained expert.

Automated detection and elimination have taken several forms. One form is that of simple voltage trigger testing where all 'high-voltage' transients are considered as artifacts (Nuwer, 1988a; Pfurtscheller et al, 1988). If analogue-to-digital conversion is being used, simple check for overflow (amplitude saturation) of the ADC input is a simple test for artifact presence.

Eye-movement artifact or ocular artifact (OA) elimination has attracted much attention. The simplest method of ensuring artifact-free raw EEG data is to monitor the electro-oculogram (EOG), and if this activity becomes significant, the data is discarded. Automated OA elimination schemes include digital subtraction techniques (Nuwer, 1988a) and more elaborate time domain techniques. Digital subtraction techniques involve modelling the effects of the EOG on each EEG channel, usually by calculating their cross-correlation. The time domain techniques are based on parameter estimation of the EOGs (Jervis et al, 1988). These method requires additional channels to record the EOG.

Pfurtscheller uses an artifact exclusion criteria based on measurements of power percentages (Pfurtscheller et al,1988). The alpha band power percentage is computed and compared to a threshold. If this is less than the threshold, movement and electrode artifacts resulting in increased activity in the low frequency range is assumed. The beta band power percentage is also computed and compared to a threshold. If this power is greater than this threshold,

myogenic artifacts are assumed.

3.3.6 Use of Colour in Topographic Maps

Colour topographic maps can be inherently deceptive. Just as the proper use of colour scaling can be used to enhance the visibility of data in topographical maps, its improper use can create false and misleading impressions. The proper choice of colour should provide an immediate sense of gradient i.e. which direction of colour change represents "more" and which "less". The use of colour scales where certain steps are dramatic (eg. yellow to red) but comparable steps of equal magnitude are much less distinct (eg. blue to green-blue), may deceptively highlight certain spatial regions, such as those in bright red.

For spectral and ERD maps, a rainbow scale is typically used with the blue to black colour group representing the lowest values and the red to white end of the spectrum highest values. An example of a rainbow scale used in the topographic mapping of alpha activity is shown in Figure 3-16. For EP data, zero microvolt readings should be encoded black or white, with red representing positive readings and blue negative. Changes of hue and saturation within the red and blue may then provide incremental steps (see Figure 3-17). The use of rainbow scaling for EP data should be avoided as it creates confusing imaging. This is due to the fact that the colour value representing zero may not stand out, the gradient is unidirectional (least to most) rather than bidirectional (zero to plus maximum and zero to minus maximum), and the distribution between negative and positive data is not usually distinct and meaningful (Duffy, 1988).

3.3.7 Statistical Treatment of Maps

There are three different cases which need to be discussed, viz. statistical significance of one map, comparison of one map with a group of maps and comparison between two groups of maps.

a) Statistical Significance of One Map

When evoked potential or EEG band powers are displayed, the mean and standard deviation can be calculated for each electrode because of the averaging procedure used. The topographical display of the variance or standard deviation gives some information about the variability of the data.

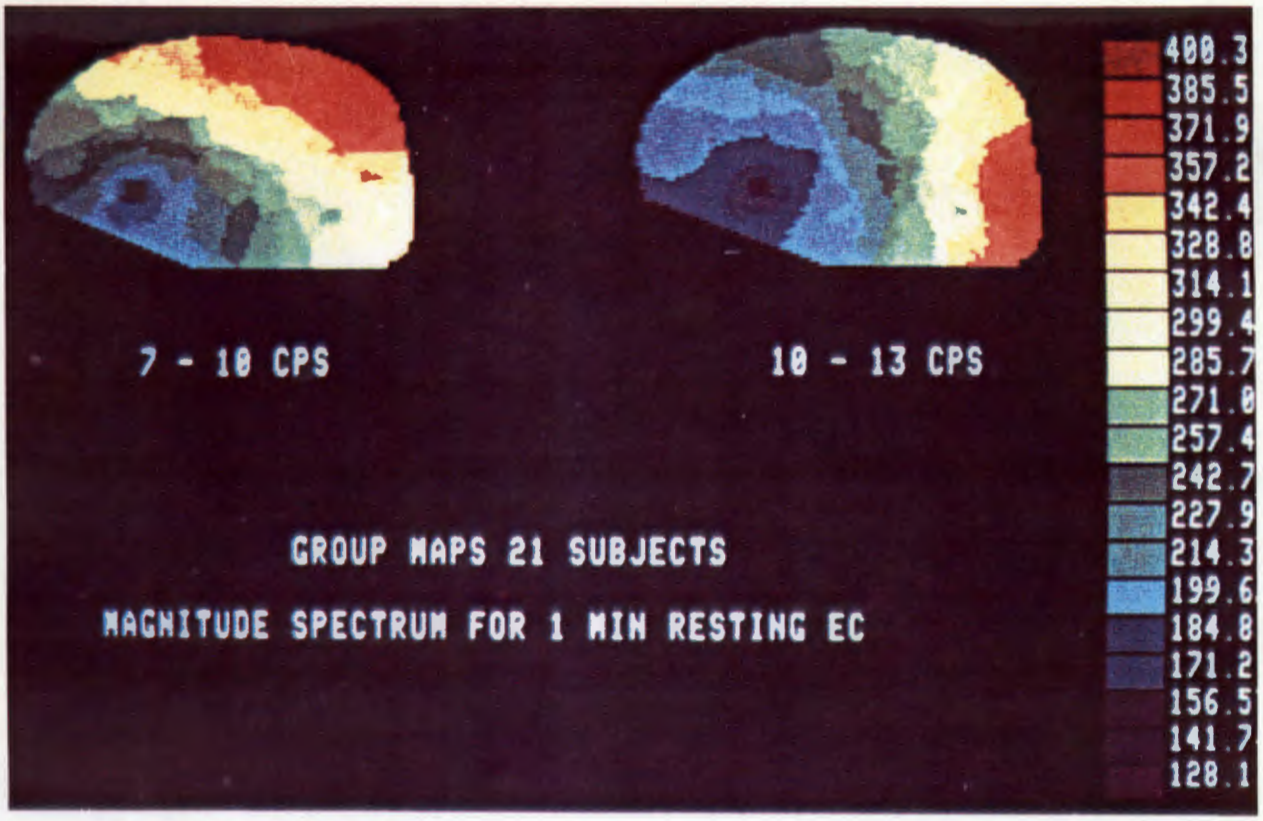

Figure 3-16 : Topographical distribution of alpha activity showing the use of a rainbow colour scale to represent the EEG intensity in μV. (Reproduced from Duffy, 1986).

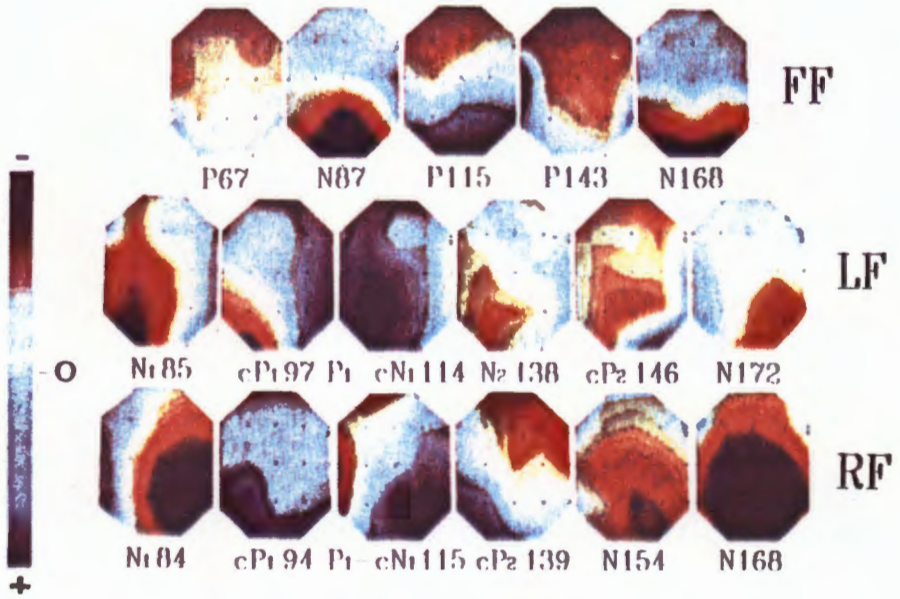

Figure 3-17 : Appropriate colour scale for EP mapping. (Reproduced from Onofrj et al, 1991).

In the case of the ERD quantification, it is possible to detect the sign of the power change (either increase or decrease) in each single trial referred to the reference interval. When there is no change in power (no ERD), the number of positive and negative signs have to be the same; when there is a significant ERD, the majority of signs will be positive. The result of this sign test can be used to define significance levels. For each electrode, the ERD and its probability can be calculated and displayed in the form of step-functions. This can be seen in Figure 3-18 (left-side). This figure shows the ERD time curve and the probability step-function. For each time interval, the ERD and its probability can be displayed topographically (Figure 3-18, right-side).

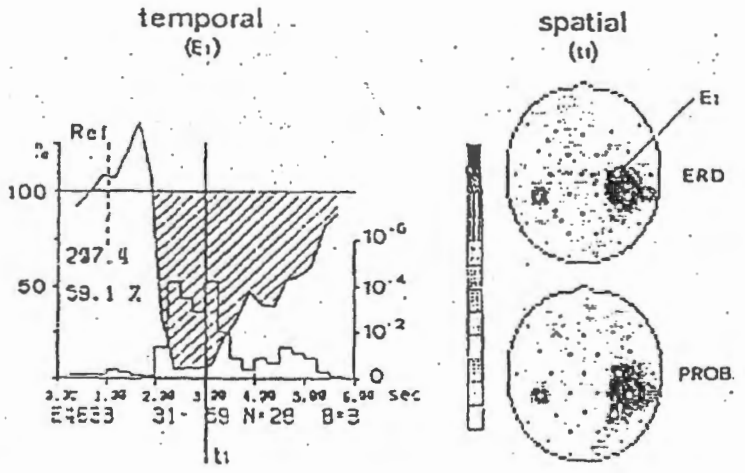

Figure 3-18 : Time curves of ERD and probability for one electrode (left); ERD map and probability map calculated at time t_1 (right). (Reproduced from Pfurtscheller, 1989b).

b) Comparison of One Map with Group of Maps

For comparison of two maps, the z-statistic can be used. Duffy et al (1981) introduced significance probability mapping (SPM). The z-transformation ($Z = (\overline{x}-x)/S$) is calculated for each pixel from an individual subject (x) in comparison to the mean ($\overline{x}$) and standard deviation (S) from a group of maps as illustrated in Figure 3-19.

The z-statistic expresses the number of standard deviations by which an individual observation differs from the mean of a group of similar observations. A prerequisite for this technique is the normal distribution of the group data. The z-statistic is then displayed in topographical form as a significance probability map.

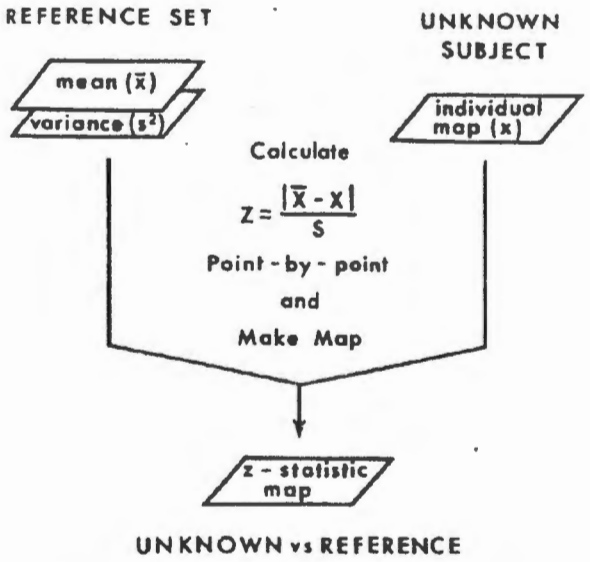

Figure 3-19 : Formation of significance probability map by z transform. (Reproduced from Duffy et al, 1981).

c) Comparison of Two Groups of Maps

For comparison of two groups of maps, the student-t statistic can be calculated and this then used to display a t-statistic SPM. The t-statistic is calculated from the mean and variance of the two groups of data (Figure 3-20), and when displayed topographically will reveal regions in which the two populations statistically differ from one another. Again, the data sets must be normally distributed.

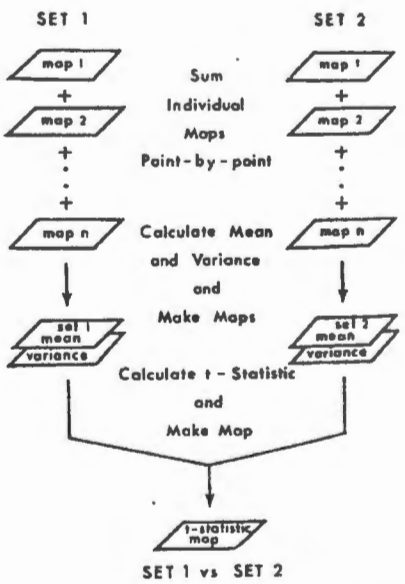

Figure 3-20 : Formulation of significance probability map by Student's t test.

CHAPTER 4

SYSTEM SPECIFICATIONS, DESIGN AND IMPLEMENTATION

Based on the requirements of the EEG Laboratory at RCWMCH, a quantitative EEG system for spectral and event-related desynchronization mapping was designed and implemented. The detailed literature survey revealed some of the decisions that needed to be made (such as choice of spectral parameters, parametric versus non-parametric spectral estimation, time domain versus frequency domain ERD quantification, type of interpolation method etc) and some of the problems (such as number of electrodes, artifact rejection, type of derivation etc) that needed to be addressed for the design and implementation of such a system.

4.1 System Overview

The system is based on an IBM-compatible computer. A 25 MHz 80386DX machine, with 4 Megabytes of RAM, a 80387 maths coprocessor and VGA graphics card and monitor was used for the development and implementation of the system. However, the system is designed to run on any 80x86 IBM compatible machine which supports VGA graphics and which uses the MS-DOS operating system (Version 5).

The computer system interfaces to the EEG recorder at RCWMCH EEG Laboratory. The Medelec 1A97A is an 18 channel recorder, with two additional channels for time and event marking. The multichannel signals recorded from the montage of electrodes placed on the patient's head are amplified, filtered and displayed as polygraphic tracings on z-fold paper. Connections on the side-panel of the Medelec recorder give access to the amplified EEG signals. These signals are passed through a pre-processor unit which preconditions the signals, and the signals are then digitized by an analogue-to-digital convertor (ADC) card which plugs into the expansion slots of the host computer. This preconditioning is required to match the output of the EEG recorder to the inputs of the ADC card, and to provide anti-aliasing filtering. Data is acquired in one of two modes depending on whether spectral analysis or ERD analysis is to be performed.

For spectral analysis, the multichannel data are recorded continuously for a period which is user selectable (typically 3-5 minutes). During this time, the patient can either be at rest with eyes open or closed (an uncontrolled state of the brain), or could be performing some test designed to maintain a particular state of the brain such as reading, listening to music, continuous fist clenching etc. The recorded data are then stored, together with patient

information, for subsequent off-line processing and display.

For ERD analysis and mapping, multichannel data are acquired in sets of short epochs (trials), each epoch being recorded during the performance of some task by the patient and the task then being repeated by the patient a number of times to give a set or ensemble of epochs. The task involves an event which might be the display of a word on a screen, the flash of a light, movement of the thumb etc. Data are acquired for a period of time prior to, during and after the event, making up the epoch of data. The pre-event time and post-event time intervals are user selectable. Typically an epoch is 6-10 seconds, with the pre-event time interval depending on whether the event is exogenous (typically between 1 and 4 seconds) or self-paced (typically 4 seconds). The number of times the task (event) is to be repeated is also user selectable and is typically 60-80 times. The ensemble of data is stored, together with patient information, for subsequent off-line processing and display.

A simple automated artifact detection scheme is implemented using a voltage threshold trigger. If any of the epochs within a block of data contain artifact, the block is discarded and not used in the processing. The user is also able to scan through recorded raw EEG data off-line and confirm the artifact-marked blocks of data, clearing any blocks which have been incorrectly classified as containing artifact. Blocks containing artifacts that were missed by the artifact detector, can also be marked by the user and these blocks are then discarded and not used in the processing of the data.

A reference-dependent derivation (i.e monopolar derivation) is used for recording of the EEG data with the left ear (A1) used as the reference site. The system allows the transformation to a reference-independent derivation giving the user a choice of transverse bipolar, longitudinal bipolar, common average or local average derivations. The user can also choose not to perform any derivation transformation, leaving the data in the reference-dependent monopolar form.

Spectral analysis is performed on the data recorded in the continuous mode of data acquisition. The recording interval (3-5 minutes) is divided up into 5 second epochs, and the non-parametric periodogram spectral estimator is calculated for each epoch. The short-time spectra thus calculated are then averaged over all epochs to produce an average power spectrum for the recording interval. The absolute and relative power in each of the delta, theta, alpha, and beta frequency bands is calculated from this averaged spectrum. After calculation of absolute and relative power in each of the bands for all channels (i.e all electrodes), topographical spectral maps are calculated using the linear three-nearest neighbour

algorithm.

Quantification of the ERD is performed in the time domain as described in the literature review and illustrated in Figure 3-5. Each epoch from the ensemble of data is bandpass filtered to a user selectable frequency band (8-10 Hz, 10-12 Hz, or 8-12 Hz), squared and averaged over all trials in the ensemble. The average power in the first second of the ERD epoch is calculated as a reference power, and the percentage power change (increase or decrease) relative to this power reference is calculated resulting in the ERD time curve. After calculation of ERD time courses for all electrodes, topographical ERD maps are calculated using the linear three-nearest-neighbour algorithm.

4.2 Design Methodology

The system was subdivided into a data acquisition module and a data processing and display module. The data acquisition module contains both hardware and software elements, while the data processing module is software based. In terms of the software, the modules were implemented as two stand-alone executable programs, with communication between modules being in the form of operations on data files which could be commonly accessed by either program. Thus the data acquisition module is responsible for generating a data file containing the acquired data, while the data processing module can access the data file, process the data and display the results.

The reason for splitting the system up into two modules was two fold. The first reason was the top-down design approach which had been adopted for the design. Top-down design is a software engineering concept which involves starting at the top and breaking the design problem down into logical components. For each of these components, there is then further division into logical sub-components, and this sub-diving is continued until each sub-component can be easily codable. The division of the system into a data acquisition module and a data processing module was thus seen as the first logical subdivision in the top-down design. The second reason, which explains why these sub-divisions were implemented as separate stand-alone executable programs, involves memory management. Running under the MS-DOS operating system where the 80x86 processor is operating in real mode, one is limited to a memory barrier of 640 Kbytes. Often with large programs where large amounts of data are to be processed, there is the risk of over stepping this memory barrier when the size of the program becomes larger than the available memory. In such cases, overlay programming is needed where sections of the program code are stored on disk and an overlay manager switches sections of the program code between disk and memory. Overlay

programming involves extra overhead both in terms of software development time as well as in program execution time, as execution of the program is slowed down by the overlaying of sections from disk. To avoid using overlay programming, the system software was implemented as two stand-alone executable programs, each program having smaller demands on memory.

Design of the data acquisition module consisted of specification of the number and placement of electrodes in the recording montage, hardware design of a pre-processor unit and software design of routines for acquisition of patient information, control of the ADC card, on-line artifact detection and storage of patient information and recorded data.

Design of the data processing module of routines for accessing data from data files, artifact handling, reference transformation, spectral and ERD quantification, interpolation and display of topographical maps.

A user interface allowing the user to make different selections and enter information required by the system, was also designed and implemented.

The software was developed in the C language using the Borland C++ development kit (Version 2).

4.3 Data Acquisition

4.3.1 Introduction

Figure 4-1 shows a block diagram of the data acquisition system. The fist two blocks in the diagram represent the technology that was already available at RCWMCH EEG Laboratory.

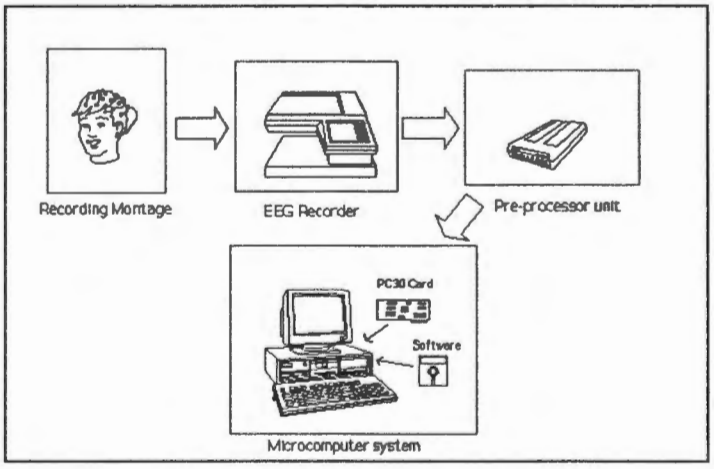

Figure 4-1 : Block diagram of data acquisition system.

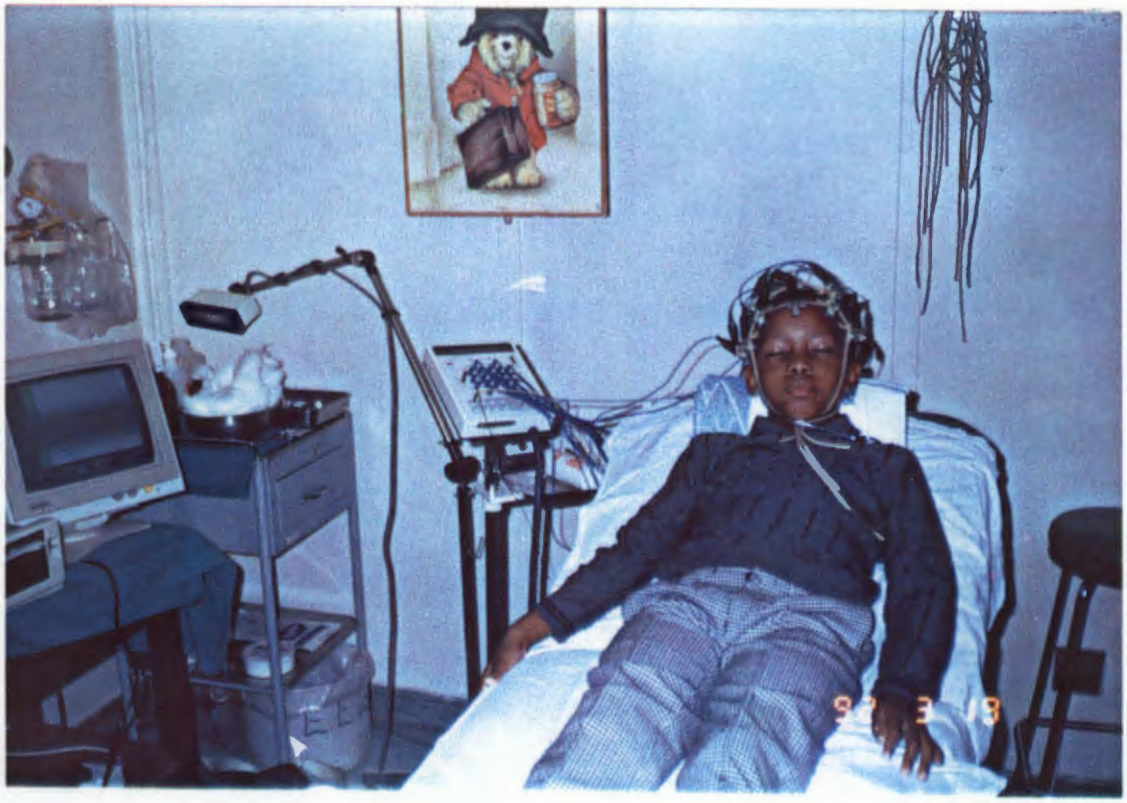

Figure 4-2 : Photograph of patient during recording session showing the recording electrodes connected to the head box.

Figure 4-3 : Photograph of computer system interfaced to EEG recorder during recording session.

Electrodes are placed on the patient's head in a particular recording montage and the multiple lead EEG is measured. The EEG channels are then amplified and displayed as polygraphic tracings by the EEG recorder. The other blocks are part of the quantitative EEG system. Figure 4-2 shows a photograph of a patient during a recording session. The electrodes from the recording montage are connected to a head-box as seen in the photograph, the head-box being connected to the EEG recorder. Figure 4-3 shows the computer system connected to the side-panel of the EEG recorder through the pre-processor unit.

4.3.2 Recording Montage

The 10-20 International system is used for electrode placement (Figure 3-12). However, only 16 electrode sites are used as compared with 19 standard sites in the 10-20 placement system. The EEG recorder is only an 18 channel recorder, and two of these channels are being reserved for recording the EOG activity for artifact detection in future development of the system.

Since only 16 electrode sites are used, it was necessary to eliminate some of the standard 10-20 sites. Since most of the areas of the brain that are functionally important (eg. MI, SI primary sensorimotor, SII secondary somatosensory, SMA supplementary motor, PM pre motor, visual association area and the primary and secondary visual areas, see Figure 3-13), lie posteriorly to sites F_3, F_z and F_4, it was decided to exclude sites F_7, F_{p1}, F_{p2} and F_8.

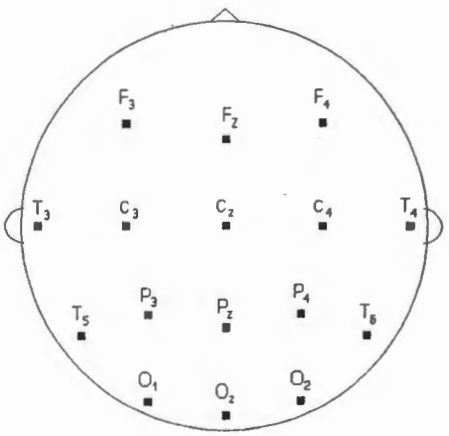

Figure 4-4 : Recording montage showing the 16 electrode sites used.

This choice was also desirable as these electrodes are most susceptible to eye movement artifacts. Electrode site Oz, midway between O_1 and O_2, which is often quoted in the literature, but not one of the standard 10-20 sites, was included. Figure 4-4 shows the

recording montage. The EEG recorder was programmed for this montage and Table 4-1 shows the assignment of the 16 channels.

Table 4-1 : EEG channel assignment of recording electrodes.

EEG channel	Recording electrode
1	$F_3 - A_1$
2	$F_z - A_1$
3	$F_4 - A_1$
4	$T_3 - A_1$
5	$C_3 - A_1$
6	$C_z - A_1$
7	$C_4 - A_1$
8	$T_4 - A_1$
9	$T_5 - A_1$
10	$P_3 - A_1$
11	$P_z - A_1$
12	$P_4 - A_1$
13	$T_6 - A_1$
14	$O_1 - A_1$
15	$O_z - A_1$
16	$O_2 - A_1$

4.3.3 Hardware

a) Pre-processor Unit

A pre-processor unit was designed to interface the EEG recorder and the ADC card. This unit provides anti-aliasing filtering and amplification for the sixteen EEG channels. The unit also contains an attenuation stage for the event-marker trigger signal, sent on one of the digital I/O lines from the ADC card and which connects to the event-marker channel of the EEG recorder.

i) Requirements

The lowpass anti-aliasing filter is used to band-limit the analogue signals, prior to digitization, to below half the sampling frequency. This ensures that no frequency components are present which would cause aliasing in the digitized signal. The highest frequency of interest in the background EEG signal is 30 Hz, thus a lowpass filter cut-off of 30 Hz was specified.

However, to meet the demands of the variable sampling rate for possible future development of the system, it was desirable for the filter's cut-off frequency to be tunable from 30 Hz to 3 kHz.

The signals from the EEG recorder also need to be amplified to the input dynamic range of the ADC in order to reduce quantization errors and thereby ensure adequate resolution of the digital signal. The input of the ADC is configured for bipolar $\pm$ 5V input, ie. a dynamic range of 10 volts. The potentials recorded on the scalp have a peak-to-peak amplitude which varies between 5 and 150 μV. The amplification of these scalp potentials depends on the sensitivity setting of the EEG recorder as shown in Table 4-2. The gain for the pre-processor was specified as the gain required to amplify the output voltage from the recorder (for an input peak-to-peak scalp potential of 100 μV at the mid-range sensitivity setting (10 μV/mm)) to the full dynamic range of the ADC. Table 4-2 shows the output peak-to-peak voltage for a 100 μV input potential. For a sensitivity setting of 10 μV/mm, the output from the recorder is 1V. To amplify this to the full-dynamic range of the ADC card, a gain of 10 times (20 dB) is required and was specified for the pre-processor.

Table 4-2 : EEG recorder gains and output voltages for an input of 100μV, for the different sensitivity settings.

Sensitivity [μV/mm]	Gain dB	Gain X	Output voltage [Vp-p]
5	86	20000	2.0
7	83	14140	1.4
10	80	10000	1.0
14	77	7070	0.7
20	74	5000	0.5
50	66	2000	0.2

The event-marker trigger signal is a TTL level signal. The input to drive the pen of the event-marker channel of the EEG recorder is specified as 1V per 10 mm pen deflection. Thus for a 5V TTL input trigger, a pen deflection of 50 mm would be obtained. This deflection is too large. An attenuation of 10 times was specified, the attenuated output signal thus triggering a 5 mm pen deflection for the marking of events.

ii) Design and Implementation

A block diagram of the pre-processor unit is shown in Figure 4-5. The 16 channels from the EEG recorder form the input to the pre-processor unit. Each channel passes through an anti-aliasing filter and an amplification stage, the outputs being connected to the inputs of the ADC card.

The cut-off frequency of the anti-aliasing filters is controlled by a clock input, coming from one of 3 sources: either an onboard timer, the clock output from the ADC card or an external clock source. The event-marker trigger signal from digital I/O line A1 of the ADC card passes through an attenuation stage, the output then being connected to the MARK IN connector on the side-panel of the EEG recorder. The ERD trigger signal from I/O line A0 of the ADC card passes through a buffer, and then connects to an external device which is being used for the ERD experiment (eg. a strobe light).

A switched-capacitor filter was used for the implementation of the anti-aliasing filter. This is a 6th order (36 dB/octave roll-off) Butterworth filter, the cut-off of the filter being set by an input clock signal. The National MF6-100 switched-capacitor filter was used; the ratio of cut-off frequency to input clock frequency for this device being 1:100. For the data acquisition system, a filter cut-off frequency of 30 Hz was specified, requiring a clock frequency of 3 kHz. This is provided by an onboard clock. The clock was implemented using a CMOS 4047 astable multivibrator configured to give a clock signal with a 50% duty cycle and a frequency of 3 kHz.

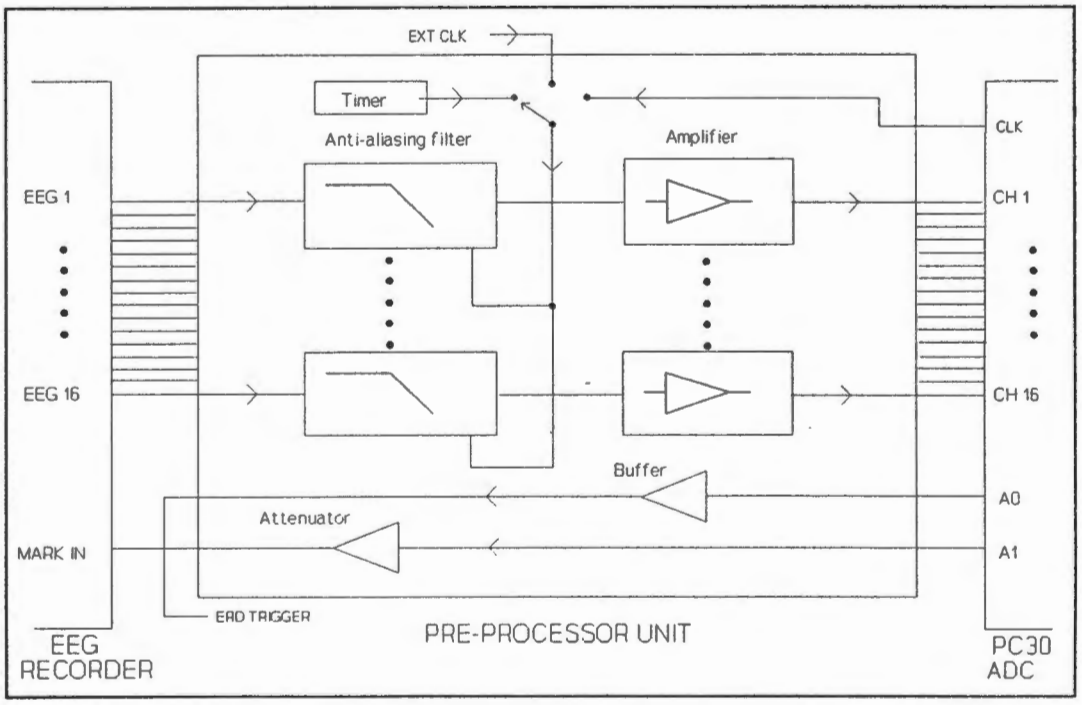

Figure 4-5 : Block diagram of pre-processor unit.

To provide flexibility for further development of the system, two other clock sources can be selected. One source is the clock output signal from the ADC card which can be programmed for a certain clock frequency, making the cut-off frequency of the filter software programmable. This would be useful if evoked potential analysis were later added to the system, necessitating the selection of a different sampling frequency depending on whether background EEG, visual evoked potential, auditory evoked potential or somatosensory evoked potential data were to be recorded. The other clock source is an external clock connected to an input on the pre-processor unit. The particular clock source to be used is selected by a hardware jumper on the circuit board.

Figure 4-6 shows the circuit diagram for the anti-aliasing filter and amplification stage for one channel.

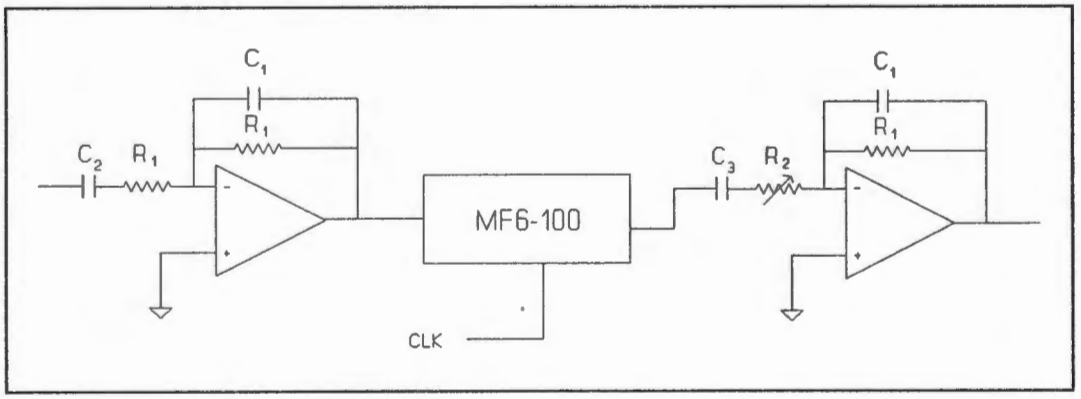

Figure 4-6 : Anti-aliasing filter and amplifier circuit

The switched-capacitor filter has two active circuits at its input and output as seen in Figure 4-6. Each of these circuits contains a lowpass filter, a highpass filter and an inverting amplifier. The switched capacitor filter operates by switching a capacitor at the input clock frequency and in effect samples the input signal at this clock rate. The lowpass filter at the input to the switched-capacitor filter prevents aliasing occurring within the switched-capacitor filter itself, by bandlimiting the input to at least half the input clock frequency. The lowpass filter at the output of the switch-capacitor filter prevents noise due to clock breakthrough. These lowpass filters are simple 1st order filters (20 dB/decade rolloff) with breakpoint frequencies ($1 / 2\pi R_1 C_1$) set at 100 Hz to give adequate attenuation at 1.5 kHz (half the clock frequency of 3 kHz), thus preventing aliasing and clock breakthrough. Simple 1st order highpass filters with breakpoint frequencies at $1/2\pi R_1 C_2$ and $1/2\pi R_2 C_3$ set at 0.5 Hz and 0.1 Hz respectively, AC couple the signal. The inverting amplifier in the active circuit at the input to the MF6 filter has unity gain ($-R_1/R_1$). The inverting amplifier of the output active

circuit is tunable as R_2 is a potentiometer and the gain is given by $-R_1/R_2$. The gain was set at 10 as specified by the requirements, by tuning $R_2 = R_1 / 10$. By using a potentiometer for R_2, the gain is adjustable and can be changed if necessary in future development.

For the attenuation stage for the event-marker trigger signal, a simple non-inverting operational amplifier configuration was used. Again, the amount of attenuation was adjustable using a potentiometer, and the attenuation was set at 10 times as specified. A simple emitter-follower operational amplifier configuration was used for the buffering of the ERD trigger signal.

The schematic circuit diagram for the pre-processor unit showing the power supply, the onboard clock and the anti-aliasing filter and amplifier for a single channel is given in Appendix E.

b) Analogue-to-Digital Conversion Card

i) Requirements

The sampling theorem dictates that the rate at which a signal is sampled must be at least twice the highest significant frequency component in the signal to prevent aliasing errors (Explained in Appendix A). The background EEG has frequency components of interest up to 30 Hz, thus requiring a sampling rate of at least 60 Hz per channel. A frequency of 100 Hz per channel was specified.

However, future development of the system might include the addition of evoked potentials analysis. Evoked potential responses have much higher frequency components than that of the background EEG, the brainstem auditory evoked potential (BAEP) being the highest having frequency components up to 3 kHz. Thus a sampling rate of at least 6 kHz would be required for the digitization of the BAEP. To provide flexibility in the system for future developments, it was desirable that the sampling frequency be variable from 100 Hz up to 6 kHz.

Only gross characteristics of the EEG signal (eg. the power) are measured for spectral and ERD analysis. An ADC resolution of 10 bits is thus adequate for digitizing of the EEG signals.

Thus an ADC card to support 16 input channels at a sampling rate of up to 6 kHz per channel, with at least a resolution of 10 bits was required. The card should also support at

least 2 digital I/O lines.

ii) PC-30D Analogue and Digital I/O Board

The PC-30D card (Eagle Electric, Cape town) is a high accuracy analogue and digital I/O board for the IBM PC/AT and PS/2 and compatible series of computers. The board plugs into any of the fully bussed expansion slots of the host computer. The board has three main subsystems: the A/D subsystem which provides analogue to digital conversion on 16 single ended analogue inputs with 12 bit resolution and a throughput of 200 kHz (12.5 kHz per channel), a D/A subsystems which provides digital to analogue conversion allowing 4 lines of analogue outputs, and a digital I/O subsystem which provides 24 TTL digital I/O lines. A detailed description of the PC-30 board is given in Appendix F.

The 16 outputs from the pre-processor unit are connected to the 16 inputs of the PC-30 card. The board is configured for bipolar $\pm$ 5V inputs, giving offset binary digital output values ranging from 0 (-5V input) to 4096 (+5V input) . The ADC is operated in continuous conversion mode, the rate of conversion (i.e the rate of A/D strobes) being set by programming the PC-30's internal timer. The board is operated in block trigger mode allowing the 16 input channels to be sampled close to simultaneously. The converted results are transferred to the host computer's memory under Direct Memory Access (DMA) control.

The card is configured to use DMA channels 6 and 7, and to use hardware interrupt IRQ5. The generation of interrupts is configured such that an interrupt is generated on each pulse from the uncommitted timer. The input clock to this timer is configured as the output from the clock prescaler and clock divider (See Figure 3, Appendix F).

The digital I/O system is operated in Mode 0 (simple I/O mode) with port A being configured as an output port. Only two of the 8 digital lines of port A are used; line A0 is used to send an ERD trigger signal and line A1 is used to send an event-marker trigger signal.

4.3.4 Software

a) Patient Information Acquisition

Information including patient name, patient folder number, patient birth date, patient sex, patient race, test date, test number and comments is entered by the user for each EEG recording. This information is stored in a data record and written to a data file together with

the recorded EEG data. Entering of this information involves user interaction with the system through a *dialog box*, and will be covered by the user interface section found later in this chapter.

b) Data Acquisition Control

The data acquisition control software comprises routines for controlling the ADC card. These include routines for initialising the A/D subsystem, setting the onboard timer, performing dual DMA sampling etc. Many of these routines are provided in the PC30 Driver Software Package which accompanies the PC30 board, and these routines were used where possible.

The sampling type (continuous or event-related), sampling parameters (either recording interval or pre-event interval, post-event interval and number of trials) and EEG recorder sensitivity setting for acquisition are entered by the user through a *dialog box*. Continuous acquisition mode for spectral analysis and event-related acquisition mode for ERD analysis will be discussed separately.

i) Continuous Acquisition Mode

The flow chart for the continuous acquisition routine is shown in Figure 4-7. The PC30D card is firstly initialized for continuous sampling. This initialization involves loading the base address of the PC30 card, setting up the mode of the 8255 ports for simple mode 0 I/O with port A being configured as an output port, and initializing the DMA system.

Next the sampling frequency is set up by programming the prescaler and clock divider registers. The input to the prescaler and clock divider is the 2 MHz master clock oscillator (see Figure 4, Appendix F). This input clock is divided down by the values programmed into the registers, so that the output from the clock divider is the required sampling frequency of 100 Hz (this output clock is the A/D strobe signal). The channel list is then loaded with the sequence of channels in the order in which they are to be sampled (this sequence follows the sequential numbering of the channels, i.e channel 1, channel 2, channel 3 ..., channel 16).

The total number of samples to be acquired is calculated from the recording time interval, the sampling frequency and the number of channels. As an example, for a recording interval of 120 seconds, the total number of samples to be acquired is 120 * 100 (sampling frequency) * 16 (number of channels) = 192 000 samples. An event-marker trigger signal is then sent

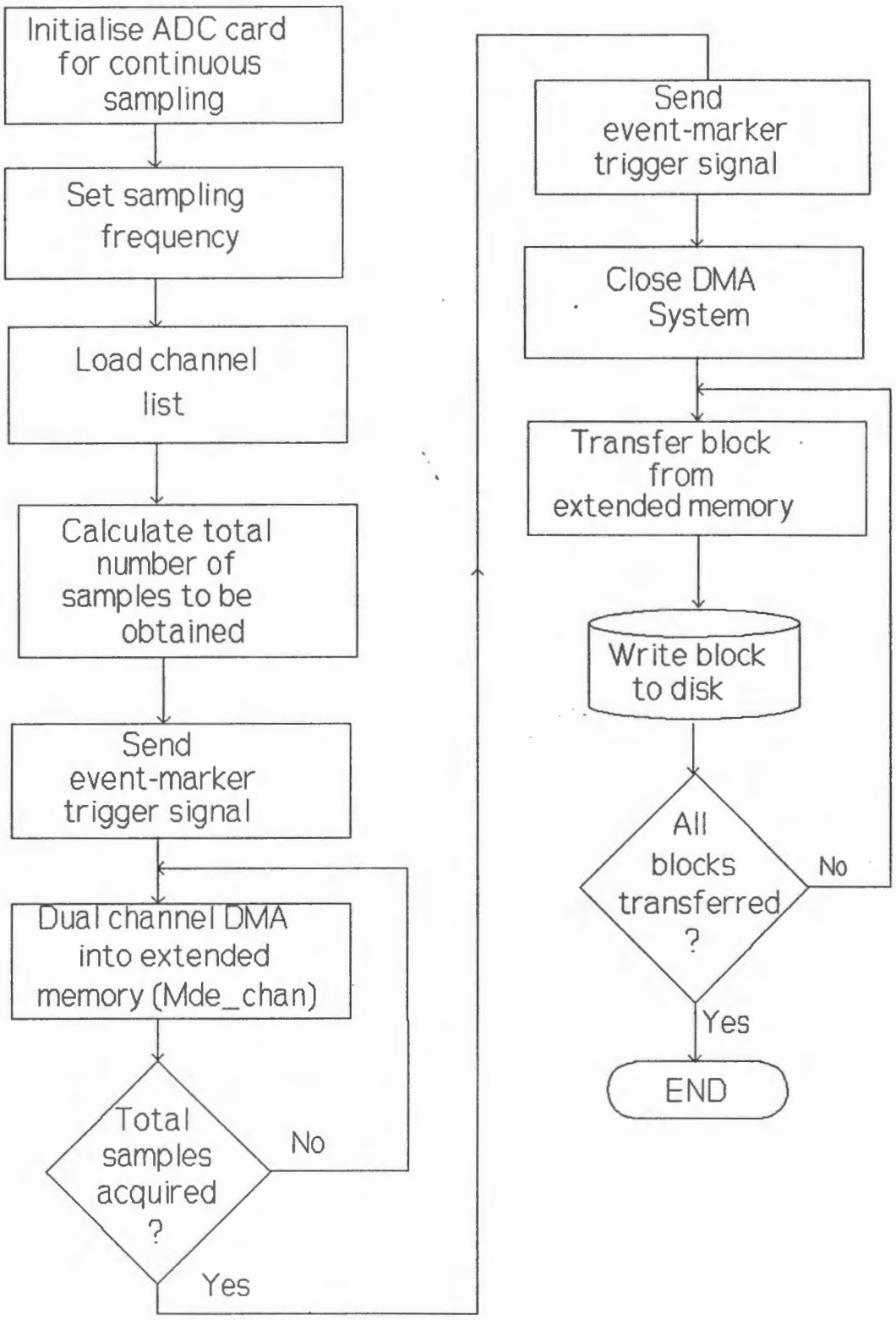

Figure 4-7 : Flow chart for continuous data acquisition routine.

to mark the beginning of data capture on the EEG paper recording. This signal is sent on line A1 of the digital I/O lines and consists of two TTL pulses. Each pulse is generated by setting bit A1 of port A, then resetting after a delay of 5 msec (the initial state of bit A1 is a reset). The EEG technologist is then able to correlate the recording made by the computer with the paper recording.

The function *Mde_chan* provided with the software driver package is used to perform dual channel DMA into extended memory. This function takes as input arguments the channel list (which has been pre-loaded with the sequence of sixteen channels to sample), the total number of samples to be captured (which has been calculated), the two DMA levels to be used for the dual DMA (levels 6 and 7), and the burst length to be used for block trigger mode (16). The function acquires data at the programmed sampling rate and transfers the data under dual DMA into extended memory until the total number of samples have been acquired. The function is explained below.

For each A/D strobe from the internal clock, occurring at intervals of 1/100 sec = 10 msec (i.e a programmed sampling rate of 100 Hz), sixteen A/D conversion pulses are generated (block trigger mode with a burst length of 16 - see Figure 3, Appendix F). Each of these A/D conversion pulses, causes an A/D conversion on the current channel in the channel list, and the result is placed into the FIFO buffer. The next channel in the channel list is then made the current channel under hardware control, and this channel is then converted and the result stored in the FIFO buffer on the next A/D conversion pulse. This process continues for all 16 A/D conversion pulses. Since the sixteen channels are sampled at maximum throughput, the sampling of the sixteen channels is close to simultaneous (5 μsecs between channels). When the end of the channel list is reached, the ADC loops back to the first channel in the channel list and the cycle is repeated when the next A/D strobe occurs. The data written to the FIFO buffer is continuously transferred under dual DMA control to extended memory as described in Appendix F.

Once the total number of samples have been acquired, another event-marker trigger signal is sent as described above to indicate the end of sampling on the paper EEG recording. The DMA system is then shut down by disabling the PC's DMA controller and the PC30's DMA subsystem.

Finally, the data which is now stored in extended memory is transferred to normal 640K memory in blocks of 512 bytes using the driver software function *Xfer_dma_res*, and these blocks of data are then written to a data file in a specific format which will be discussed later

in this section.

ii) Event-related Acquisition Mode

For the event-related acquisition mode, sampling of data is synchronised with an event, with data being acquired prior to, during and after the event. The event is then repeated a number of times resulting in an ensemble of epochs. The flow chart for the event-related acquisition routine is shown in Figure 4-8.

For the acquisition of each epoch of data, a timing mechanism for synchronizing the sending of the ERD trigger signal used to trigger the event, is needed. The ERD trigger signal must be sent after data has been acquired for the pre-event time interval. This timing mechanism is provided by the uncommitted timer and interrupt system. The PC30 card is configured to generate an interrupt on every pulse from the timer, signalling the instant that the ERD trigger signal should be sent.

Initialization for event-related acquisition mode involves initializing the PC30 card and setting up the interrupt system. The initialization is the same as that for continuous acquisition. A description of interrupts and their operation is given in Appendix G. The PC30 is configured to use hardware interrupt IRQ5. Thus initialization of the interrupt system involves saving the address of the old interrupt service routine for IRQ5 and loading the address of the ERD interrupt service routine into the interrupt vector table.

The same procedures are used for setting up of the sampling frequency and the channel list for the event-related acquisition mode, as was the case for continuous acquisition mode. The frequency of the interrupt timer (uncommitted timer) also needs to be programmed. This frequency needs to be set so that there is a delay corresponding to the pre-event time interval between when the timer is started and the first clock pulse. For example, if the pre-event time interval is 4 seconds, a timer frequency of 0.25 Hz is required, ensuring that the first clock pulse occurs 4 seconds after the timer is started. The timer frequency is set by programming the timer register.

The total number of samples to be acquired for each epoch is calculated from the pre and post-event time intervals, the sampling frequency and the number of channels. Data acquisition in the event-related mode also uses dual channel DMA, except that the data is transferred to a buffer set up in memory, rather than to extended memory as was the case for the continuous mode. The buffer is implemented as an array, its size dependent on the total

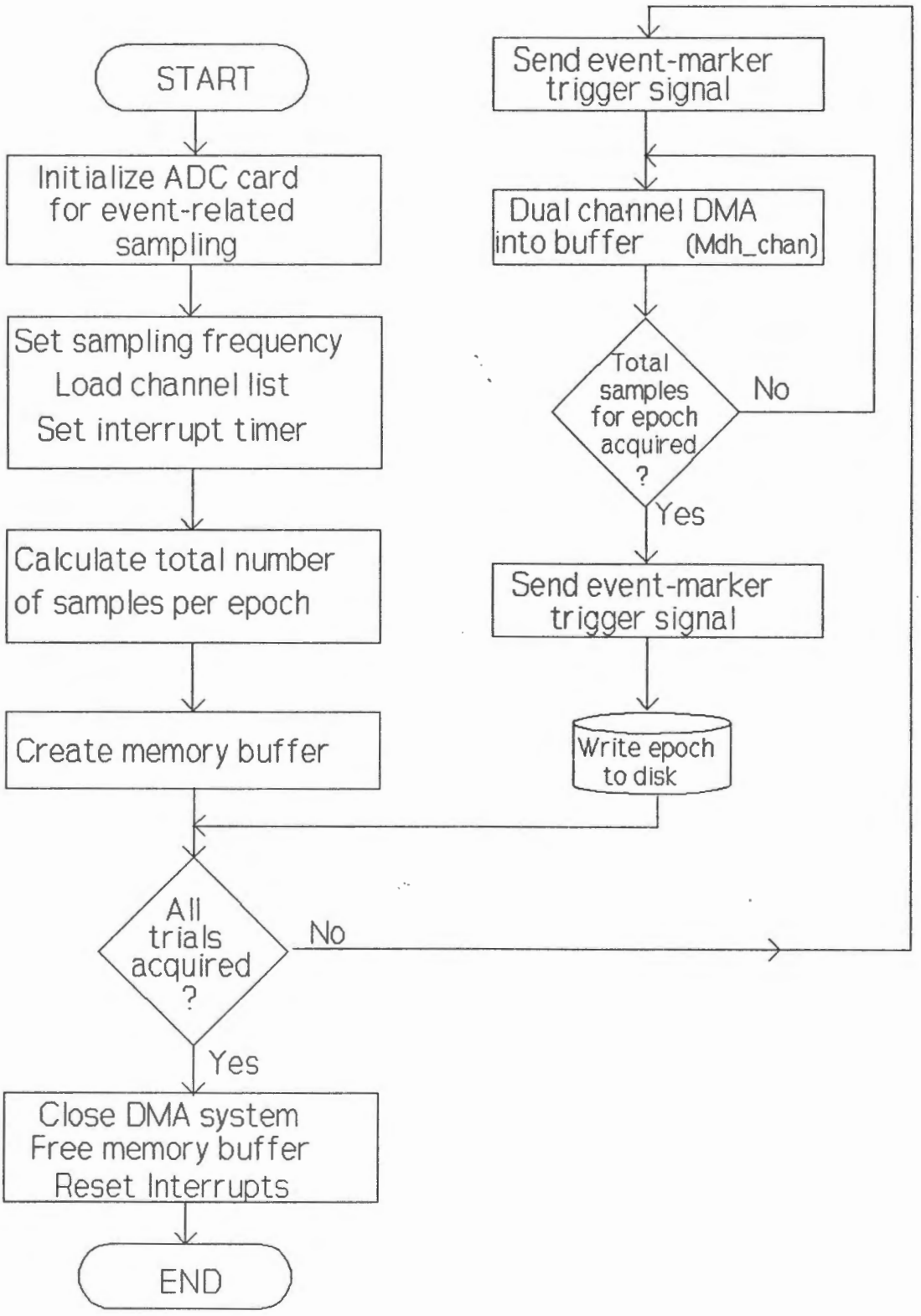

Figure 4-8 : Flow chart for event-related acquisition routine.

number of samples per epoch. The buffer is created by allocating sufficient space in memory for this array.

The commencement of sampling of each epoch is marked on the EEG paper recording by sending an event-marker trigger signal on digital I/O line A1 in the same way as was done for the start of continuous sampling.

The function *Mdh_chan* provided with the software driver package is used to perform dual channel DMA into an array. The channel has the same input arguments as the *Mde_chan* function used for continuous sampling, with the addition of the starting address of the array in memory to which the data is to be transferred. The function acquires data at the programmed sampling rate and transfers the data under dual DMA into the array until the total number of samples for the epoch have been acquired. One change was made to the *Mdh_chan* function. Normally when using the function, interrupts are not enabled (i.e they are masked) as they are not required for DMA transfer. However, for the event-related acquisition mode, interrupts are used for controlling the timing of the ERD trigger signal and thus are enabled in the modified *Mdh_chan* function. When the sampling is started by the *Mdh_chan* function, the interrupt timer is also started. The function continues operating, sampling the sixteen input channels and transferring the data to the array in memory at the programmed sampling frequency, until an interrupt occurs. This causes the execution of the *Mdh_chan* function to be temporarily halted, and the program is vectored to the address of the ERD interrupt handler.

The ERD interrupt handler is responsible for the generation of the ERD trigger signal. This signal is sent on line A0 of the digital I/O lines and consists of a single, TTL pulse generated by the setting and resetting of bit A0 of port A. At the same time that the ERD trigger signal is sent, a single, TTL pulse is also sent on line A1. This event-marker trigger signal causes a mark to be made on the event-marker channel of the EEG paper recording, thus indicating the instant at which the event occurred. Finally, the interrupt handler disables any further interrupts by masking the interrupt on the PC30 card. This is to allow the sampling of the post-epoch time period to proceed without being further interrupted by a pulse from the interrupt timer.

On completion of execution of the interrupt handler, the program continues executing at the location in the *Mdh_chan* function at which it was when the interrupt occurred. It continues to sample the sixteen input channels, transferring the data to the memory buffer until the total

number of samples for the epoch have been acquired. Execution time of the interrupt handler is negligible, and as data can be stored in the FIFO buffer, no data is lost during the time when the interrupt handler is executing.

Once the total number of samples for the epoch have been acquired, another event-marker trigger signal is sent to indicate the end of sampling on the paper EEG recording. Thus each epoch recorded by the computer is marked on the EEG paper recording. A double mark indicates the start of sampling, a single mark indicating the instant at which the event occurred, and another double mark the end of sampling for the epoch. The technologist is thus able to correlate the recordings made by the computer with the epochs marked on the paper recording.

The data stored in the memory buffer is then added to the data file which contains the data from all the trials performed (i.e. the whole ensemble of data). The format in which this data is stored will be discussed later in this section. The time interval between trials is dependent on the time taken to write the data from the memory buffer to the disk data file, as this is the time between the end of sampling of one epoch and the beginning of sampling of the next epoch. This is dependant on the number of samples but typically 10 seconds.

On completion of acquisition of data for all trials, the DMA system is closed, the interrupt system is reset by loading the address of the old interrupt handler back into the interrupt table, and the space in memory reserved for the data buffer is freed.

c) Artifact Detection

An artifact detection scheme based on voltage trigger testing is implemented. With this detection scheme, all 'high voltage' transients are considered as artifact. Since A/D conversion is being used, voltage trigger testing can be implemented by checking for overflow of the ADC.

The PC30 board is configured for bipolar $\pm$ 5V inputs. If an ADC overflow occurs, ie. if the input voltage is greater than or equal to + 5V, or less than or equal to - 5V, then the output from the ADC will be 4095 or 0 respectively. Thus by checking the output from the convertor, one is able to determine whether an ADC overflow occurred.

Before each block of data is written to the data file, it is checked for overflow errors. This involves checking each group of sample values obtained from the sixteen input channels at

each sampling instant. If any of these values from the sixteen channels are 0 or 4095, then an artifact flag is set and this is stored in the data file together with these sixteen values. The specific file format will be given in the following section.

d) Data File Format

The data file must contain all the information and data required by the data processing and display system. This includes patient information, test information, sampling information, artifact information and the recorded data. The data file is stored as an ASCII file, the format of the file being shown in Figure 4-9.

```
BODDINGTON
RICHARD
MALE
WHITE
08-10-1962
02-04-1992
1
E/C AT REST
1
0
0
0
180
1
0
0
0
2161 2401 2377 1835 2158 2200 2289 2215 2166 2179 2090 2148 2210 2260 2085 2188 0
2142 2443 2309 1700 2266 2265 2311 2244 2077 2159 2184 2148 2196 2230 2139 2201 0
2278 2544 2370 1625 2353 2447 2414 2248 2041 2261 2373 2265 2222 2096 2222 2204 0
2405 2509 2447 1655 2336 2583 2500 2264 2013 2434 2535 2392 2295 1914 2233 2265 0
2414 2562 2429 1716 2443 2586 2503 2275 1966 2464 2534 2412 2308 1786 2125 2297 0
2363 2513 2340 1668 1863 2508 2443 2244 1947 2304 2352 2285 2189 1785 1972 2178 0
2258 2372 2148 1517 1725 2340 2279 2150 1936 2109 2078 2084 2038 1853 1904 1994 0
2095 2123 1875 1439 1692 2100 2014 2004 1906 1967 1836 1919 1915 1888 1914 1891 0
2084 2038 1780 1515 1654 2031 1889 1925 1912 1889 1801 1905 1875 1859 1933 1932 0
2228 2185 1926 1590 1695 2181 2002 1939 1952 1892 1928 1997 1914 1826 1943 2043 0
```

Figure 4-9 : Section of data file showing the data file format.

The first 8 lines of the file contain patient and test information. This includes the patient's surname, name, folder number, race, sex and birth date and the test date, number and comments.

The next 6 lines contain sampling information. This includes the sampling type (continuous (1) or event-related (0)), the sampling parameters (pre-event time interval, post-event-time interval, number of trials and recording interval) and the EEG recorder sensitivity setting (sensitivity setting of 5 μV (0), 7 μV/mm (1), 10 μV/mm (2), 14 μV/mm (3), 20 μV/mm (4), 50 μV/mm (5)).

The next 3 lines contain artifact information. This includes the type of artifact detection. Presently, voltage trigger testing is the only detection scheme implemented, but future developments of the system may include other artifact detection schemes.

The remainder of the file contains the recorded data. The data is stored in a matrix 17 columns wide with length being dependent on the total number of samples per channel. Each row corresponds to one multichannel sample: 16 EEG channels and an artifact flag. This flag is set if an overflow error occurred during the sampling of any of the 16 channels at that specific sampling instant.

The data files generated using typical sampling parameters are very large. For continuous recording with a typical recording interval of 3 minutes, the size of the data file is approximately 1.5 Mbytes. For event-related sampling with a pre-event interval of 4 seconds, a post-event interval of 2 seconds and 60 trials, the size of the data file is approximately 3 Mbytes.

4.4 Data Processing and Display

4.4.1 Data File Accessing

To access the data recorded during a specific experiment for a specific patient, the user enters the patient's surname and first name, and the test number of the recording. The filename is generated from this information and the required data file can then be accessed.

The additional patient information (folder number, birth date, sex, race), the additional test information (test date, comments), the sampling information and the artifact information are accessed from the file and stored as global data records in memory. Since these are stored as global variables, they are available to all the routines of the data processing and display software.

Since the size of the data matrix is far larger than the memory available for storing and processing the data, the data is accessed in blocks. Each block is then processed (either spectral analysis or ERD analysis depending on the mode of data acquisition), and the results stored. The next block is then accessed, processed and the results stored. This is repeated until all blocks have been processed. The results can then be combined to give the final result.

For spectral analysis processing, the data is divided up into 5 second epochs, with spectra being calculated for each epoch. Each epoch contains 500 samples (5 seconds at 100 Hz sampling rate). The length of the data block accessed from the file is thus a (500 x 17) matrix. The block is stored in memory as two separate arrays. A data array of dimension

(500 x 16) contains the samples from the 16 EEG channels. This is an integer array, as the recorded values are in the digital form output from the ADC. The second array of dimension (500 x 1), contains the artifact flags for each sample point in the epoch. The number of data blocks to be accessed from the data file can be calculated by dividing the recording interval (in seconds) by the epoch length (5 seconds). As an example, a typical recording interval of 2 minutes requires the accessing of 24 blocks.

For ERD analysis, the length of the epochs to be processed depends on the pre-event and post-event time interval parameters. Thus the epoch size is not fixed and varies depending on the ERD experiment being performed. The number of data points in the epoch is given by: (pre-event time interval + post-event-time interval) * 100. As an example, with a pre-event interval of 4 seconds, a post-event interval of 2 seconds, an epoch of 600 data points would be used. The dimension of the data block accessed from the data file, for this example, would be (600 x 17). Again, this block is stored in memory as two separate arrays: a data array and an artifact array. The number of blocks to be accessed from the data file depends on the number of trials recorded for the ERD experiment.

4.4.2 Artifact Handling

Handling of artifacts which occur during recording of the EEG data includes detection of the artifacts and elimination of the section(s) of the data containing the artifacts. Both automated and manual detection is performed. Automated detection is executed during data acquisition and involves voltage trigger testing as described in Section 4.3.4.

If an epoch contains artifact, that epoch of data is eliminated from the data to be processed. In this way only a small amount of data (i.e the epoch in which the artifact occurred) needs to be discarded with minimal loss of accompanying "real" (artifact-free) data. For topographical mapping, where multichannel recordings are used, the presence of artifact in an epoch of data on just one channel, necessitates the discarding of data from the other channels. Thus, a complete block of data (containing 16 channels of data) is discarded if artifacts are found anywhere in the block.

The decision of whether a block of data contains artifacts and should therefore be eliminated, depends on the percentage of overflow errors occurring in that block. An artifact checking routine calculates the percentage of overflow errors occurring in a block. The artifact array for the block is passed to this routine, and the number of set artifact flags extracted. The percentage of set artifact flags to the length of the block is then compared to a threshold, and

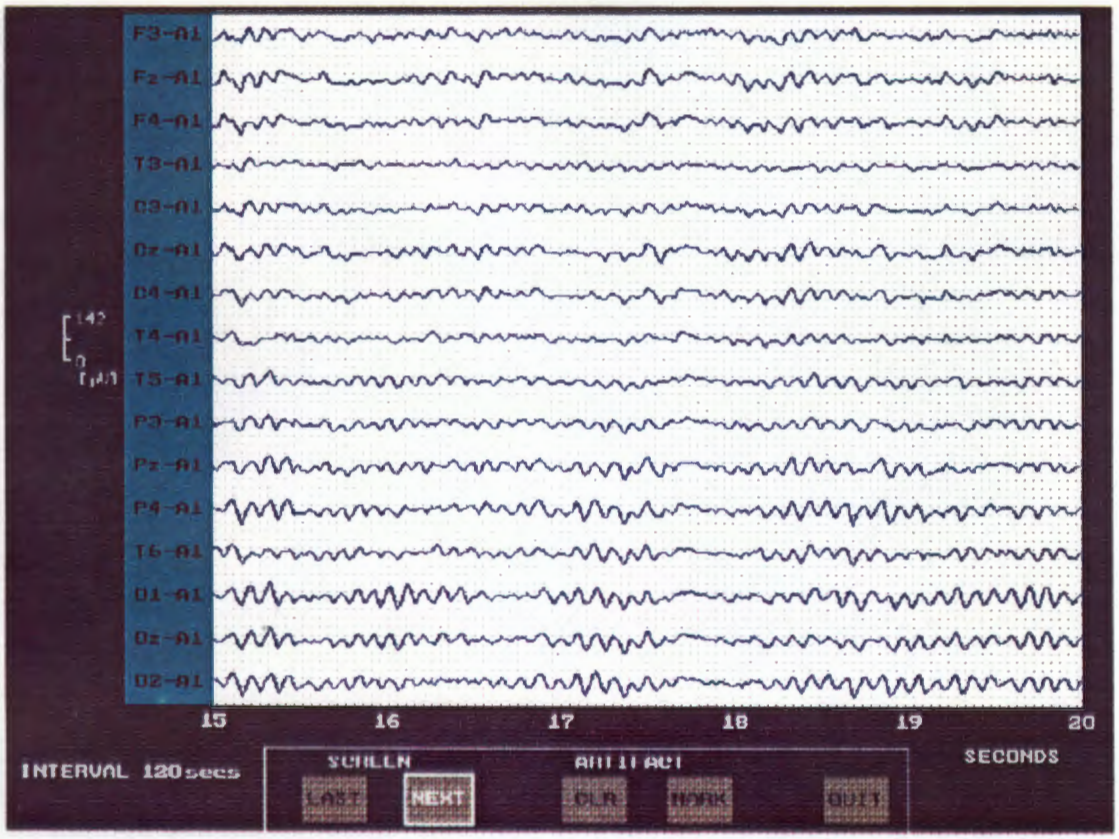

Figure 4-10 : Multichannel screen display for scanning of blocks for artifacts. The blue EEG tracing indicate that the block is artifact-free.

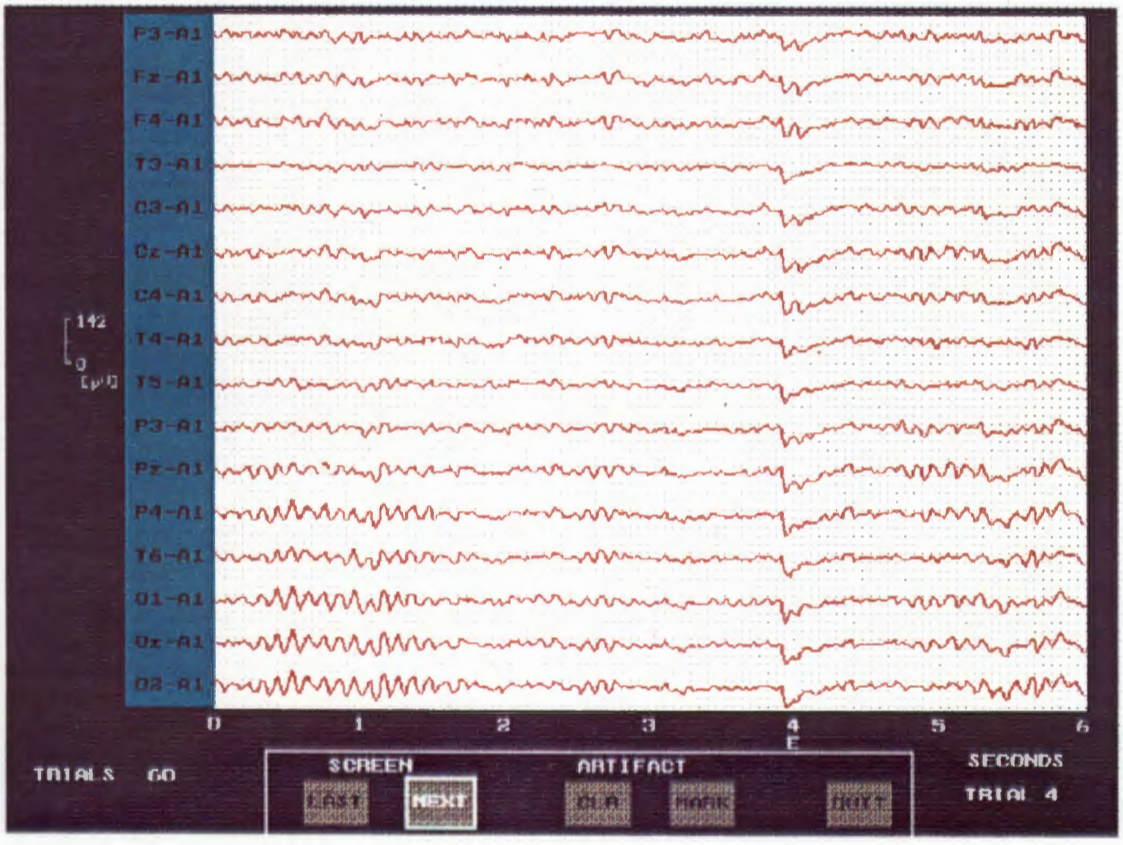

Figure 4-11 : Multichannel screen display for scanning of blocks for artifacts, the red EEG tracing indicate that the block contains artifact.

if this threshold is exceeded, the block is marked as containing artifact. The artifact array for each block to be processed is first passed to the artifact checking routine. If the result returned from this routine indicates that the block is free of artifacts, the data array of the block is used for processing. If not, the data array is discarded.

The data can also be manually scanned for artifacts. This then allows the marking of blocks which the user decides contain artifacts, but which are marked as being artifact-free. Also, the user can confirm blocks which have been marked as containing artifact, clearing any blocks considered to have been incorrectly classified. A multichannel display of the 16 EEG channels is provided for the scanning of the raw (unprocessed) EEG data. This display shows a block of data on the screen at a time. If the block of data is found to be artifact-free by the artifact checking routine, the colour of the EEG tracings is made blue, as shown in Figure 4-10. However, if the block of data is marked as containing artifacts by the artifact checking routine, then the colour of the EEG tracings are red (Figure 4-11). The user is able to page forwards or backward through the EEG data one block at a time.

The user can mark a block which is indicated as artifact-free, but which the user considers to contain artifact. All the artifact flags for this block in the data file are then set, and the EEG tracings are re-plotted in red giving the user visual feedback that the block has been marked. When this block is re-accessed and re-tested by the artifact checking routine, the percentage of artifacts will exceed the threshold and the data array of the block will be rejected from being used for processing. Similarly, if a block marked as containing artifacts is cleared by the user, the EEG tracings are re-plotted in blue and the artifact flags in the data file are reset. When this block is re-accessed and re-tested by the artifact checking routine, the percentage of artifacts will be below the threshold and the data array of the block will be used for processing.

4.4.3 Reference Transformation

The EEG data is recorded using a monopolar montage with the left ear (A1) as the reference site. This is a reference-dependent derivation. The data can be transformed to a reference-independent derivation. The transverse bipolar, longitudinal bipolar, common average and local average derivations are supported.

The topographical map is composed of pixel points that are enclosed by a circle inscribed in an 81 x 81 pixel grid. The electrode sites for the monopolar montage, as projected onto the 2-dimensional map of the head, are shown in Figure 4-12.

Electrode Number	Electrode	X Co-ord	Y Co-ord
1	F3	20	20
2	Fz	40	22
3	F4	60	20
4	T3	2	40
5	C3	20	40
6	Cz	40	40
7	C4	60	40
8	T4	78	40
9	T5	9	62
10	P3	22	58
11	Pz	40	60
12	P4	58	58
13	T6	71	62
14	O1	25	75
15	Oz	40	78
16	O2	55	75

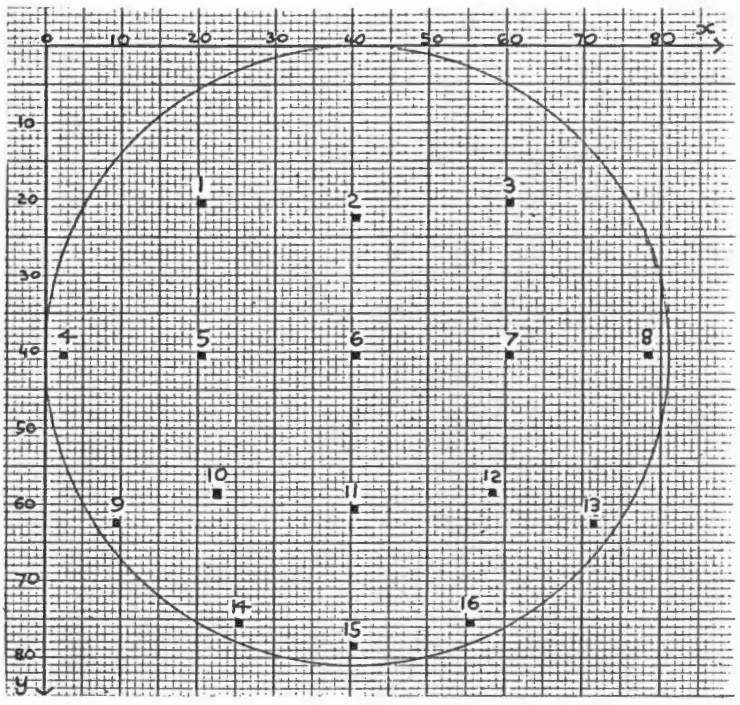

Figure 4-12 : Electrode sites for monopolar montage.

The electrode positions are given by the (x,y) co-ordinates on the grid, with the x-axis running horizontally and the y axis running vertically. For the common average and local average derivation transformations, the electrode locations remain the same as for the recording montage. However, for the transverse and longitudinal derivation, where the difference between the potentials at two adjacent electrodes is calculated, a new electrode position midway between the two electrode sites is used. Thus the locations of the electrode sites for the transverse and longitudinal bipolar derivations, differ from those in the recording montage (see Sections 4.4.3b and 4.4.3c).

Figure 4-13 shows a block diagram of the reference transformation routine. The routine takes as input the data array (N x 16) for a block of data, calculates the appropriate reference transformation, and outputs an array of transformed data.

The dimension of the output array depends on the derivation. In addition, the routine also converts the data from the ADC digital integer values of the input array, to the equivalent scalp potentials (in microvolts). The different derivations are discussed below.

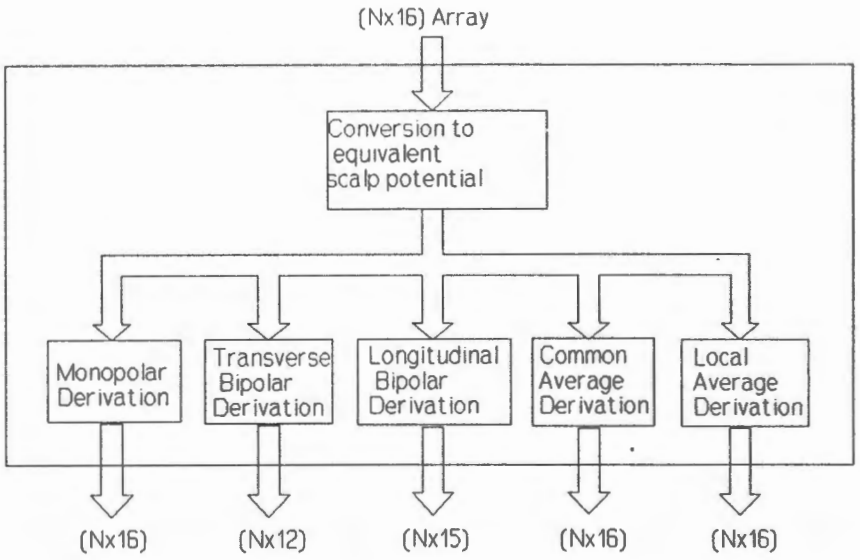

Figure 4-13 : Block diagram of reference transformation routine.

a) Monopolar

For monopolar derivation, the data is to be left in the reference-dependent form in which it was recorded. Thus, the only processing needed is the conversion of the integer values into equivalent scalp potentials.

The ADC digital output is in offset binary format, ranging from 0 to 4095 for an input voltage range of -5V to +5V. The analogue voltage at the ADC input for a given output digital value is given by:

$$Voltage = \frac{(Digital\,value - 2048) * 5}{2048} \qquad (4\text{-}1)$$

The potential recorded at the scalp is amplified by the EEG recorder and the pre-amplifier unit. By working backwards, the scalp potential can be calculated from the input voltage at the ADC, provided that the EEG recorder and pre-processor gains are known. The pre-processor gain is fixed at 10 times. The recorder gain depends on the recorder sensitivity setting (Table 4-2), this being provided as part of the sampling information. The recorder gain can be found from a data lookup table of recorder gains for different sensitivity settings which is programmed into the software.

The output from the routine for the monopolar case is thus an array of data (N x 16) in the original reference-dependent form with data values converted to equivalent scalp potentials (in microvolts).

b) Transverse Bipolar

For bipolar derivations, the potential difference between two electrodes is measured. Bipolar derivations can be obtained from monopolar reference recordings by subtracting the referentially-recorded potential at one of the electrodes in the pair, from the referentially-recorded potential at the other electrode, provided the two electrodes are recorded relative to a common reference. In the data acquisition system, a left ear reference site is used, with all electrodes potentials measured relative to this reference. Therefore, bipolar derivations can be calculated for any pair of electrodes in the montage.

Electrode Number	Electrode Pair	X Co-ord	Y Co-ord
1	Fz-F3	30	21
2	Fz-F4	50	21
3	C3-T3	11	40
4	Cz-C3	30	40
5	Cz-C4	50	40
6	C4-T4	69	40
7	P3-T5	16	60
8	Pz-P3	31	59
9	Pz-P4	49	59
10	P4-T6	64	60
11	Oz-O1	33	77
12	Oz-O2	47	77

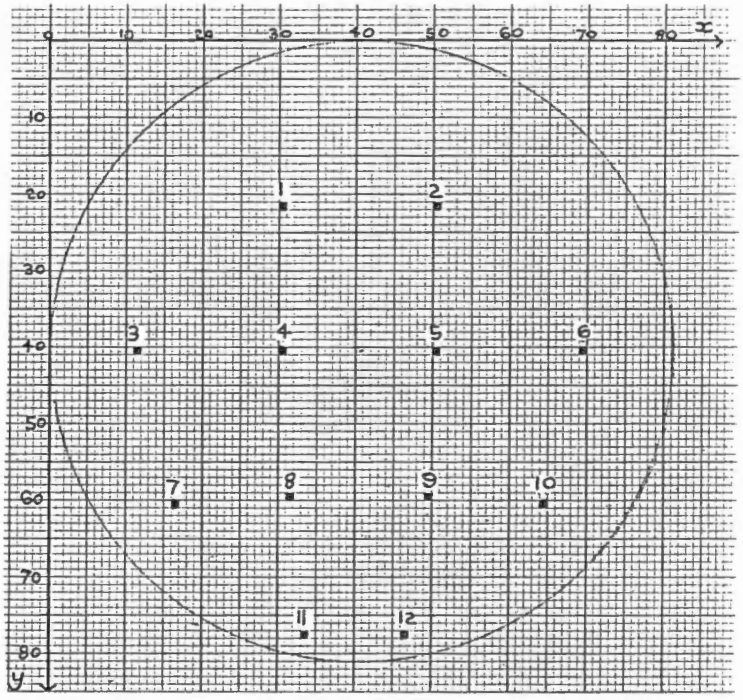

Figure 4-14 : Electrode sites for transverse bipolar derivations.

For transverse bipolar derivations, the pair of electrodes to be used in the bipolar calculation must lie roughly on an axis which is parallel to the line running from ear to ear. Twelve transverse bipolar derivations are calculated from the 16 electrodes in the monopolar recording montage; these derivations are listed in the table in Figure 4-14. New electrode sites midway between the two electrodes used in each bipolar derivation replace these electrode sites. The bipolar derivation electrode sites thus formed are shown in Figure 4-14, with the grid co-ordinates of the electrodes given in the table.

For each row (sample point) of the input data array (N x 16), each of the bipolar differences listed in the table in Figure 4-14 is calculated. The results from the bipolar calculations are

placed in the corresponding row of the output array. This is then repeated for each row in the input array until all the data has been transformed. Since only 12 bipolar derivations are calculated from the original 16 EEG channels, the output array is an (N x 12) dimensional array.

c) Longitudinal Bipolar

Longitudinal bipolar calculations are the same as the transverse bipolar calculations, except the pairs of electrodes used in the bipolar calculation must lie roughly on an axis perpendicular to the line passing from ear to ear.

Electrode Number	Electrode Pair	X Co-ord	Y Co-ord
1	F3-T3	11	30
2	F3-C3	20	30
3	Fz-Cz	40	31
4	F4-C4	60	30
5	F4-T4	69	30
6	T3-T5	6	51
7	C3-P3	21	49
8	Cz-Pz	40	50
9	C4-P4	59	49
10	T4-T6	74	51
11	T5-O1	17	69
12	P3-O1	24	67
13	Pz-Oz	40	69
14	P4-O2	56	67
15	T6-O2	63	69

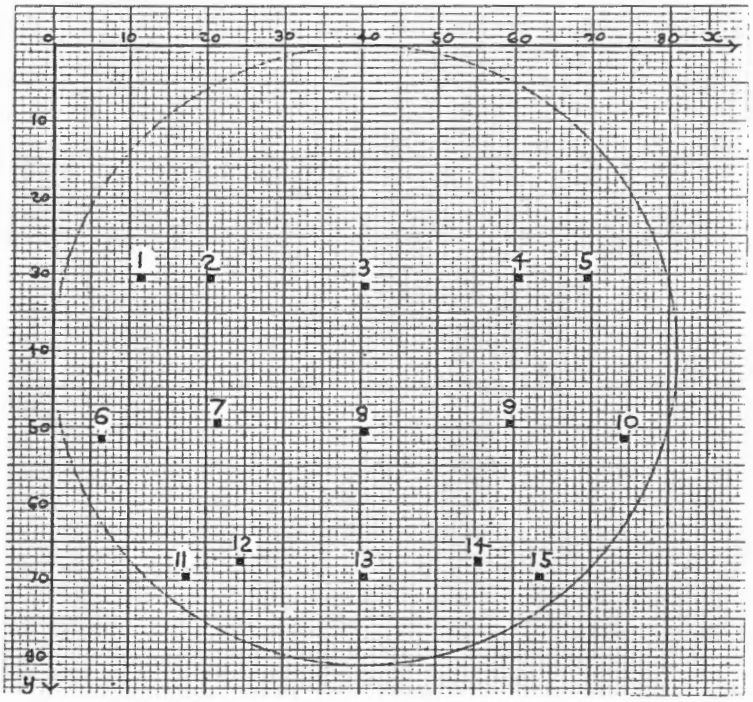

Figure 4-15 : Electrode sites for longitudinal bipolar derivations.

Fifteen longitudinal bipolar derivations are calculated from the 16 electrodes in the monopolar recording montage; these derivations are listed in the table in Figure 4-15 together with the grid co-ordinates. The new electrode sites for the longitudinal derivations are shown in this figure. The output from the reference transformation routine is an (N x 15) dimensional array.

d) Common Average

The potentials recorded from all electrodes are averaged to produce a reference potential and

each active electrode is then measured relative to this average reference. If data is recorded using a monopolar montage with a common reference site (reference-dependent recording), then the common average reference can be derived from the referentially recorded data. The reference-dependent potentials are summated and the average computed by dividing by the number of electrodes. This average is subtracted from the reference-dependent potentials at each electrode, to yield the common average derivation for each electrode. It can be shown that the reference recording is truly reference-independent. If we assume the following:

R	:	potential at reference (unknown)
U_i	:	potential at i th electrode
C-R, U_i-R	:	reference-dependent recorded potentials
M	:	number of electrodes (16 in this case)

then the common average potential at electrode C is calculated as:

$$
\begin{aligned}
C_{com\ av} &= (C-R) - \frac{\sum_{i=1}^{M}(U_i-R)}{M} \\
&= C - R - \frac{\sum_{i=1}^{M}U_i}{M} + \frac{\sum_{i=1}^{M}R}{M} \\
&= C - R - \frac{\sum_{i=1}^{M}U_i}{M} + R \\
&= C - \frac{\sum_{i=1}^{M}U_i}{M}
\end{aligned}
\qquad (4-2)
$$

and the cancelling of the reference is clearly noted. The electrode positions for the common average derivation are the same as for the original monopolar recording montage.

For each row (sample point) in the input data array (N x 16), the 16 data values are converted to equivalent scalp potentials, the average of these 16 values is found, and then this average value is subtracted from each of the 16 values to give the common average derivation. The result of this subtraction is stored in the corresponding row in the output

array. This is then repeated for each row, until all the data in the input array has been transformed. The output array from the reference transformation routine is thus an (N x 16) dimensional array.

e) Local Average

The local average reference or source derivation is an approximation to the Laplacian operator as discussed in the literature review and shown in Appendix D. The formula for the source derivation for electrode C, is given by:

$$C_{loc\ av} = (C-R) - \sum_{i=1}^{M} (U_i-R)\, g_i \qquad (4-3)$$

where M is the number of electrodes used in the local average and g_i is the normalized distance from electrode i to electrode C.
The normalized distance is calculated as

$$g_i = \frac{d_i}{D} \qquad (4-4)$$

where d_i is the distance from electrode i to electrode C, and D is the summation of all distances d_i for the M electrodes. Again by expanding Equation 4-3 it easy to verify that the references cancel, the local average derivation thus being reference-independent.

The number of electrodes, M, used in the local average depends on whether a five-point or three-point operator is used. For a five-point operator, the four electrodes surrounding the electrode to be transformed are used in Equation 4-3. However, in the 10-20 system, the electrodes on the periphery of the recording montage are not surrounded by four electrodes. Thus, for these peripheral electrodes, three-point operators are used, and the two electrodes lying on the periphery on either side of the electrode to be transformed are used in Equation 4-3.

Table 4-3 shows the five and three point operators used by the processing software for the electrodes in the recording montage (Figure 4-12). Column 1 of the table gives the electrode (channel) number of the electrode for which the local average is to be calculated (this electrode position can be seen in Figure 4-12). The four channel numbers of the four electrodes that surround the electrode to be transformed and that are used in the five-point operator are shown in columns 2,3,4 and 5. The normalized distances from each of these surrounding electrodes to the electrode to be transformed is given in columns 6,7,8 and 9 of

the table. If columns 4,5,8 and 9 are blank, this indicates that the electrode to be transformed lies on the periphery, in which case a three-point operator is used.

Table 4-3 : Five and three-point operators for local average derivation.

Local Av	Electrodes				Norm. Distances			
	u_1	u_2	u_3	u_4	g_1	g_2	g_3	g_4
1	2	4	-	-	.43	.57	-	-
2	1	3	-	-	.50	.50	-	-
3	2	8	-	-	.43	.57	-	-
4	1	9	-	-	.54	.46	-	-
5	1	4	6	10	.26	.24	.26	.24
6	2	5	7	11	.22	.26	.26	.26
7	3	6	8	12	.26	.26	.24	.24
8	3	13	-	-	.54	.46	-	-
9	4	14	-	-	.53	.47	-	-
10	5	9	11	14	.27	.20	.27	.26
11	6	10	12	15	.28	.24	.24	.24
12	7	11	13	16	.27	.27	.20	.26
13	8	16	-	-	.53	.47	-	-
14	9	15	-	-	.57	.43	-	-
15	14	16	-	-	.50	.50	-	-
16	15	13	-	-	.43	.57	-	-

For each row (sample point) in the input data array, each of the 16 electrode potentials is transformed to a local average derivation using Equation 4-3. For the transformation of each channel (electrode), the electrodes used in the five or three point operator, together with the normalized distances, are accessed from a lookup table containing the same information as shown in Table 4-3. The reference-dependent potentials at each of the electrodes specified in the lookup table, are converted to equivalent scalp potentials and each one is then multiplied by its respective normalized distance. Each of these results is then subtracted from the recorded potential of the electrode being transformed, this also first being converted to its equivalent scalp potential. The transformed results for each channel in the row are then stored in the corresponding row in the output data array. This is then repeated for each row until all the data has been transformed. The output array from the reference transformation routine is thus an (N x 16) dimensional array.

4.4.4 Quantification

Spectral analysis and ERD analysis are the two quantitative analysis techniques implemented by the system. The implementation of each of these analysis techniques will be discussed

separately.

a) Spectral Analysis

For spectral analysis, the average power spectrum of the EEG over the recording interval, for each of the EEG channels is required. The absolute and relative power in each of the delta, theta, alpha and beta frequency bands can then be calculated.

The recording interval is divided into five second epochs. The power spectrum for each of these epochs is calculated and the spectra are then averaged over all epochs, resulting in an average spectrum. This is done for each channel of the multichannel recording. The assumption is made that a five second epoch is short enough to ensure that the signal will be stationary over the epoch. This assumption was based on findings from the literature review. The periodogram method of spectral estimation, as discussed in Appendix B, is used for the calculation of power spectra for each epoch. For each channel of the data block, the periodogram defined by Equation 4-5 is calculated.

$$P_{xx} = \frac{1}{N}|X(f)|^2 \qquad (4-5)$$

where X(f) is the Fourier transform of the EEG signal.

The flow chart for the periodogram routine is shown in Figure 4-16. This routine takes as input a (500 x 1) array corresponding to a 5 second epoch, and calculates the periodogram from this input data according to Equation 4-5. The input sequence is zero-padded (see Appendix A) by adding 12 zeros to the end of the sequence, thereby expanding the input sequence to 512 points ($=2^9$). A radix 2, in-place, decimation-in-time FFT routine using trigonometric recombination optimization is used for calculation of the Fourier transform (see Appendix A). This FFT routine takes as input a data sequence of length N, and returns the N/2 length FFT sequence. The radix 2 FFT algorithm requires that the length of the input sequence be a power of 2 and hence the need for zero-padding. The output sequence from the FFT routine is then used in the calculation of the periodogram according to Equation 4-5.

The output sequence of the FFT routine contains only N/2 (256 in our case) frequency points. For a real input sequence, the FFT values in the upper half of the spectrum are complex conjugates of the values in the lower half of the spectrum - therefore the upper half of the spectrum contains redundant information and need not be calculated. The N/2 frequency point

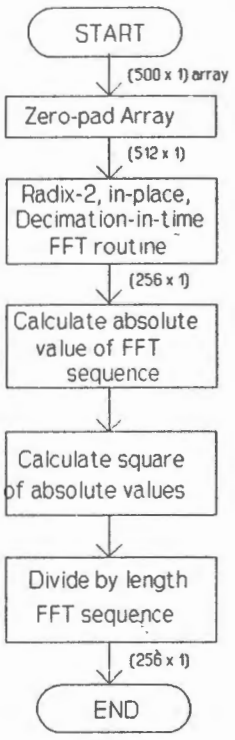

Figure 4-16 : Flow chart for periodogram routine.

(in our case the 256 th frequency point) corresponds to the Nyquist frequency of 50 Hz. Thus the frequency resolution of the periodogram will be 50/256 = 0.195 Hz. The periodogram is output as a (256 x 1) dimensional array.

The upper graph in Figure 4-17 shows a five second epoch of recorded data for EEG channel 0_2. The lower graph shows the periodogram (power spectrum).

The flow chart for the complete spectral calculation routine is shown in Figure 4-18. A block of data is accessed from the file as described in the Data File Accessing section. The block is checked for artifacts by passing the artifact flag array to the artifact checking routine. If the block contains artifacts, then the block is not used for processing and the next block of data is accessed from the file.

If the block is artifact-free, then it is processed. The (500 x 16) dimension data array is sent to the reference transformation routine. The output from this routine is a (500 x M) data array, M being dependent on the type of derivation (M = 16 for monopolar, common average and local average derivations; M = 12 for transverse bipolar; M = 15 for longitudinal bipolar). Each column of the 500 x M data array is passed as a one dimensional array (500 x 1) to the periodogram routine. This array represents one epoch of data for a single channel. The periodogram routine returns a (256 x 1) dimensional array. A (256 x M)

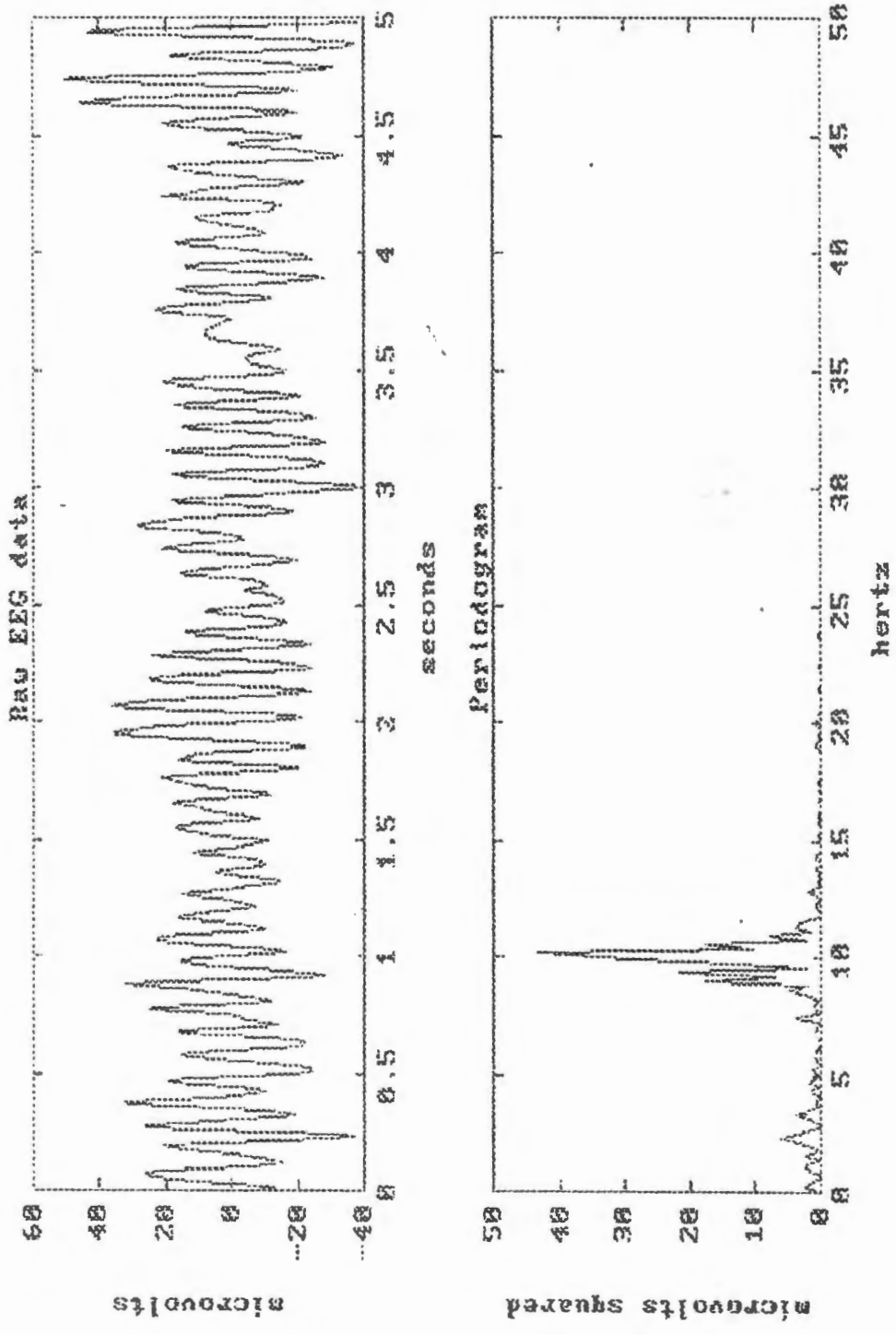

Figure 4-17 : A single 5 second epoch of raw EEG data for electrode O_2 and the resulting power spectrum calculated by the periodogram routine.

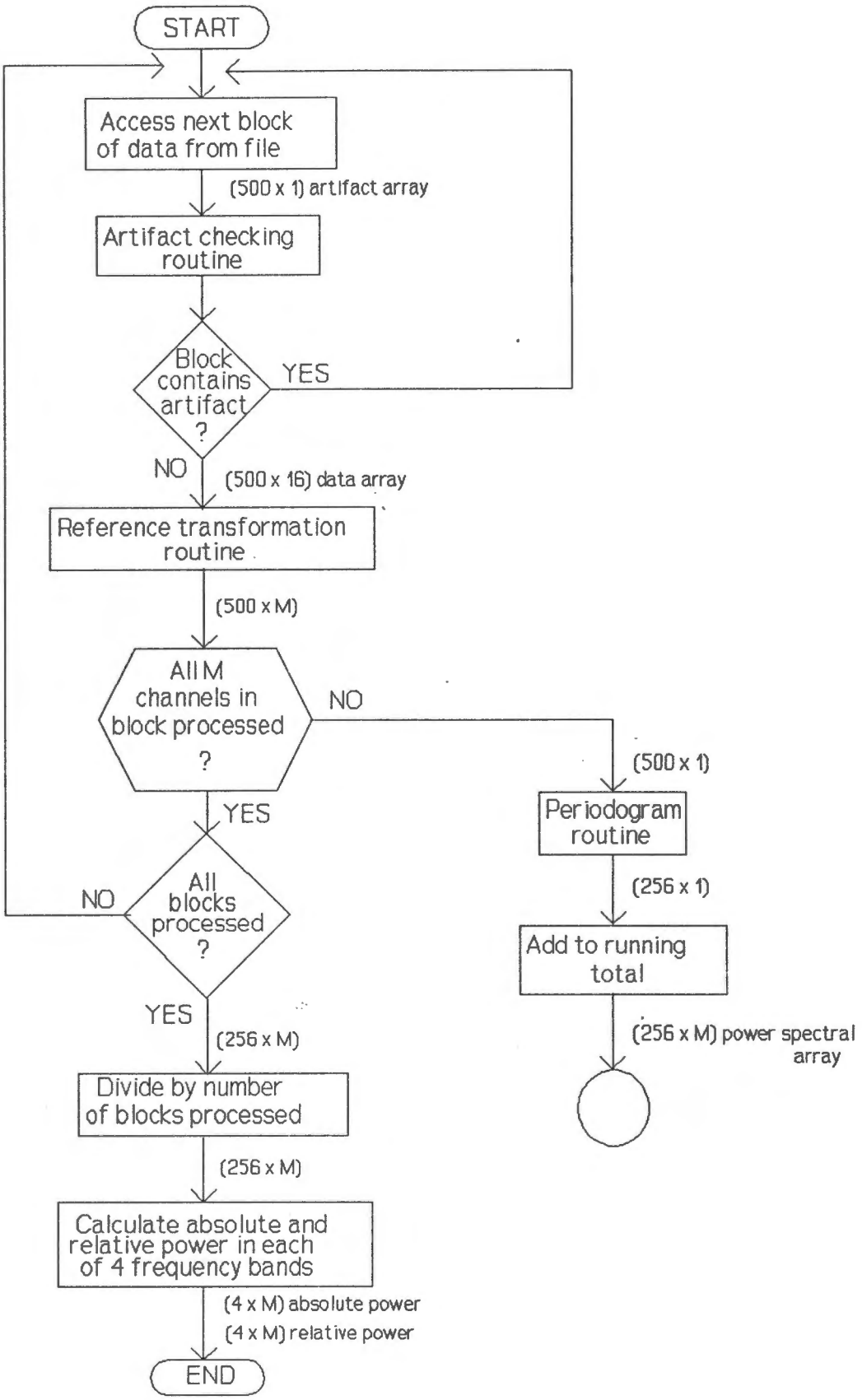

Figure 4-18 : Flow chart for complete spectral calculation routine.

dimensional power spectral array contains the running total of the summation of the periodograms calculated for each of the M channels. The array is initialized to zero at the start of the spectral calculation. The periodogram values returned from the periodogram routine as a (256 x 1) dimensional array, are added to the values of the corresponding column in the power spectral array. The next column (i.e the epoch of data for the next channel) in the data array is then passed to the periodogram routine, the returned array being added to the corresponding column of the power spectral array. This is repeated until periodograms for all M channels in the current block of data have been calculated and added to the running total. The next block of data is then accessed from the file and the block checked for artifacts. If the block is free from artifacts, then reference transformation is performed and the periodograms for each of the channels in the block are calculated and added to the running total in the power spectral array as described.

This procedure is repeated until all blocks have been processed. The final result is a (256 x M) dimensional power spectral array containing the summation of the periodograms calculated for all epochs for each channel. To calculate the average periodogram for each channel, the summated values in each column of the array are divided by the number of blocks processed. This is given by the recording interval divided by the epoch size, minus the blocks which were rejected by the artifact checking routine.

The absolute power in each of the four EEG frequency bands for each channel is then calculated. The power spectra for each channel contain 256 frequency points, from d.c. to the Nyquist frequency of 50 Hz. The absolute power for a particular frequency band is calculated by summation of the power values at each frequency point which fall into this frequency band. The frequency bands are defined in Table 4-4.

Table 4-4 : Definition of the four frequency bands.

Frequency Band	Lower frequency [Hz]	Upper frequency [Hz]
Delta	0.5	3.5
Theta	4.0	7.5
Alpha	8.0	13.0
Beta	14.0	30.0

The relative power in each frequency band is also calculated as the ratio of absolute power in each frequency band to the total power (0.5-30 Hz). "Absolute power" and "relative

power" arrays are output from the spectral calculation routine. These are (4 x M) dimensional arrays: the first row of the array contains the delta power for each of the M channels, the second row theta power, the third row alpha power and the last row beta power.

b) ERD Analysis

It was decided to use quantification in the time domain for the ERD calculation as this allows calculation of the time course of the phasic blocking and allows the production of a series of ERD maps throughout the ERD trial. A flow chart of the ERD processing in the time domain is shown in Figure 3-5. The processing of each channel in the multichannel recording is as follows: each ERD epoch is bandpass filtered, the instantaneous power at each of the sample points in the epoch is calculated, and P consecutive instantaneous power samples are averaged (thereby reducing the temporal resolution of the time sequence). After the epochs from all trials have been processed, they are averaged. One second at the start of the epoch is assigned as a reference period, and the average power in this reference period calculated. The ERD time sequence is then obtained, with each sample point in the time series being calculated as the percentage change between the instantaneous power at that sample point and the average reference power.

For the filtering of the ERD epochs, bandpass digital filters were used. A brief description of digital filters, including some of the different methods of design and implementation of these filters is given in Appendix H. Three filters were designed with passbands of 8-10 Hz, 10-12 Hz and 8-12 Hz.

Finite impulse response (FIR) filters were chosen since these have linear phase response and therefore a constant phase delay for all frequencies. For a constant filter phase delay of N, the filtered signal is simply delayed by N time steps. This is important for ERD studies, since the ERD time course is correlated to the occurrence of an event and tasks performed by the patient. A time shift between the recorded data and processed data would upset this correlation. Thus the output signal from the filter needs to be shifted by the phase delay of the filter. The bandpass filters were required to be very narrow band with steep roll-off in the transition bands. This requirement shows the disadvantage of using a FIR filter (as opposed to an IIR filter) as large filter lengths are required to obtain steep roll-offs.

The filters were designed using the Matlab (Mathworks Inc.) filter design package. The window method was used for the design of the filters. Table 1 of Appendix A list the main lobe widths and side lobe amplitudes for different windows. The Hanning window was

selected as this window gave a good balance between main lobe width and side lobe attenuation. In filter terms, this corresponds to a good balance between steepness of roll-off and amount of attenuation at the stopband frequency. A filter length of 50 was used and the 50 filter coefficients for each filter were stored in separate files. A phase delay of 25 data points was found for each filter. This corresponds to a time delay of 0.25 seconds (25 data points at 100 Hz sampling frequency).

The filters were implemented using the 'fast convolution' method discussed in Appendix H. A filter routine was written which accepted as input an array of data (N x 1). The filter coefficients for the particular filter selected are accessed from the filter file, and stored in a filter coefficient array (50 x 1). The input data array and the filter coefficient array are zero-padded to the required length of (N+50-1), and the FFT for each of these sequences calculated. If (N+50-1) is not a power of 2, the sequences are further zero-padded to the length which is the closest power of 2 greater than (N+50-1). A radix 2, decimation-in-time FFT routine is used for computation of the discrete Fourier transform. The two FFT sequences are then multiplied together and the inverse DFT performed using a radix 2, decimation-in-time inverse FFT routine. The real part of the inverse FFT routine gives the output of the filter. This output sequence is then shifted by 25 sample points (the time delay of the filter), and the filter routine returns an (N x 1) dimensional array of the filtered data.

The flow chart for the complete ERD calculation is shown in Figure 4-19. A block of data is accessed from the file as described in the Data File Accessing section. The block length N depends on the pre-event and post-event time intervals. The block is checked for artifacts by passing the artifact flag array to the artifact checking routine as already. If the block contains artifacts, then the block is not used for processing and the next block of data is accessed from the file.

If the block is artifact-free, then it is processed. The (N x 16) dimension data array is sent to the reference transformation routine. The output from this routine is thus a (N x M) data array, M being dependent on the type of derivation. Each column of the (N x M) data array is passed as a one dimensional array (N x 1) to the filter routine. This one dimensional array represents one epoch of data (i.e a single trial) for a single channel. The filter routine returns an (N x 1) dimensional array of band-limited data. Each value in the array is then squared to calculate the instantaneous power, and 10 consecutive power samples are averaged. This band-limited instantaneous power is stored in an (R x 1) dimensional array, where R = N/10. An (R x M) dimensional ERD array contains the running total of the summation over the epochs for each of the M channels. Each column of this array contains a running total of the

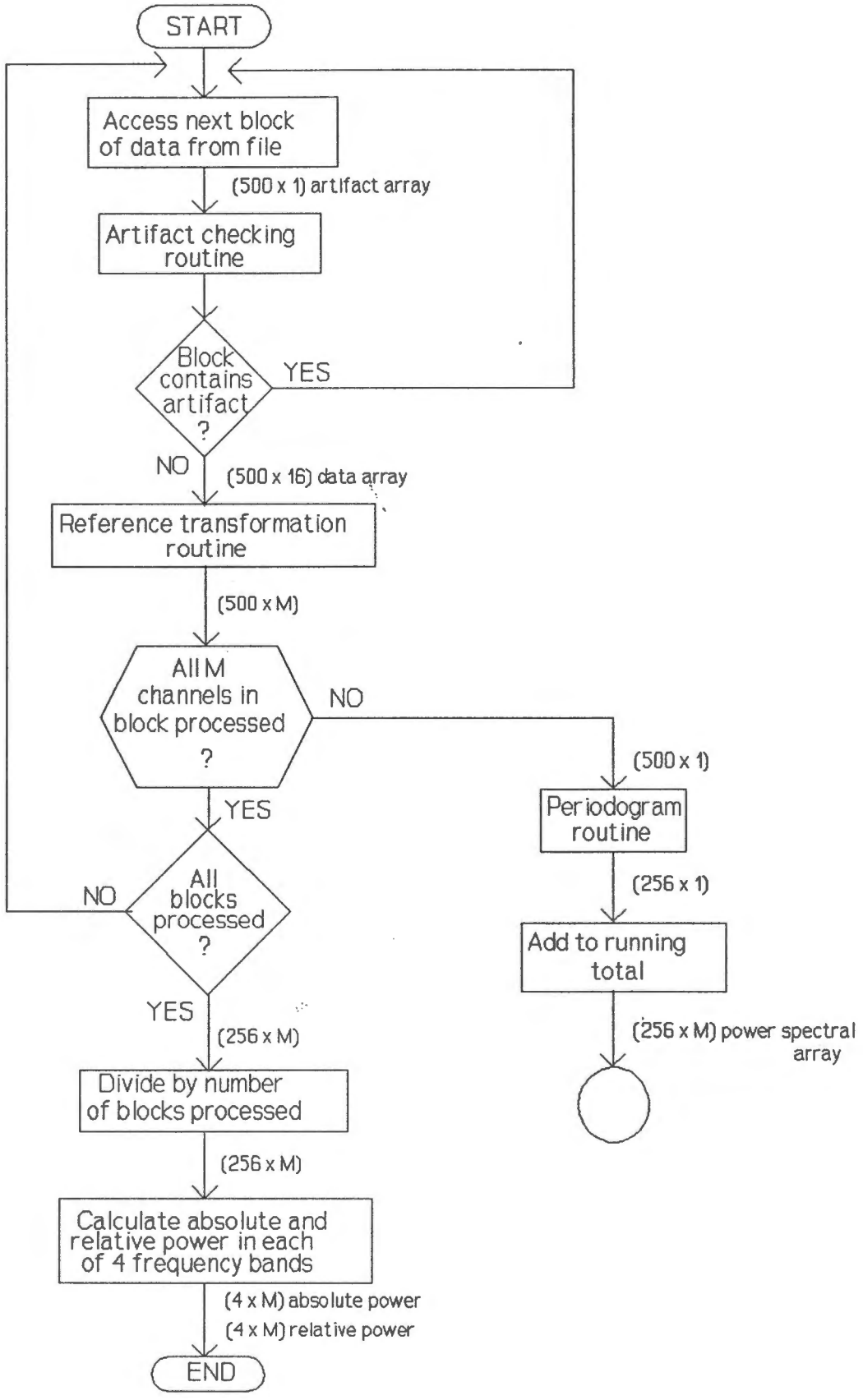

Figure 4-19 : Flow chart for complete ERD calculation routine

summation of the band-limited instantaneous power calculated for each trial for a single channel. The array is initialized to zero at the start of the ERD calculation. The R band-limited instantaneous power values are added to the corresponding column in the ERD array. The next column (i.e the epoch of data for the next channel) in the data array is then passed to the filter routine and the band-limited instantaneous power calculated. These values are then added to the corresponding column of the ERD array. This is repeated until epochs of band-limited instantaneous power for all M channels in the current block of data have been calculated and added to the running total. The next block of data (i.e the next trial) is then accessed from the file and the block checked for artifacts. If the block is free from artifacts, the reference transformation is performed and the band-limited instantaneous power for each of the channels in the block is calculated and added to the running total in the ERD array as described.

This procedure is repeated until all blocks (trials) have been processed and the results added to the running total. The final result is a (R x M) dimensional ERD array containing the summation of the band-limited instantaneous power calculated for all trials for each channel. The instantaneous power is then averaged over all trials for each channel by dividing each column of the ERD array by the number of blocks used in the summation, ie. the number of trials minus the number of blocks rejected by the artifact checking routine.

The ERD time series is then obtained by calculating the average power in a reference interval. This interval is defined as the interval from 0.5 seconds to 1.5 seconds of the epoch. For each column of the ERD array (i.e each channel), the sample points within this reference interval are averaged to produce the reference power, and then the percentage power change is calculated at each of the R sample points in the column, by subtracting this reference power from the instantaneous power at each sample point, dividing this result by the reference power and multiplying by 100. The final output from the ERD routine is an (R x M) dimensional ERD array, each column containing the ERD time series for one of the M channels. The time resolution of the original data is 10 milliseconds (100 Hz sampling rate), but 10 instantaneous power values are averaged thus reducing the resolution of the ERD time series to 100 milliseconds.

Figure 4-20 shows results of the ERD calculation for a single channel. The upper left-hand graph shows one of the epochs from a set of trials recorded for EEG channel O_2 during an ERD experiment. This experiment involved an exogenous event, viz the flashing of a strobe light in front of the subject's eyes. The upper right-hand graph shows the computed band-limited instantaneous power for this epoch, and the lower left-hand graph shows the average

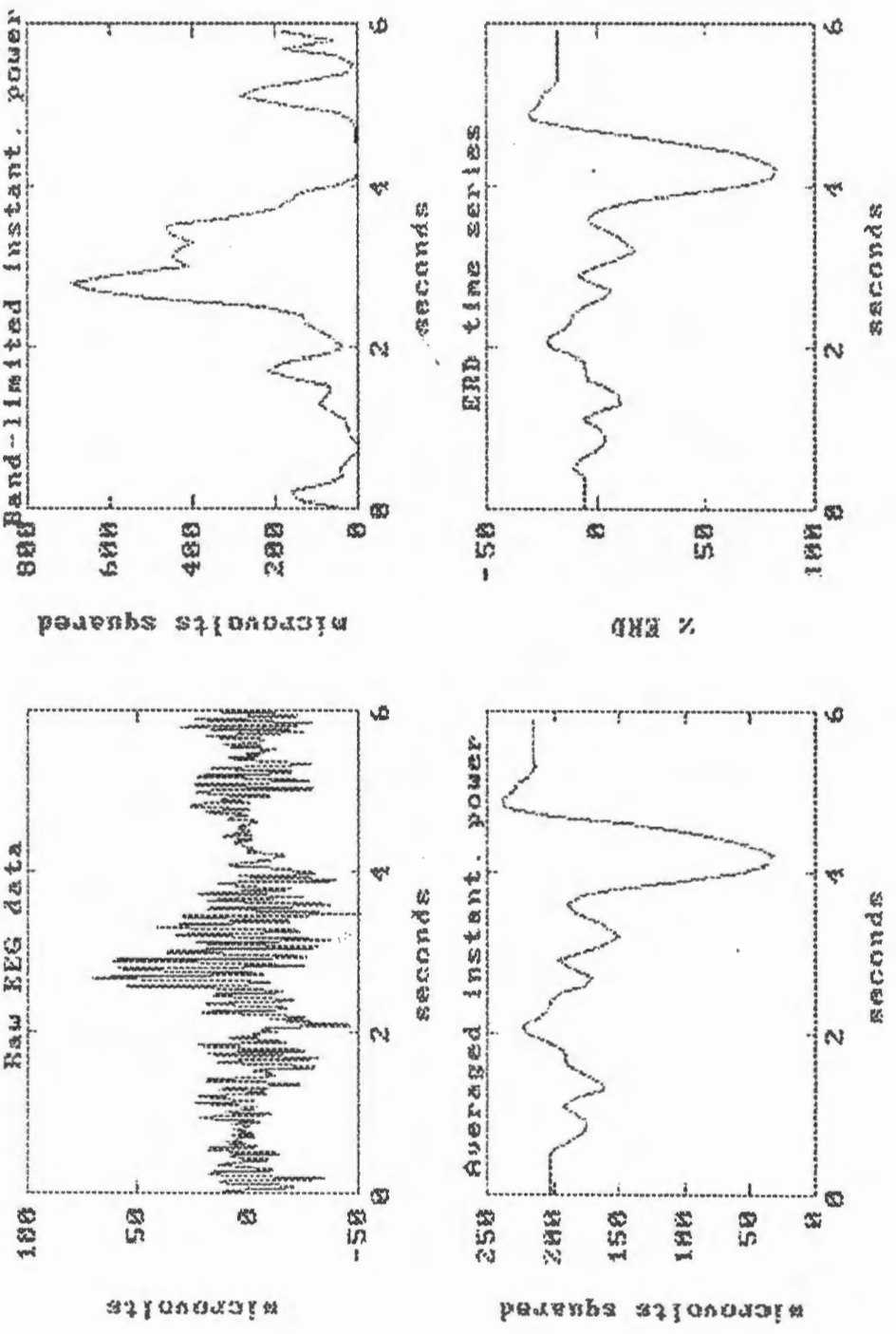

Figure 4-20 : Results from different stages of the ERD calculation. (Upper left) : An epoch of raw EEG data from channel O_2. (Upper right) The band-limited instantaneous power graph for the raw data. (Lower left) The average instantaneous power over 60 trials. (Lower right) The computed ERD time series.

of this instantaneous power over 60 trials. The lower right-hand graph shows the ERD time series computed from the epoch-averaged power of the lower left-hand graph.

4.4.5 Interpolation

The topographical map is composed of 5025 pixel points which fill the circle inscribed in a square grid of 81 pixels per side as shown in Figure 4-12. The spectral power values (for spectral maps) or ERD percentage values (for ERD maps) are only known at a limited number of these pixel points. The pixel points at which the values are known are the electrodes sites: 16 for monopolar, common average or local average (Figure 4-12), 12 for transverse bipolar (Figure 4-14) and 15 for longitudinal bipolar (Figure 4-15). To construct a map of 5025 pixel points, the values for the remainder of the pixel points are interpolated from these known values.

The linear three-nearest neighbour algorithm is used for the interpolation. The value at each pixel point is calculated from the known values at the three closest electrode sites: the value at each electrode site, is multiplied by its normalized distance to the unknown pixel point and these summated to yield the interpolated value.

The pixels in the topographical map are numbered by starting at the left ear, and numbering the pixels from bottom to top and column to column - the last pixel (next to the right ear) is numbered as 5025. A program was written to calculate the three nearest electrodes together with their normalized distances, for each of the 5025 pixel points in the topographical map. This program reads in the grid co-ordinates of each of the electrode sites from an electrode file into an (M x 2) dimensional array, with a column for each of the x-grid and y-grid co-ordinates. Then starting at pixel point 1, the distances from this pixel point to all M electrodes are calculated using Pythagoras' theorem. For the three closest electrodes, the normalized distances are calculated and the electrode numbers together with the distances are stored in the first row of an interpolation file. This is then repeated for all 5025 pixel points in the maps, resulting in an interpolation file containing 5025 rows. Since the electrode sites differ depending on the derivation, three electrode files were used as input to the program: one containing the 16 co-ordinates for the monopolar, common average and local average derivation, one containing the 12 co-ordinates for the transverse bipolar derivation, and one containing the 15 co-ordinates for the longitudinal bipolar derivation. The program thus generated three separate interpolation files. These files can then be used by the data processing software.

An interpolation routine accepts as input an (M x 1) dimensional array containing the processed values at each of the M electrode sites. For spectral mapping, the processed values will be absolute or relative power values, while for ERD mapping the values will be ERD percentages. The interpolation routine then interpolates the map, calculating values at each of the 5025 pixel points in the map. This is done by first accessing one of the three interpolation files, depending on the derivation setting. For each pixel point, the three values in the input array specified by the three electrode numbers from the corresponding row of the interpolation file, together with the three normalized distances, are used to calculate the value at this pixel point. The output from the routine is a (5025 x 1) map array, containing the values (power or ERD percentages) for each of the pixels in the topographical map.

4.4.6 Displays

There are three different displays: one spectral and two ERD displays. The different elements making up these displays are first discussed briefly, followed by a description of each of the different types.

There are six basic elements used by the different displays: the patient information box, the test information box, the push-button selection box, the multichannel time series screen, the topographical map and the scale bar. Not all these elements are used in each of the display types.

The **patient information box** displays the name, folder number, birth date, sex and race of the patient whose processed data results are being displayed. The **test information box** displays the test number, the test date, comments, and the derivation type. For the spectral display, the test information box also displays the lower and upper frequencies of each of the four spectral bands, while for the ERD displays, the filter used for the ERD calculation is displayed.

The **push-button selection box** displays a number of push buttons which can be selected using the cursor keys. The currently selected button is indicated by a white border around the button. The button is pressed by hitting Return on the keyboard. The push button function is marked on the button in white text.

The **multichannel time series screen** displays M channels of time series data, with M being 16, 15 or 12 depending on the derivation setting. A cursor running the length of the display

can be moved backwards and forwards through the displayed data.

The **topographical map** consists of a circular head representation comprising 5025 pixel points, two solid semi-circles forming the left and right ears, and a solid triangle forming the nose. The map can have a header describing the map and a footnote giving additional information. The data to be displayed in the topographic map; ie. the (5025 x 1) dimensional map array of spectral power or ERD percentages, first undergoes colour transformation. Each value in the map array is mapped to one of thirteen colours, thus producing a (5025 x 1) dimensional colour array (this colour mapping procedure will be discussed in more detail later). Each of the 5025 pixels in the circular head region is then plotted as a colour, starting at pixel 1 and finishing at pixel 5025.

The **scale bar** provides the scale for the topographical maps. A rainbow scale of 13 colours is used: from dark blue, through different shades of blue, through cyan, green, yellow, different shades of red to dark red. Dark blue is at the bottom of the scale and dark red at the top. The scale bar consists of a thin rectangle divided up into thirteen segments. The scale is marked by displaying at the bottom and top of the bar, the values (power or percentages) that the dark blue colour and the dark red colour represent, respectively. The colour scale is linear.

a) Spectral Display

An example of the spectral display is shown in Figure 5-1. At the top of the screen, the patient information box and test information box are displayed. In the middle of the screen, the four spectral maps are displayed, and in the bottom right-hand corner the scale bar.

The user has three options for the spectral display: whether absolute or relative power is to be displayed, whether the scaling of the maps is auto-ranging or fixed (if fixed then the user must specify the maximum value in μV^2 or % depending on whether absolute or relative power is being displayed), and which of the spectral maps are to be displayed (eg. delta and/or theta and/or alpha and/or beta). The absolute power array (4 x M) or relative power array (4 x M) from the spectral calculation routine is then used to produce the maps. Each row of the chosen array (i.e. delta power for each of the M channels, theta power for each of the M channels, etc) are passed to the interpolation as an (M x 1) array, and four (5025 x 1) map arrays are interpolated, one each for delta, theta, alpha and beta power.

Each map array is then colour mapped. This involves dividing up the power range into thirteen equal size bins, and then assigning a colour to each of the 5025 power values, depending on which bin this value falls into. The range is determined by the range setting. If auto-ranging is selected, then the maximum power value over the four map arrays is found, and this forms the upper limit of the range. The lower limit of the range for spectral mapping is always 0 μV^2 or 0% (absolute or relative power). These upper and lower limits are then marked on the scale bar. If the range is fixed, then the upper limit of the scale is set at the value provided by the user.

Four colour maps are produced, each then being used to plot the spectral maps. The name of the frequency band is shown as a header for each of the maps.

b) ERD Display

i) ERD Time Series

An example of the ERD time series display is shown in Figure 5-8. The patient information box and test information box are displayed in the top right-hand corner of the screen. Most of the left half of the screen is taken up by the multichannel time series screen. The ERD array (R x M) is used to display the ERD time series for each of the M channels (electrodes) with each ERD epoch having R data points. The bottom of the multichannel display shows the time scale in seconds. An 'E' indicates the instant during the trial at which the event occurred. The user is able to move the cursor a sample point at a time (i.e 100 millisecond steps - time resolution of the ERD series) or in steps of five sample points (0.5 second). The user can then select an instant during the trial, and produce a topographical map at this instant.

The M values at that sample point are passed (from the (R x M) ERD array) to the interpolation routine as an (M x 1) array. The map is interpolated and a map array of 5025 ERD percentages is returned. This array is then colour mapped. For the ERD display, the scale is fixed, with the top of the scale representing +100% ERD and the bottom of the scale -100% ERD. This range is then divided up into thirteen colour bins, and the ERD value is mapped to a colour value depending on the bin into which it falls. The resultant (5025 x 1) colour array is then used to plot the topographical map which is displayed, together with the scale bar, at the bottom right-hand corner of the screen. The map is given a header to indicate that it is an ERD map, and a footnote indicates the sample instant (in milliseconds) at which the map was produced. The user is able to store a sequence of ERD maps which have been

produced at different time instances, for display as an ERD map series.

Two push-button selection boxes are displayed, one below the multichannel time series screen and one above the topographical map. The former provides the functions for controlling the movement of the cursor in the ERD time series screen, for generating a map for the sample instant at the cursor position, and for exiting from the display. The latter selection box provides the functions for adding a map to a stored series of ERD of maps, deleting a map from the stored series of maps, changing the sequence of maps stored in the series, and displaying the series of ERD maps.

ii) ERD Map Series

An example of such a display is shown in Figure 5-9. The patient information box and test information box are displayed at the top of the screen. The ERD map series is displayed in the middle of the screen, each map having a footnote indicating the time instant of the map. The scale bar for the maps is displayed in the bottom right-hand corner of the screen.

4.5 User Interface

Both the data acquisition system and the data processing and display system have interfaces made up of three basic elements: a menu bar, a pull-down menu and a dialog box.

4.5.1 Menu Bar

The menu bar is the primary access to all the menu commands. The bar consists of a single bar at the top of the screen containing a number of menu titles, each providing the user with a choice of menu commands. The menu titles can be highlighted and selected using the cursor keys and the Return key. The selection of a menu bar command can have one of three effects; the command can cause an action, or lead to another menu (pull-down menu), or result in a dialog box being displayed. Some of the menu commands in the bar are unavailable when it would make no sense to choose them.

4.5.2 Pull-Down Menu

A pull-down menu consists of a rectangular window containing a list of menu titles. Each of these menu titles can be selected by highlighting and selecting the required menu title to execute the required menu command. The selection of a command from the pull-down menu

Figure 4-21 : A screen from the user interface for the data processing system, showing menu bar, pull-down menu and dialog box.

can have one of two effects: the command can cause an action or it can result in a dialog box being displayed. Again, some of the commands in the pull-down menus are unavailable when it would make no sense to choose them.

4.5.3 Dialog Box

The dialog box is the principal means through which the user communicates with the system. The user is able to enter information, select items from a list, or set multiple options. Dialog boxes are composed of five basic types: check boxes, radio buttons, input boxes, list boxes, and action buttons.

Check boxes consist of a box [ ] followed by an item which can either be turned ON or OFF. When a check box is selected, an X appears in the box to show that it is ON: [X]. An empty box indicates that the item is OFF. Often a group of check boxes appear together when applying to a common topic. **Radio buttons** consist of a box ( ) followed by an item which can either be selected or not. If the item is selected, a dot appears in the box: (·). Radio buttons differ from check boxes in that they present mutually exclusive choices. For this reason, radio buttons always come in groups, and only one (no more, or less) radio button in any group can be on at any one time. **Input boxes** allow the user to enter text. The most basic text-editing keys (eg. *Home*, *End*, *BkSpace*, etc) are available in a text box. **List boxes** let the user scroll through and select from variable-length lists. The dialog box has two standard **action buttons**: OK and CANCEL. If OK is chosen, then the settings in the dialog box are accepted and the dialog box is removed; if CANCEL is chosen, no changes to the settings which were current when the dialog box was accessed are made, but the dialog box is removed.

Figure 4-21 shows a screen from the user interface for the data processing system. The bar menu at the top of the screen, the pull-down menu near the top and centre of the screen, and the dialog box in the middle of the screen can be seen. This dialog box consists of three groups of radio buttons, a single group of check boxes, an input box and two action buttons.

The user is able to navigate around the system by choosing the different options of the menu bar and the pull-down menus, and is able to enter the information that the system requires by entering and making selections in the dialog boxes.

CHAPTER 5

CLINICAL TESTS AND RESULTS

To test and verify the quantitative EEG system, a pilot study was undertaken. Volunteers and patients were used for the recording of EEG data during simple experimental set-ups, designed so that results obtained from the processing of the recorded data could be compared with expected results based on the findings of the literature survey. Five volunteers (4 males and 1 female), aged between 20-30 years, and two patients (a male aged 10 years and a female aged 15 years) were used as subjects for the pilot study. Only spectral tests were performed on the patients.

5.1 Spectral Analysis Tests

5.1.1 Experimental Set-up

For spectral analysis testing, two different experimental set-ups were used. For the one, the subjects were comfortably reclining, at rest with their eyes closed, and data acquired in the continuous acquisition mode for a period of 3 minutes. For the other, the subjects were reclining, at rest, but with eyes open, and data acquired again for a period of 3 minutes in continuous acquisition mode.

The acquired signals were then processed and spectral maps of both absolute and relative power, for the five different reference derivations, were produced for each subject.

5.1.2 Results

Figure 5-1 shows the absolute power for the four spectral bands (delta, theta, alpha, and beta) with a transverse bipolar derivation for Subject 1 with "eyes closed". Dominant alpha activity in the parieto-occipital region can be seen from the alpha spectral map. The alpha activity in this case is concentrated more in the right hemisphere. Figure 5-2 shows the absolute power for just the alpha band, again with a transverse bipolar derivation, for Subject 2 with "eyes closed". The alpha activity is localized to the parieto-occipital region, with a slight right hemisphere dominance. The peak alpha power in the occipital region for Subject 2 is far less than the peak occipital power for Subject 1 (8 μV^2 compared to 49 μV^2).

Since each of the four spectral maps in Figure 5-1 is displayed with the same colour scale,

only the alpha map is displayed using the full dynamic range of the colour scale. For the delta, theta and beta maps, the spectral power falls into the lower end of the colour scale and the spatial distribution of the power in each of these maps is therefore not very clear due to the inadequate dynamic range. Figures 5-3, 5-4, and 5-5 show delta, theta and beta spectral maps respectively for Subject 1 with eyes closed and again with a transverse bipolar derivation. Since only one map is computed for each of these spectral displays, the map shown in each display is scaled to the full dynamic range, thereby showing more clearly the spatial distribution of these frequency bands. From Figure 5-3, it can be seen that the delta power is localized to the frontal and temporal regions. The theta power is localized to the temporal regions (Figure 5-4) and the beta power is localized to the frontal and temporal regions (Figure 5-5).

The spatial distribution of the delta, theta, alpha and beta power for the seven subjects with "eyes closed" showed the same general trends. Delta power was localized mainly to the frontal and temporal regions, with the peak power varying from subject to subject between 8 μV^2 and 21 μV^2. Theta power was localized to the frontal and temporal regions, with the peak power of approximately 8 μV^2 being fairly constant amongst subjects. Alpha power was localized to the parieto-occipital and temporal regions. There was a great variation in inter-subject peak alpha power, ranging from clear dominant alpha activity (49 μV^2) to non-existent alpha activity (2 μV^2). The beta peak power was fairly constant amongst subjects (approximately 5 μV^2) and was localized to the frontal, temporal and central regions.

The theta and beta spectral maps for the "eyes open" case did not differ significantly from the "eyes closed" case. However, there was some variation in the delta and alpha maps. The delta power was again localized to the frontal regions. However, for some of the subjects, the peak power was found to be higher for the "eyes open" case when compared with the "eyes closed" state, while for other subjects, there was very little difference between the peak power for the two states. For the alpha map, although the power was still localized to the parieto-occipital region, the peak power was reduced for the "eyes open" state. Figure 5-6 and Figure 5-7 show comparisons between the alpha maps (transverse bipolar) for the "eyes closed" and "eyes open" cases for Subject 1 and Subject 2 respectively. The reduction in alpha power in the parieto-occipital region is clearly evident from these maps.

The results from the spectral analysis test are discussed in the following chapter.

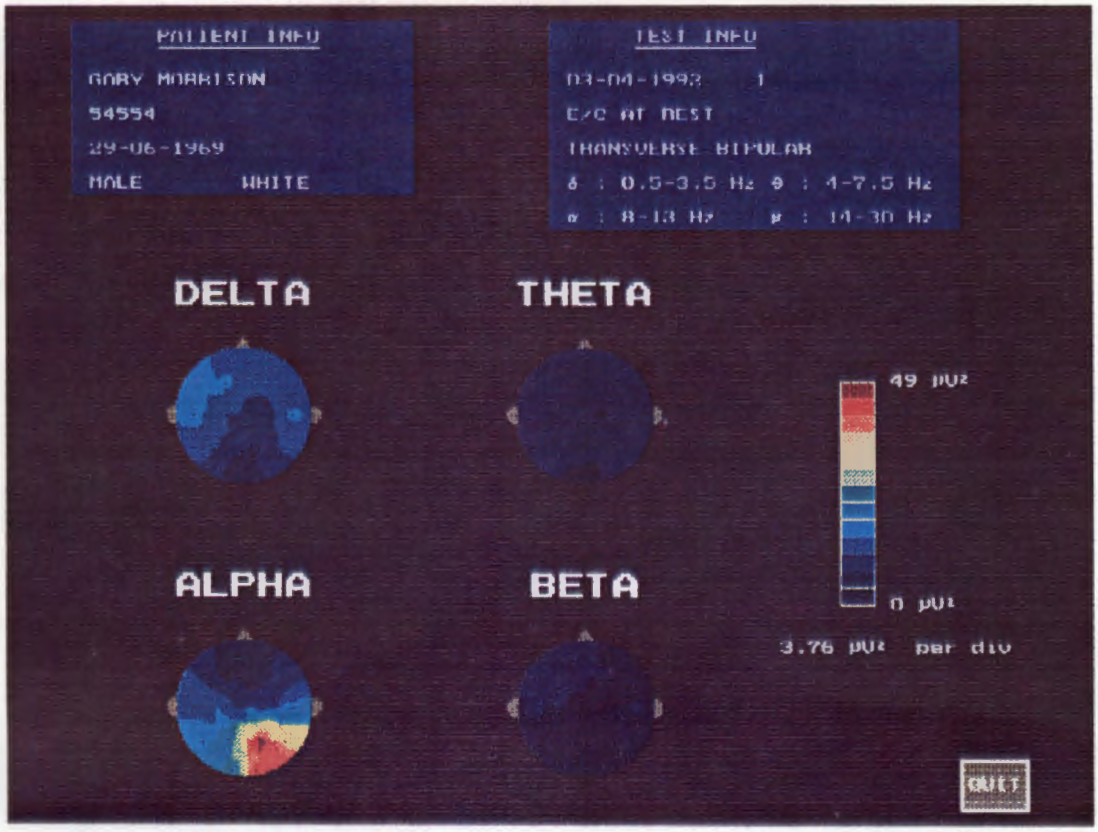

Figure 5-1 : Spectral maps showing absolute power in each of the delta, theta, alpha and beta bands for Subject 1 for the "eyes closed" case.

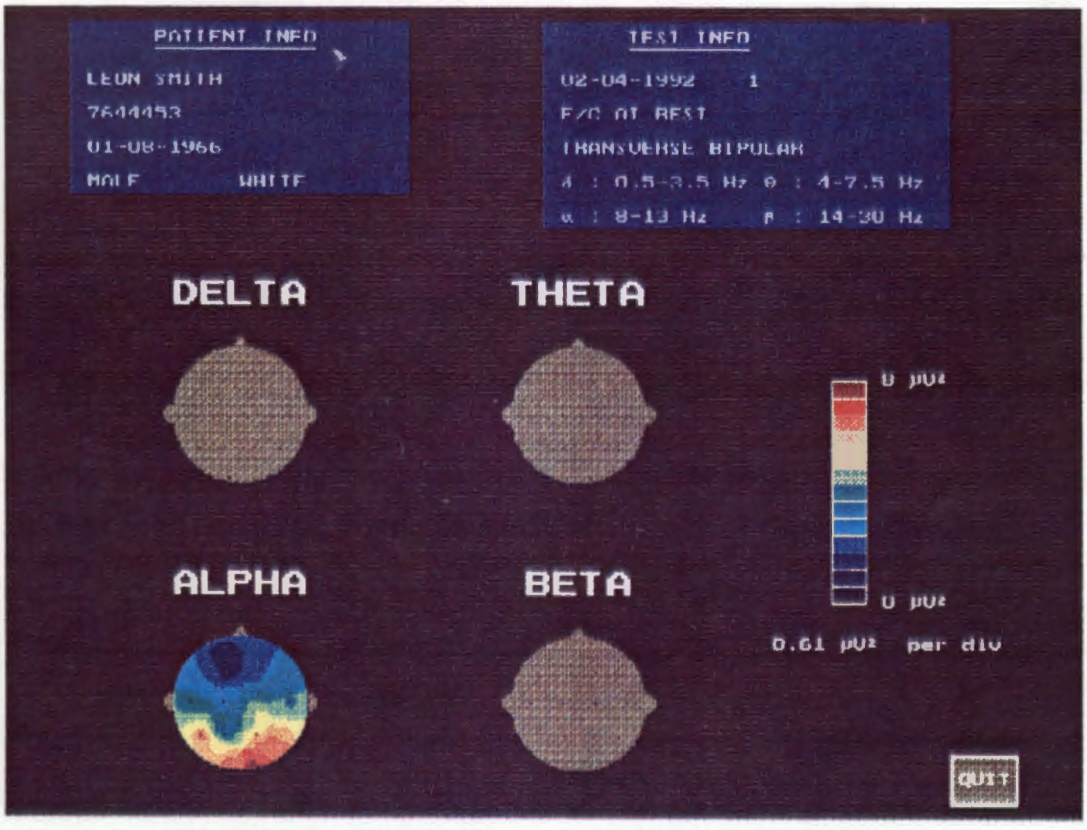

Figure 5-2 : Spectral map showing absolute power in the alpha band for Subject 2 for the "eyes closed" case.

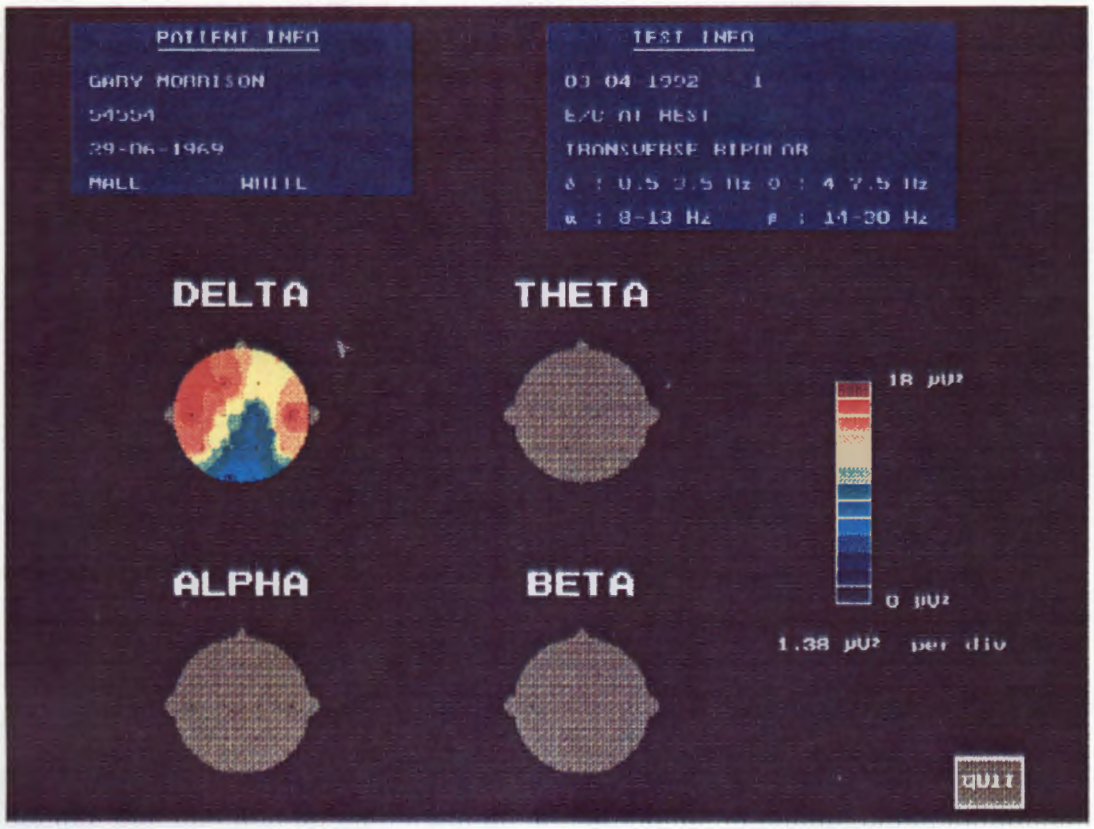

Figure 5-3 : Spectral map showing absolute power in the delta band for Subject 1 for the "eyes closed" case.

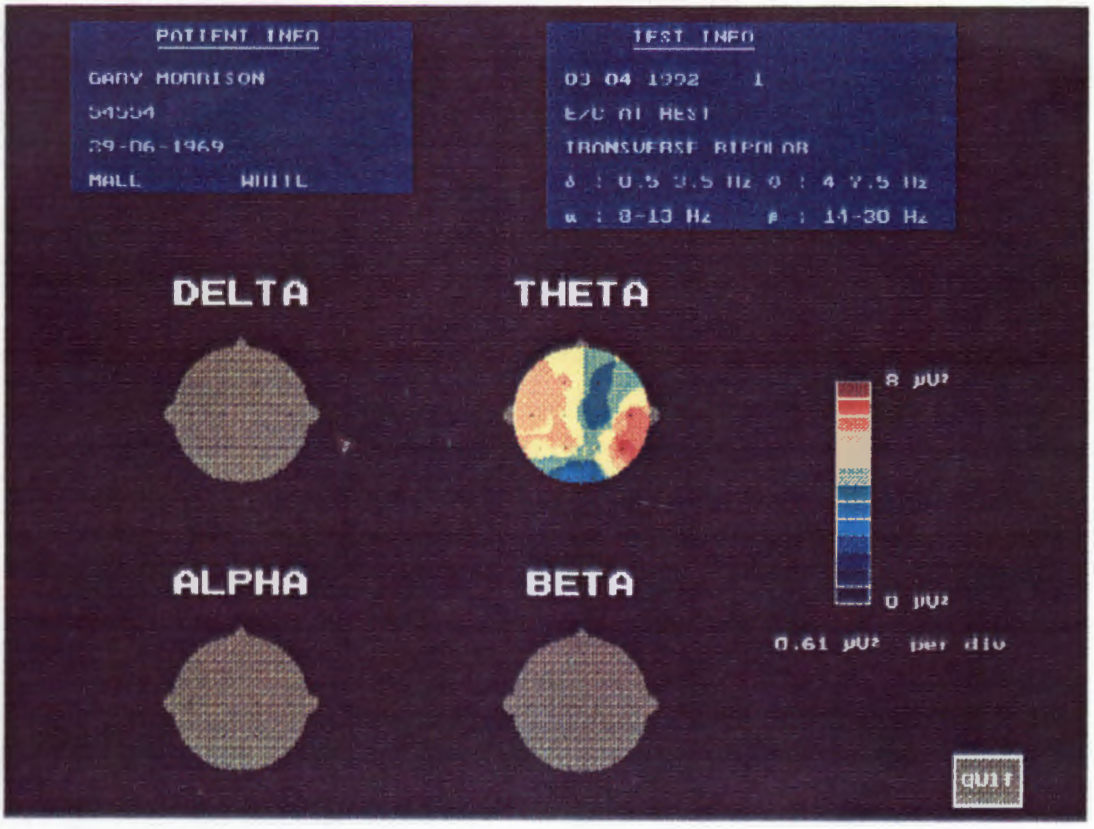

Figure 5-4 : Spectral map showing absolute power in the theta band for Subject 1 for the "eyes closed" case.

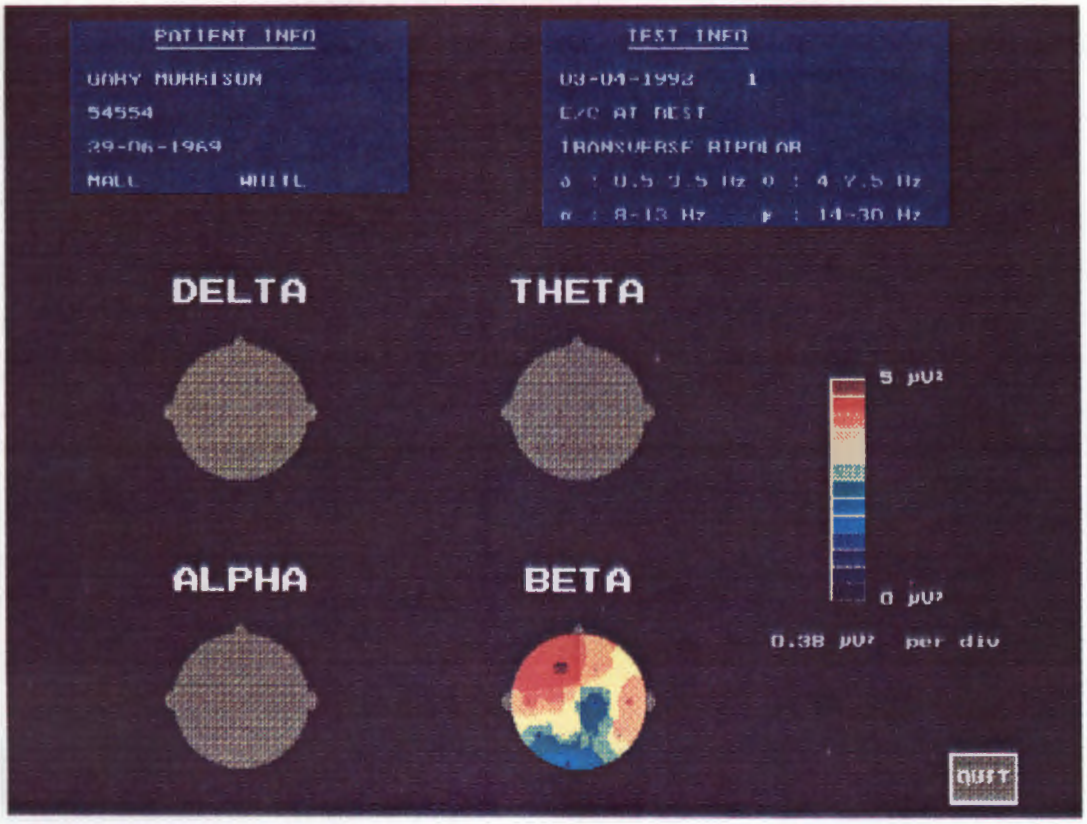

Figure 5-5 : Spectral map showing absolute power in the beta band for Subject 1 for the "eyes closed" case.

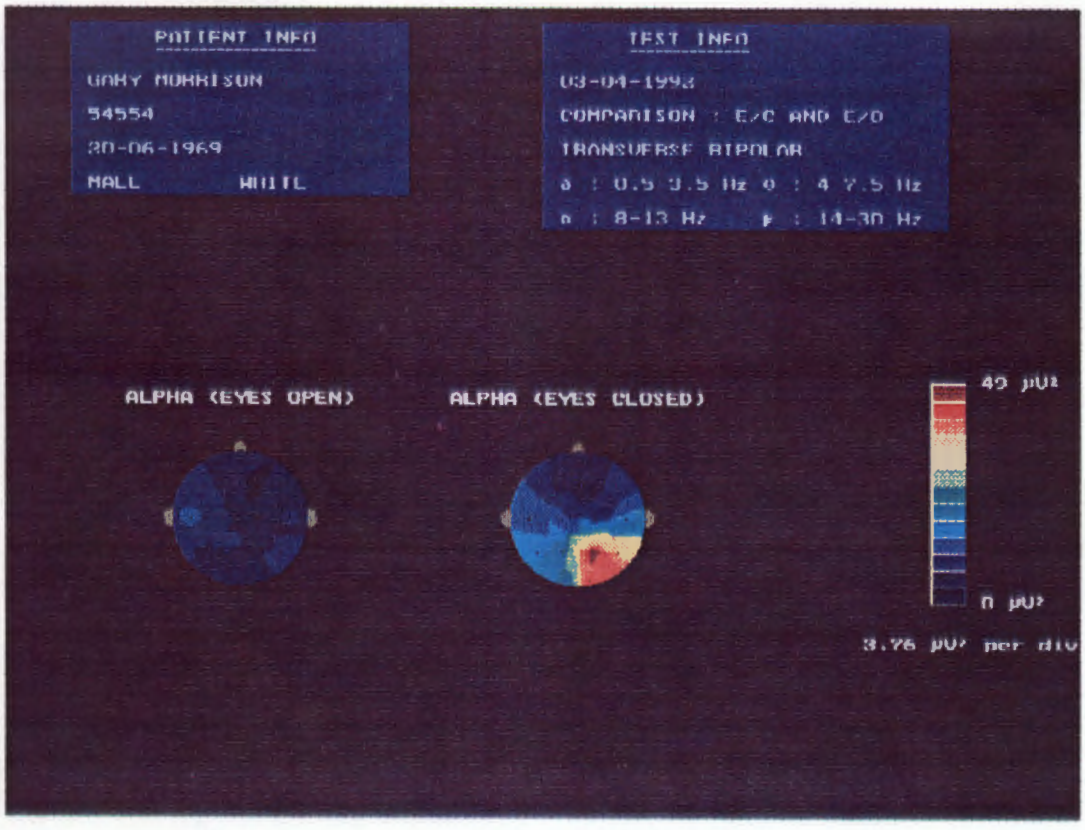

Figure 5-6 : Alpha maps for the "eyes open" and "eyes closed" cases for Subject 1.

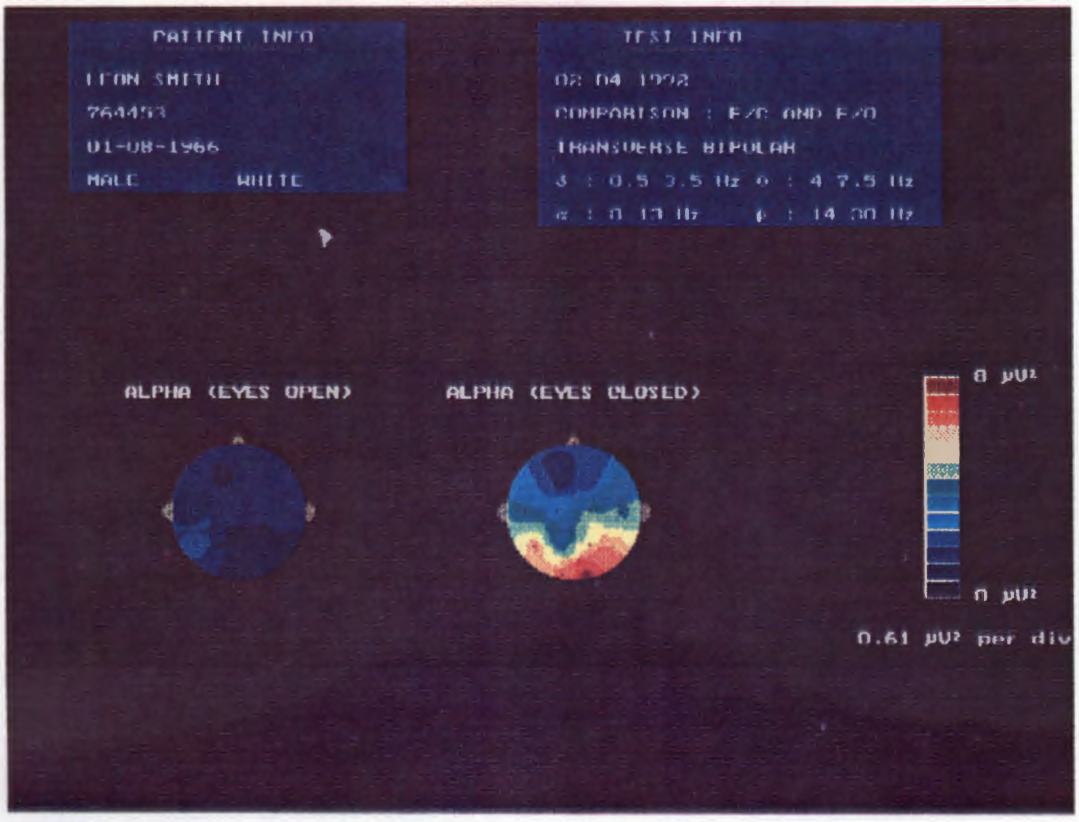

Figure 5-7 : Alpha maps for the "eyes open" and "eyes closed" cases for Subject 2.

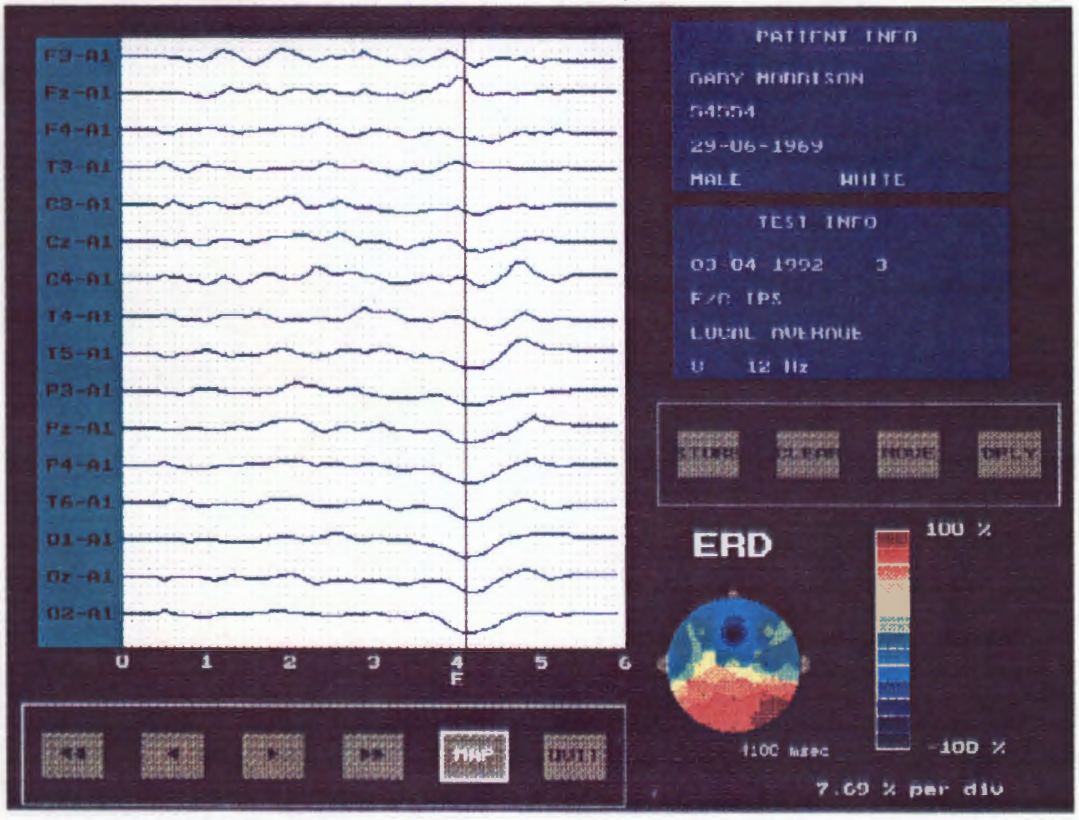

Figure 5-8 : ERD time series for the 8-12 Hz band for Subject 1. Derivation is local average.

5.2 ERD Analysis Tests

5.2.1 Experimental Set-up

For ERD testing, data were acquired in event-related mode. The event was a single flash of a strobe light. For each trial, data were recorded for 4 seconds prior to the light flash (pre-event time interval) and for 2 seconds after the flash (post-event time interval). Sixty trials were performed per subject.

For data acquisition, the subjects were reclining with the strobe light placed approximately 10 cm from their eyes. The strobe light of the Medelec EEG recorder was used, with the ERD trigger output from the pre-processor unit connected to the TRIGGER IN connector on the side-panel of the EEG recorder to trigger the strobe. Subjects kept their eyes closed during the entire recording session.

The acquired signals were then processed and ERD time series computed. For each subject, ERD time series were calculated for each of the five different derivations (monopolar, transverse bipolar, longitudinal bipolar, common average and local average). For each derivation, ERD time series for each of the three different filter bands (8-10 Hz, 10-12 Hz and 8-12 Hz) were calculated, thus resulting in a total of fifteen ERD time series for each subject. For each ERD time series, a sequence of eight maps at different time instances in the ERD series were stored and displayed as an ERD map series.

5.2.2 Results

Figure 5-8 shows the ERD time series for the 8-12 Hz band with a local average derivation for Subject 1. An ERD map is displayed for the time instant indicated by the cursor position (i.e at 4100 milliseconds). The event (the flashing of the strobe) occurred at 4 seconds and is indicated by an 'E'. Maps at eight time instants during the ERD epoch were calculated and displayed as an ERD map series as shown in Figure 5-9. Three maps prior to the event (at 3000, 3700 and 3900 msecs) and five maps after the event (at 4100, 4200, 4400, 4600 and 4900 msecs) are displayed in this map series. Figure 5-10 shows the ERD map series for Subject 2. Again, the ERD is computed with a local average derivation in the 8-12 Hz band. In this map sequence, three maps prior to the event (at 2700, 3700 and 3800 msecs) and five maps after the event (at 4100, 4200, 4300, 4400 and 5000 msecs) are displayed.

It can be clearly seen that the ERD is localized to the occipital and parietal areas. The ERD

reaches its maximal magnitude about 200 milliseconds after the event and has a duration of 400 to 500 milliseconds. The ERD is followed by an enhancement of alpha activity in the occipital and central areas occurring approximately 1 second after the event.

The ERD map series for four of the five subjects had the ERD localized to the occipital and parietal regions, lasting some half a second, followed by an enhancement of alpha activity in the occipital and central regions. For one of the subjects, no significant ERD was found; however, the recording for this subject contained a high percentage of artifact, and more than 50% of the recorded data was discarded. This meant that the number of averages used in the ERD calculation was greatly reduced.

The ERD maps shown thus far are for the 8-12 Hz band and use a local average derivation. Figures 5-11 and 5-12 compare the five different derivations and the three different frequency bands. The maps in these figures are for Subject 1, and are produced at the instant of maximum ERD (i.e. at 4200 milliseconds). For the comparison of the different derivations, the ERD is calculated in the 8-12 Hz frequency band, while for the comparison of the different frequency bands, a local average derivation is used.

The results from the ERD analysis tests are discussed in the following chapter.

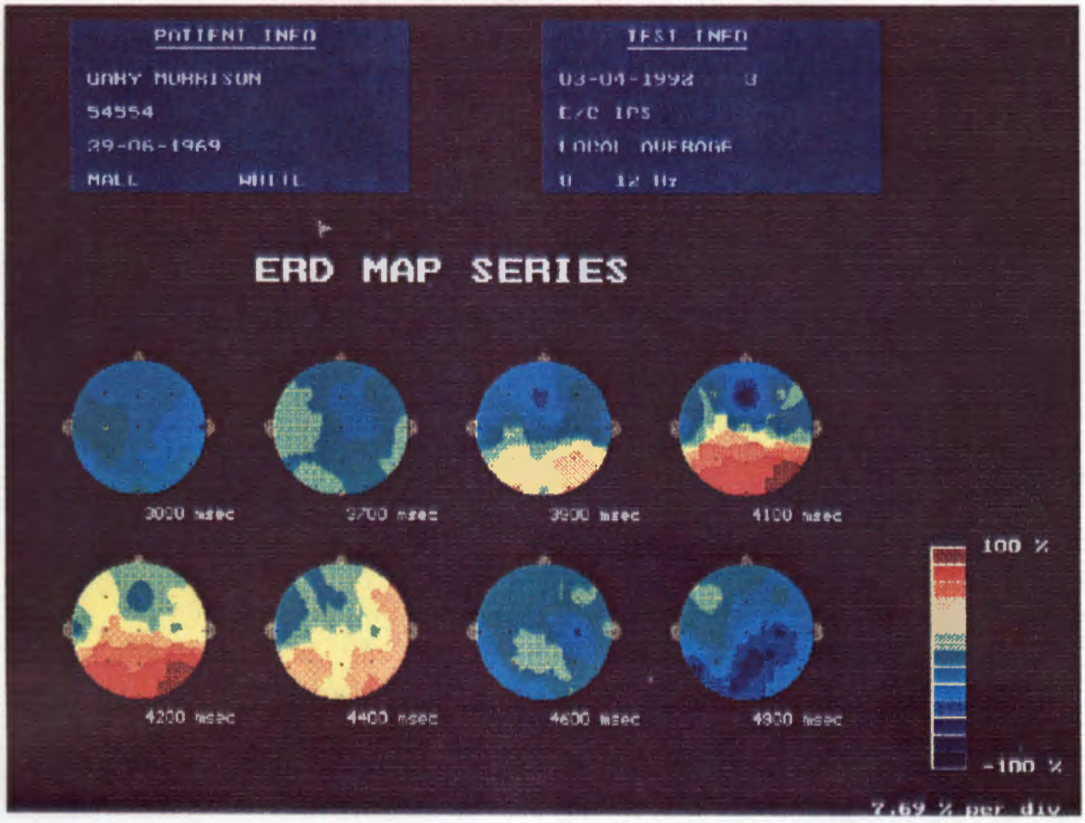

Figure 5-9 : ERD maps series for the 8-12 Hz band for Subject 1. Derivation is local average.

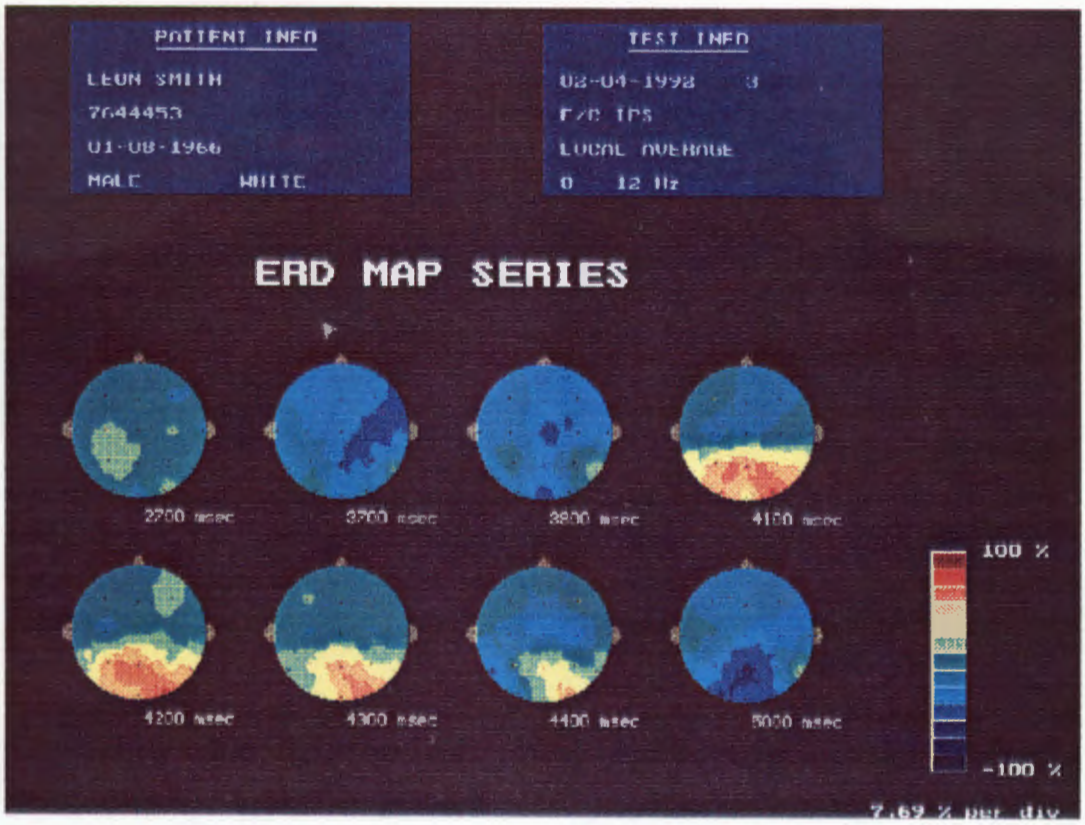

Figure 5-10 : ERD map series for the 8-12 Hz band for Subject 2. Derivation is local average.

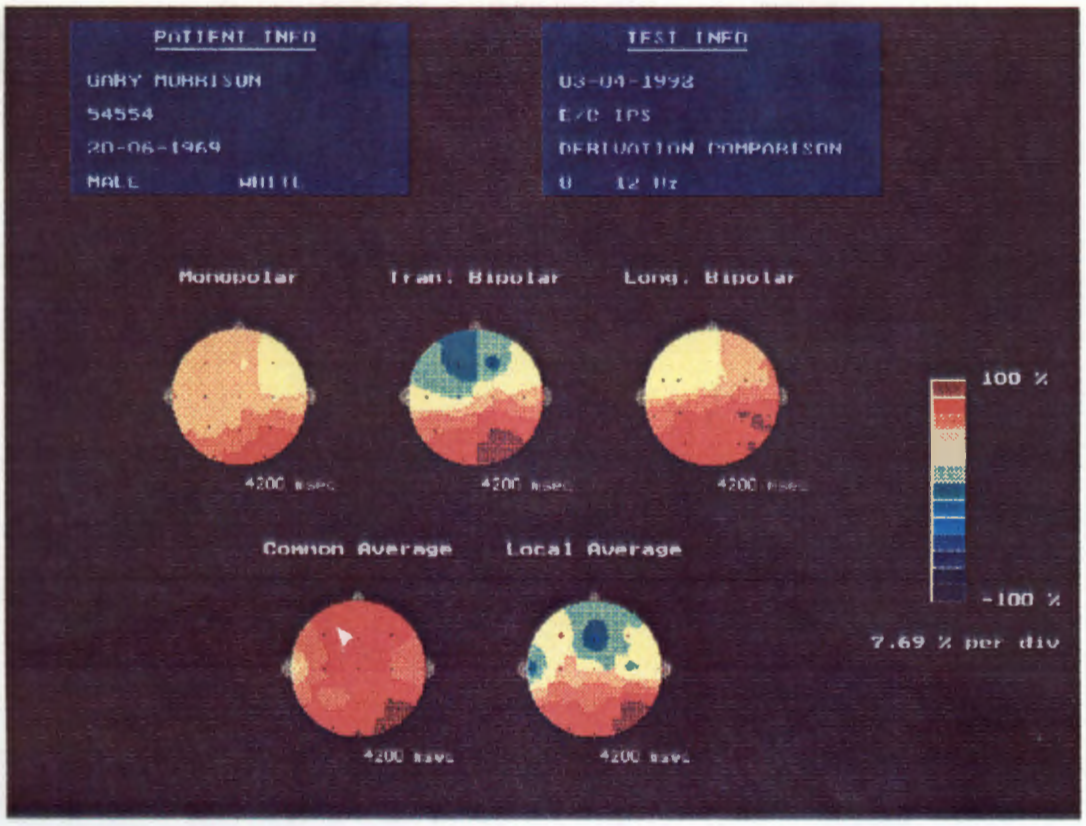

Figure 5-11 : ERD maps for the five different derivations. Maps are computed in the 8-12 Hz band for Subject 1 at instant of maximum ERD (4200msec).

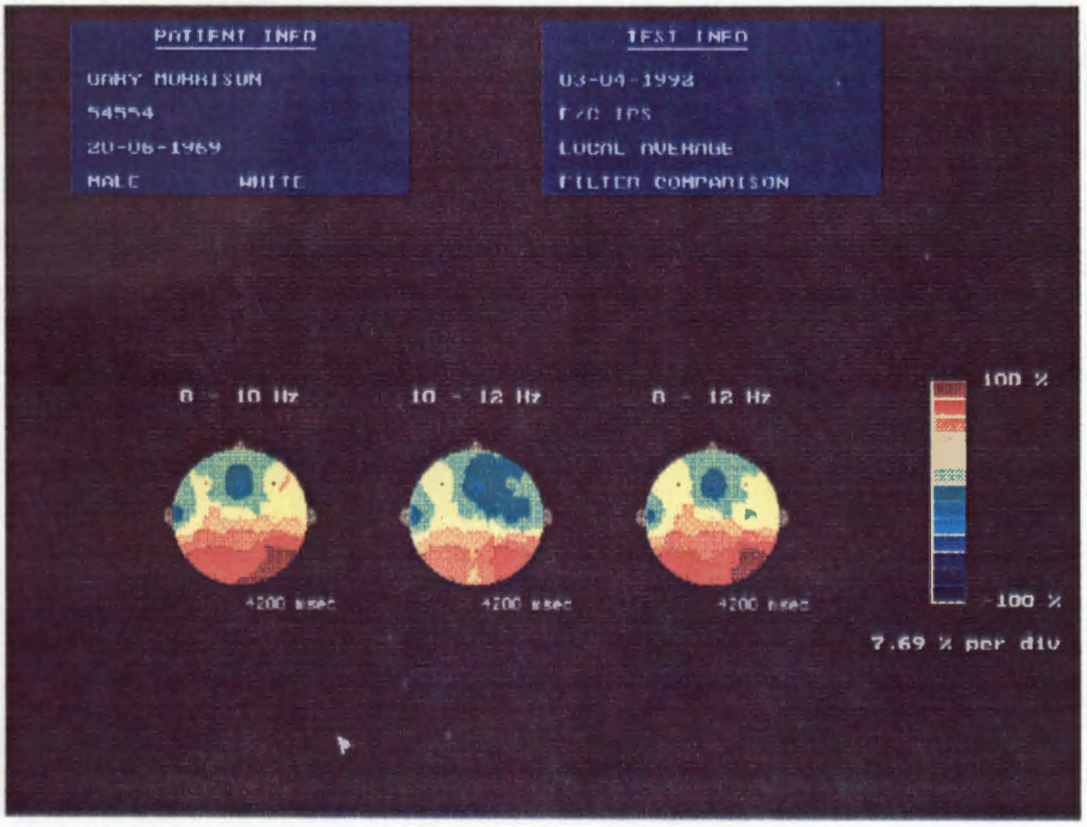

Figure 5-12 : ERD maps for the three different frequency bands. Maps are for Subject 1 at instant of maximum ERD (4200msec) with a local average derivation.

CHAPTER 6

DISCUSSION

6.1 System Design, Implementation and Performance

One of main shortcomings of the quantitative EEG system is the **number of recording electrodes.** The system is limited to 16 channels since the Medelec 1A97A recorder has only eighteen channels with two of these reserved for EOG monitoring in future development of the system. The electrodes dropped from the standard 10-20 sites were the four frontal electrodes F_{p1}, F_{p2}, F_7 and F_8, since these sites do not overly any of the important cerebral regions involved in functional studies (see Figure 3-13). However, the interpolation of the pixel values forming the greater part of the frontal region of the topographical map now rely on the potentials recorded at electrodes F_3, F_z and F_4 (as these are the 3 nearest electrodes to the pixel points in this frontal region, see Figure 4-12). The calculation using the 3-nearest neighbour algorithm thus becomes an extrapolation, rather than an interpolation, and the results obtained in these frontal regions must be treated with caution.

Also, additional electrodes between the 10-20 sites would give a denser electrode array over the scalp. This is important for bipolar derivations, as the spectral power increases and ERD decreases with increasing interelectrode distance (as explained in the literature survey). Thus, for studying localized blocking (ERD), especially over the sensorimotor cortex, bipolar derivations with closely spaced electrodes are more appropriate. A denser electrode array is also important for local average derivations. With the recording montage used for the system, only 6 of the 16 electrodes do not lie on the periphery (see Figure 4-12). Thus the local averages for the majority of the electrodes in this montage (10 of the sixteen electrodes) are calculated using three-point, rather than five-point operators. The three-point operators do not give as good an approximation to the Laplacian operator as the five-point operator. By inserting additional electrodes between the 10-20 sites, the percentage of five-point operators used for the local average reference will be increased.

The number of electrodes used in the recording montage should therefore be increased. The four frontal electrodes of the 10-20 system should be used, plus additional electrodes between the 10-20 electrode sites. This means, however, that either the system will have to be interfaced to another EEG recorder with more channels, or a front-end will have to be designed and built to support the required number of channels. Adaptions to the pre-processor unit will also need to be made, although this is a fairly simple task. Also, the PC30D

analogue-and-digital I/O card only supports 16 channels. A new ADC card supporting the required number of channels could be used, but this would require re-writing of the data acquisition control software for the new ADC card. The alternative approach is to use the PC30 card with an input multiplexer to increase the number of input channels. A multiplexer for the PC30D card which expands the number of input channels up to 64 is available. This approach would require modifications to the data acquisition control software.

The design and implementation approach for the **management of patient information** was very simple. Patient and test information is entered for each test, and this information is then stored, with the recorded data, in each data file. When using the system to perform the clinical tests, the patient information had to be re-entered for each test, this being extremely tedious. Each data file for a patient contains a copy of the patient information, this redundancy increasing the amount of storage space on disk. Also, the user needs to keep a record of what tests were performed for each patient, together with the respective test number, for accessing the data for processing. This method of managing the patient information is not conducive to the implementation of a database, whereby searches for certain patients, or groups of patients (i.e. all patients with a certain pathology, or all patients who were tested on a certain date etc) could be made.

Thus a more elaborate information and data management scheme is required to make the system a useful tool in the clinical and research environment. A scheme based on a hierarchial approach is suggested. A record containing a list of patients who have been tested could be kept. Such a record could be stored in a file, with each entry in the record containing the patient's name, together with a pointer to a patient information record. The patient information record could then store all the required information, together with information on all the tests which were performed on that patient. This patient record could also be stored in a file, in which case the pointer to the patient information record in the patient list, would contain the filename of the specific patient information file. For each test that has been performed, pointers (filenames) to records (files) containing the raw recorded data and processed data would be stored with the test information.

Thus for data acquisition with such a scheme, the name of the patient to undergo a test could be entered, resulting in the patient list record being accessed and searched for that patient. If the patient is found (i.e. if the patient has been tested previously), the required tests can be performed with the relevant information being appended to the patient information file, together with the filenames of the data files in which the recorded data is saved. If the patient

is not found, then the patient information can be entered by the user and stored in a new patient information file, the patient's name and this filename then being added to the patient list record. For data processing and display, the user can enter the patient's name and a complete list of the tests performed for that patient can be displayed. The user is then able to select a particular test, and the data contained in the associated record can be accessed and processed.

The data files that are generated are extremely large: about 3 Megabytes for a typical ERD recording. Thus a **storage medium** with a large capacity such as an optical disk is required for data storage. One way of reducing the size of the data files is to store the files in binary format, rather than ASCII format. This would result in a 50% reduction in size. Different methods of **data compression** could also be investigated to lessen the demands on disk storage space required by the data files. However, data compression is at the expense of system performance, as processing time is required for the compression algorithm when writing and reading the data file.

During the performance of the clinical tests, the EEG technologists had a chance to use the system and make comments about the system. One of the criticisms was that the EEG signals are not displayed on the screen during data acquisition, thus giving no **visual feedback** to the user. Displaying the EEG data as it is recorded would also facilitate the selection of the recorder sensitivity. This setting needs to be set for each patient as the peak-peak amplitude of the scalp potentials varies across patients. To set this sensitivity, the recorded data needs to be displayed in order to see whether the signals have been amplified too much and are therefore clipped (sensitivity setting too high) or whether the signals have not been amplified sufficiently resulting in very small signals with poor resolution being displayed (sensitivity too low). The sensitivity can then be changed until the most suitable setting is selected for each patient.

The **artifact detection algorithm** based on voltage trigger testing was found to be satisfactory for detecting gross movement artifacts. However, the majority of artifacts during the clinical tests were due to eye movements (mainly eye blinks) and were not detected by this voltage trigger testing. These artifacts had to be manually marked by scanning through the recorded data. This problem of eye movement artifact will be intensified when more complex experimental paradigms involving reading are used, where the percentage of eye movement artifacts will be increased. The problem of eye artifact detection therefore needs to be

addressed. A second problem with artifact handling by the system, is that blocks of data which are marked as containing artifacts are still physically stored in the data file, even though they are not used for processing. This results in large amounts of redundant data being stored. If for example, 25% of the data recorded for a typical ERD study contains artifact, then 0.75 Megabytes of redundant data will be stored. Also more data than would normally be required for processing needs to be recorded. This is to ensure that at least the minimum amount of artifact-free data are obtained. Thus, if for an ERD calculation, 60 trials are required, then between 80-100 trials should be recorded in the hope that at least 60 of these trials will be artifact-free.

Much more research and development needs to be applied to the area of **artifact handling** in future development of the system. One change to the way in which the system handles artifacts might be to physically eliminate the blocks of data containing artifact from the data file. Thus once the user has scanned the data, verifying the epochs marked as being contaminated, and marking any epochs which were not marked but which contain artifact, the system could then remove these blocks of data from the data file. Thus, the data file would contain only artifact-free data, and each block accessed would not need to be checked for artifacts prior to being processed. This would speed up the processing time and prevent the storing of redundant data, at the cost of the overhead involved in managing the removal of data from the data file.

On-line examination of the recorded EEG data as described in the literature survey could be implemented. With this method, data containing artifact could be identified by the user during recording, with the user pressing a button to suspend the digitizing and storage of that particular epoch of data. This method has two advantages. Firstly, the artifact contaminated data would not be stored in the data file. Secondly, it would not be necessary to record more data than are required for processing, since the data which are saved have already been passed as artifact-free and can therefore be used for processing. In practise, the data would normally be scanned again off-line to ensure that no artifacts were missed during the on-line inspection, and a few epochs of data containing artifact might need to be marked.

A method for the detection and elimination of **eye-movement artifact** should also be implemented. Most of these methods require the monitoring of the EOG, and thus two of the 18 EEG channels were reserved for this purpose for future development of the system. On-line ocular artifact detection might involve calculating the cross-correlation of the EOG signal and the EEG signal from one of the frontal electrodes. From this calculation, the amount of

EOG activity recorded from the frontal EEG electrode can be calculated, and if this amount exceeds some threshold, then an artifact flag could be set for the epoch currently being recorded. More elaborate methods might involve the subtraction of the EOG activity from the EEG data, thus producing artifact-free epochs from data which was contaminated with ocular artifact. For this type of on-line artifact detection, real-time processing of the signal is required. Many plug-in digital signal processing (DSP) boards are now available which would make such real-time processing of the EOG possible. To obtain the required amount of EEG data completely free of ocular artifact is often very difficult for some patients, for a particular experimental paradigm . EOG subtraction methods would thus be extremely advantageous in these circumstances.

The **spectral and ERD calculations** require a large amount of computational time. Spectral analysis calculations for the three minute recording interval used, required about 2 minutes of computation. For the ERD calculation of the sixty 6 second epochs recorded, the computation requires about 15 minutes. Thus methods of reducing this computation time need to be found.

The software for the quantitative EEG system runs under the MS-DOS **operating system.** Since the 80386 processor of the computer operates in real mode under MS-DOS, this limits the size of the code and data of any application software to 640 Kbytes. It was for this reason that the processing software was written to access and process a block of data at a time, as the amount of data to be processed was far too large for all of the data to be loaded into memory and processed at one time. Having to access a number of smaller blocks from disk is more time consuming than just accessing the complete block. Thus one way to decrease the computation time would be to read all the data into memory, and then process the data. However, this would require using a different operating system which allows the processor to run in protected mode (for example OS/2), thereby allowing the accessing of the full-address space. It would also require a large amount of onboard memory. Another possibility for decreasing the computational time would be to port the system to a higher performance machine, such as a 80486 machine. If a DSP board was being used for on-line detection of artifacts, then the DSP processor could be used for doing some of the "number-crunching" required by the spectral and ERD calculations to reduce the computational time. The architecture of DSP processors is designed for the efficient handling of demanding DSP algorithms such as digital filters and FFTs. However, the data needs to be transferred to and from the DSP board, and this transfer time must be taken into account.

6.2 Clinical Tests and Results

The data recorded from the clinical tests contained mainly ocular artifacts, with a few gross movement artifacts. The gross movement artifacts were automatically detected and marked. However the ocular artifacts were not detected and had to be manually marked by the user. The ocular artifacts consisted of eye blinks rather than horizontal or vertical eye movements artifacts, and were present in higher numbers for the "eyes open" state than for the "eyes closed" state. To try and reduce these eye blinks during the eyes open recordings, subjects were provided with a small fixation target and instructed to view the target and avoid blinking. Some subjects were able to control their blinking in this manner. Eye blinks were also a problem for the ERD recording, where for some subjects, the flashing of the strobe caused an eye blink even though the subject's eyes were closed.

The two patients used as subjects did not have any specific pathology (such as a tumour) which may have presented as a change in the background EEG activity. The spectral maps produced for the patients therefore did not differ significantly from those for the volunteers. However, the recorded data for the patients contained many more artifacts than for the volunteers, including more gross movement artifacts. The patients were not as cooperative as the volunteers and were very restless during the recording. They also struggled to control their eye blinking. Part of the reason for this was that a routine EEG test had been performed on the patients prior to the spectral tests (this takes about 15 minutes). Children are, in general, less cooperative and more restless than adult subjects, and it is often necessary to sedate them to perform routine EEG tests. This presents a problem for spectral and ERD mapping. The ERD depends on the degree of activation, arousal and attention, and sedation will thus affect the ERD measurement. Therefore sedation cannot be used during ERD analysis and hence the importance of efficient artifact handling algorithms.

6.2.1 Spectral Test Results

The literature survey revealed that for the normal awake, relaxed adult, the dominant cerebral activity is the alpha rhythm, arising predominantly from the parieto-occipital and to some extent the temporal regions. The amount of alpha activity varies from individual to individual, and approximately 10% of normal individuals have little or no demonstrable alpha activity. The alpha rhythm is blocked by the opening of the eyes, thus resulting in a decrease in alpha amplitude or power. Beta activity is found predominantly in the frontal regions of the cortex. A small amount of theta activity is seen in normal alert adults, with the amount of theta activity increasing as the patient becomes drowsy. Delta activity in the normal, awake adult

is considered abnormal.

Three of the subjects showed clear dominant alpha activity in the parieto-occipital and temporal regions, while another three subjects demonstrated significant alpha power in these regions, although the alpha rhythm was not as dominant. One subject showed very little alpha activity. There was also a decrease in alpha power between the alpha maps produced for the "eyes closed" state and the "eyes open" state. These results correlate well with the expected results. The alpha activity is localized to the parieto-occipital and temporal regions as expected, the inter-subject variability in the amount of alpha power being a normal variant. The decrease in power for the "eyes open" state is due to the blocking of the alpha activity. A small amount of spectral power within the beta band was found, this being localized to the frontal regions as expected.

The delta spectral maps generated from the tests did not correlate with the expected results as some subjects displayed a significant amount of delta activity in the frontal region, which, as the literature survey revealed, should not be present in the normal alert, awake adult. One possible explanation for this result is that these subjects became drowsy during the 3 minute recording, thereby increasing the amount of slow wave activity in the delta and theta bands. However, a comparison of the theta spectral maps between two subjects, one who had a significant amount of delta activity, and one who had very little delta activity, revealed not much difference in the amount of power in the theta band. An increase in theta power would be expected to accompany the increase in delta power if drowsiness was responsible. A second possible explanation for the presence of delta activity is ocular artifact, which has frequency components of 2-3 Hz. Although the EEG recording was scanned for artifacts, some minor ocular artifacts that should have been marked, may have been passed because of the concern for discarding too much data. This possibility is re-enforced by the fact that the delta activity was found to be localized to the frontal areas which are most sensitive to ocular artifact, and by the fact that the delta activity increased during the "eyes open" state when more ocular artifact is present.

6.2.2 ERD Test Results

From the literature survey, it was seen that the visual ERD is strongly localized to the occipital and parietal areas (visual cortex), with the ERD reaching its maximum amplitude about 200 milliseconds after the stimulus. This was confirmed by Aranibar and Pfurtscheller (1978), with studies of blocking after light stimulation. These studies revealed that the blocking of the alpha rhythm was localized to the occipital and parietal areas, beginning

approximately 200 milliseconds after stimulus onset, and lasting for some seconds.

The results obtained from the ERD clinical tests correlated well with the results found by Aranibar and Pfurtscheller. The ERD's calculated from the clinical tests were localized to the occipital and parietal areas, with the maximum ERD occurring about 200 milliseconds after stimulation. However, one notable difference between the clinical test results and Aranibar and Pfurtscheller's results, was the duration of the ERD. The ERD's calculated for the clinical tests lasted for about half a second. This difference may be explained by the difference in experimental paradigms. For Aranibar and Pfurtscheller's studies, the event consisted of a 1 second train of flashes of the strobe light, at 100 flashes per second. For the clinical tests, the event was a single flash of the strobe light. It thus appears that the single flash causes activation of the visual cortex for a shorter period than the prolonged flashing. Further tests using a paradigm similar to that of Aranibar and Pfurtscheller should be performed to see if a longer duration ERD is obtained.

For most of the ERD studies performed by Pfurtscheller, subjects selected showed clear dominant alpha activity in their EEG records. For the clinical tests, no such screening was performed, and the subjects' alpha activity varied from dominant alpha activity, to very little alpha activity, as seen from the spectral tests. However, the amount of alpha activity did not seem to affect the percentage of blocking. This can be seen when comparing the ERD's of Subject 1 and Subject 2 in Figures 5-9 and 5-10 respectively. The peak percentage ERD between these two subjects are very similar (92% versus 86%), even though the alpha power for the two subjects as seen in Figures 5-1 and 5-2 (Subject 1 and Subject 2 respectively) differs greatly (49 μV^2 versus 8 μV^2).

Very little was found in the literature on what effect the number of trials used in the averaging has on the ERD time curve and no minimum for the number of averages to obtain reasonable results was given. Most of the ERD studies reported used between 60-80 single trials for the computation of the ERD. For the ERD tests performed, 60 trials were recorded. Not all these trials were used in the ERD calculation as those trials containing artifact were rejected. For one subject, the recorded data contained many artifacts, and more than 50 % of the data had to be discarded. Thus, less than 30 ERD trials were used in the ERD calculation for this patient, and no ERD was observed. Thus, a study of the effects of the number of trials on the ERD time curve needs to be undertaken to try and find the minimal number of trials that need to be averaged to provide reasonable ERD time curves.

Figure 5-11 shows a comparison between the different types of derivations. This can be

compared with Figure 3-14. The topographical display of the ERD for the monopolar and common average derivation is more widespread as seen in Figure 3-14. This was also found for the monopolar, common average and longitudinal bipolar derivations in the ERD maps calculated for the clinical tests, as seen in Figure 5-11. For the common average derivation, there is always the problem that if a large number of electrodes pick up similar signals, the common average becomes contaminated and a focus of activity in the occipital region, say, can appear in the frontal region. In this case, the ERD focus in the occipital region encompasses 8 of the 16 electrodes, causing contamination of the common average, and results in a widespread ERD which covers the greater part of the scalp. The ERD is localized and enhanced using a transverse bipolar and local average derivation as seen in Figures 5-11 and 3-14.

Figure 5-12 shows the comparison between the two frequency bands within the alpha band. As described in the literature survey, the upper frequency components within the alpha band of the visual ERD are related to the activation of primary and secondary visual areas, while the lower frequency components are more related to the activation of the visual association cortex and extrastriate cortical areas. For this reason, the lower frequency components are more widespread than the upper frequency components, as seen in Figure 3-9. Examination of Figure 5-12 also shows this difference, with the 8-10 Hz band being slightly more widespread than the 10-12 Hz band.

CHAPTER 7

CONCLUSIONS AND RECOMMENDATIONS

7.1 Conclusions

1) A detailed literature survey was performed. Three quantitative EEG techniques, viz. spectral analysis, event-related desynchronization analysis and topographic mapping were investigated. The literature survey revealed some of the decisions that needed to be made for the specification of a quantitative EEG system.

2) A quantitative EEG system for spectral and event-related desynchronization mapping was specified. This system is to be used by the EEG Laboratory at RCWMCH for evaluation of children with learning disabilities.

3) The system is implemented as a PC-based system which interfaces to the EEG recorder in the EEG Laboratory. Hardware consisting of a pre-processor unit was designed, which matches the signals from the EEG recorder to the input of an ADC card. The greater part of the design and implementation consisted of software development, which was written in the C programming language.

4) For spectral mapping, signals are acquired continuously for a period. During this recording period, the subject is either at rest with eyes open or closed, or is performing some specified test to maintain a particular state of the brain. Topographical maps of absolute and relative power, representing the average of the activity over this period, are produced.

5) For ERD mapping, signals are recorded during an event-related task which is repeated a number of times. The paradigm for the ERD experiment is designed for the particular study undertaken. A sequence of ERD maps showing cortical activation patterns during the task is produced.

6) A pilot study provides results which are in accordance with expected results revealed by the literature survey. The only discrepancy found was in the spectral tests, where some subjects showed a significant amount of delta activity.

7.2 Recommendations for Future Development

The following recommendations for future development and improvements to the system are made:

1) The number of electrodes used in the system's recording montage should be increased.

2) An improved information and data management system with database facilities needs to be provided.

3) A simultaneous display of EEG signals during data acquisition should be provided.

4) Data compression techniques should be investigated for reducing the amount of storage space required by the data files. Also, the use of an alternative long-term storage device with a high capacity (such as an optical disk drive) needs to be considered.

5) Improved artifact handling needs to be provided. This might include on-line monitoring of the EOG, and the provision of a subtraction algorithm for removing ocular artifacts from the recorded EEG.

6) Different methods for reducing the amount of computational time required by the quantification algorithms need to be examined.

7) Additional quantitative techniques which would aid functional studies should be incoporated into the system, eg. evoked potential analysis. This should include some type of statistical analysis such as significance probability mapping, so that comparisons between maps can be made.

REFERENCES

ADRIAN ED, MATTHEWS B
1934
Berger rhythm: Potential changes from occipital lobes in man.
Brain, 57: 355-385

AKAIKE H
1981
Recent developments of statistical methods for spectrum estimation.
pp 63-79 In: Recent Advances in EEG and EMG Data Processing, Yamaguchi N, Fujisawa K (eds), Amsterdam: Elsevier

ALLEN PJ, FISH DR, SMITH SJM
1992
Very high-frequency rhythmic activity during SEEG suppression in frontal lobe epilepsy.
Electroenceph Clin Neurophysiol, 82: 155-159

ARANIBAR A, PFURTSCHELLER G
1978
On and off effects in the background EEG activity during one-second photic stimulation.
Electroenceph Clin Neurophysiol, 44: 307-316

AUTRET A, AUVERT L, LAFFONT F, LARMANDE P
1985
Electroencephalographic spectral power and lateralized motor activities.
Electroenceph Clin Neurophysiol, 60: 228-263

BALDOCK GR, WALTER WG
1946
A new electronic analyzer.
Electronic Eng, 18: 339-44

BALZAAR E, SALETU B, KHOSS A, WAGNER U
1986
Quantitative EEG: Investigation in children with end stage renal disease before and after haemodialysis.
Clin Electroenceph 4: 195-201

BANKMAN IN, GATH I
1987
Feature extraction and clustering of EEG during anaesthesia.
Med & Biol Eng & Comp, 25: 474-477

BARLOW JS, BRAZIER MAB
1954
Note on correlator for electroencephalographic work.
Electroenceph Clin Neurophysiol, 6: 321-5

BERGER H
1930
Uber das Elektroencephalogramm des Menschen II. Mitteilung.
J Psychol Neurol, 40: 160-179

BERGER H
1932
Uber das Elektroencephalogramm des Menschen IV. Mitteilung.
Arch Psychiatr Nervenkr, 97: 6-26

BERGER H
1934
Uber das Elektroencephalogramm des Menschen IX. Mitteilung.
Arch Psychiatr Nervenkr, 102: 538-57

BERGER H
1936
Uber das Elektroencephalogramm des Menschen XI. Mitteilung.
Arch Psychiatr Nervenkr, 104: 678-89

BLINOWSKA KJ, FRANASZCZUK PJ, MITRASZEWSKI P
1988
A new method of presentation of the average spectral properties of the EEG time series.
Int J Biomed Computing, 22: 99-106

BRAZIER MAB, CASBY, JU
1956
Some applications of correlation analysis to clinical problems in electroencephalography.
Electroenceph Clin Neurophysiol, 8: 325-31

BRESLAV J, STARR A, SICOTTE N, HIGA J, BUCHSBAUM MS
1989
Topographical EEG changes with normal aging and SDAT.
Electroenceph Clin Neurophysiol, 72: 281-289

BRUNET D, NISH D, MACLEAN AW, COULTER M, KNOWLES JB
1988
The time course of 'process S' : Comparison of visually scored slow wave sleep and power spectral analysis.
Electroenceph Clin Neurophysiol, 70: 278-287

BUCHSBAUM MS, HAZLETT E, SICOTTE N, BALL R, JOHNSON S
1986
Geometric and scaling issues in topographic electroencephalography.
pp 325-337 In: Topographic Mapping of Brain Electrical Activity, Duffy (ed), Boston: Butterworths

BUCHSBAUM MS, RIGAL F, COPPOLA R, CAPPELLETI J, KING C, JOHNSON 1982
A new system for gray-level surface distribution maps of electrical activity.
Electroenceph Clin Neurophysiol, 53: 237-42

BYRING RF, SALMI TK, SAINIO KO, ORN HP
1991
EEG in children with spelling disabilities.
Electroenceph Clin Neurophysiol, 79: 247-255

CANDY JV
1988
Signal Processing. The Modern Approach.
New York: McGraw-Hill

CHALLIS RE, KITNEY RI
1991
Biomedical signal processing. Part 2: The frequency transforms and their inter-relationships.
Med & Biol Eng & Comp, 29: 1-17

CHATRIAN GE
1976
The mu rhythm.
pp 46-69 In: The EEG of the waking adult: Handbook of EEG and Neurophysiology, Chatrian GE, Lairy GC (eds), Amsterdam: Elsevier

CHATRIAN GE, PETERSEN MC, LAZARTE JA
1959
The blocking of rolandic wicket rhythm and some central changes related to movement.
Electroenceph Clin Neurophysiol, 11: 497-510

COBEN LA, DANZIGER WL, BERG L
1983
Frequency analysis of the resting awake EEG in mild senile dementia of the Alzheimer type.
Electroenceph Clin Neurophysiol, 55: 372-80

COBEN LA, DANZIGER WL, STORANDT M
1985
A longitudinal EEG study of mild senile dementia of the Alzheimer type: changes at 1 year and 2.5 years.
Electroenceph Clin Neurophysiol, 41: 379-86

COHEN A
1986
Biomedical Signal Processing. Volume I : Time and frequency domains analysis.
Florida: CRC Press

COHN R
1942
A cycloscopic study of the human electroencephalogram.
J Gen Physiol, 25: 517-22

COLON E, NOTERMANS SL, DE WEERD JP, KAP J
1979
The discriminating role of EEG power spectra in dyslexic children.
J Neurol, 221: 257-62

COOLEY JW, TUKEY JW
1965
An algorithm for the machine calculation of complex Fourier series.
Math Comput, 19: 297-301

COPPOLA R
1979
Isolating low frequency activity in EEG spectrum analysis.
Electroenceph Clin Neurophysiol, 73: 179-187

COPPOLA R
1986
Issues in topographical analysis of EEG activity.
pp 339-346 In: Topographic Mapping of Brain Electrical Activity, Duffy (ed), Boston: Butterworths

CORSI-CABRERA M, RAMOS J, MENESES S
1989
Effect of normal sleep and sleep deprivation on interhemispheric correlation during subsequent wakefulness in man.
Electroenceph Clin Neurophysiol, 72: 305-311

DEEKE L, GROZINGER B, KORNHUBER HH
1976
Voluntary finger movement in man: cerebral potentials and theory.
Biol Cybernet, 23: 99-119

DIETCH G
1932
Fourier-Analyse von Elektroencephalogrammen des Menschen.
Pflugers Arch, 230: 106-12

DONEGAN JH
1985
The Electroencephalogram.
pp 323-343 In:Monitoring in Anesthesia and Critical Care Medicine, Blitt CD (ed), New York, Churchill Livingstone

DUCKROW RB, SPENCER SS
1992
Regional coherence and the transfer of ictal activity during seizure onset in the medial temporal lobe.
Electroenceph Clin Neurophysiol, 82: 415-421

DUFF TA
1980
Topography of scalp recorded potentials by stimulation of the digits.
Electroenceph Clin Neurophysiol, 49: 452-460

DUFFY FH
1986
Brain electrical activity mapping : Issues and answers.
pp 401-17 In: Topographic Mapping of Brain Electrical Activity, Duffy (ed), Boston: Butterworths

DUFFY FH
1988
Issues facing the clinical use of brain electrical activity mapping.
pp 149-160 In: Functional Brain Imaging, Pfurtscheller G, Lopes da Silva DA (eds), Toronto: Hans Huber

DUFFY FH, BARTELS PH, BURCHFIELD JL
1981
Significance probability mapping. An aid in the topographical analysis of brain electrical activity.
Electroenceph Clin Neurophysiol, 51: 455-62

DUFFY FH, BURCHFIELD JL, LOMBROSO CT
1979
Brain electrical activity mapping (BEAM): a method for extending the clinical utility of EEG and evoked potential data.
Ann Neurol, 5: 309-21

DUFFY FH, DENCKLA MB, BARTELS PH, SANDINI G
1980
Dyslexia: Regional differences in brain electrical activity by topographic mapping.
Ann Neurol, 7: 412-420

EHLERS CL, WALL TL, SCHUCKIT MA
1989
EEG spectral characteristics following ethanol adminastration in young men.
Electroenceph Clin Neurophysiol, 73: 179-187

ETEVENON P
1986
Applications and perspectives of EEG cartography.
pp 113-141 In: Topographic Mapping of Brain Electrical Activity, Duffy (ed), Boston: Butterworths

ETEVENON P, PEROW-MAGNAN P, GUILLOU S, TOUSSAINT M, GUEGUEN B, DENIKER P, LOO H, ZARIFIAN E
1988
A pharmacological model of "local cerebral activation" EEG cartography of caffeine effects in normals.
pp 171-180 In: Functional Brain Imaging, Pfurtscheller G, Lopes da Silva DA (eds), Toronto: Hans Huber

FEIN G, GALIN D, YINGLING CD, JOHNSTONE J, DAVENPORT L
1986
EEG spectra in dyslexia and control boys during resting conditions.
Electroenceph Clin Neurophysiol, 63: 87-97

FISCH B, PEDLEY TA, KELLER DL
1988
A topographic background symmetry display for comparison with routine EEG.
Electroenceph Clin Neurophysiol, 69: 491-494

GALIN D, RAZ J, FEIN G, JOHNSTONE J, HERRON J, YINGLING C
1992
EEG spectra in dyslexic and normal reading during oral and silent reading.
Electroenceph Clin Neurophysiol, 82: 87-101

GASTAUT H, TERZIAN H, GASTAUT Y
1952
Etude d'une activite electroencephalographique meconnue: le rythme rolandique en arceau.
Marseille Med, 89: 296-310

GEVINS AS, BRESSLER SL
1988
Functional topography of the human brain.
pp 99-116 In: Functional Brain Imaging, Pfurtscheller G, Lopes da Silva DA (eds), Toronto: Hans Huber

GOLDMAN D
1950
The clinical use of the 'average' reference in monopolar recording.
Electroenceph Clin Neurophysiol, 2: 209

GOLDMAN S, VIVIAN WE, CHIEN CK, BOWES HN
1948
Electronic mapping of the activity of the heart and brain.
Science, 108: 720-3

GOTMAN J, SKUCE D, THOMPSON C, GLOOR P, IVES J, RAY W
1973
Clinical applications of spectral analysis and extraction of features from electroencephalograms with slow waves in adult patients.
Electroenceph Clin Neurophysiol, 35: 225-35

HARNER RN
1986
Clinical applications of computed EEG topography.
pp 347-356 In: Topographic Mapping of Brain Electrical Activity, Duffy (ed), Boston: Butterworths

HILFIKER P, EGLI M
1992
Detection and evaluation of rhythmic components in ictal EEG using short segments spectra and discriminant analysis.
Electroenceph Clin Neurophysiol, 82: 255-265

HJORTH B
1975
An on-line transformation of EEG scalp potentials into orthogonal source derivations.
Electroenceph Clin Neurophysiol, 39: 526-530

HJORTH B
1986
Physical aspects of EEG data as basis for topographical mapping.
pp 175-193 In: Topographic Mapping of Brain Electrical Activity, Duffy (ed), Boston: Butterworths

IVANOVA LA
1988
Orthostatic changes in the EEG power spectra of normal subjects: effect of aging.
Electroenceph Clin Neurophysiol, 70: 363-365

JACKEL RA, DHADUK V, HOOKER M, MAWHINNEY-HEE M, HARNER RN
1987
Computed EEG topography in acute stroke.
Neurology, 37: 364

JANSEN BH, BOURNE JR, WARD JW
1981
Autoregressive estimation of short segment spectra for computerized EEG analysis.
IEEE Tran. Biomed. Eng, 28: 630-638

JASPER HH, PENFIELD W
1949
Electrocorticograms in man: Effect of voluntary movement upon the electrical activity of the precentral gyrus.
Arch Psychiat Nervenkr, 183: 163-174

JERVIS BW, COELHO M, MORGAN GW
1989
Spectral analysis of EEG responses.
Med & Biol Eng & Comp, 27: 230-238

JERVIS BW, IFEACHOR EC, ALLEN EM
1988
The removal of ocular artefacts from the electroencephalogram : a review.
Med & Biol Eng & Comp, 26: 2-12

JONKEMAN E, LELIEVELD M
1981
EEG computer analysis in patients with migraine.
Electroenceph Clin Neurophysiol, 52: 652-5

KOPRUNER V, PFURTSCHELLER G
1984
Multiparametric asymmetry score (MAS) - distinction between normal and ischemic brains.
Electroenceph Clin Neurophysiol, 57: 343-6

KOWELL AP, REVELER MJ, NUWER MR
1987
Topographic mapping of EEG and evoked potential in epileptic patients.
J Clin Neurophysiol, 4: 233-4

KUHLMAN WN
1978
Functional topography of the human mu rhythm.
Electroenceph Clin Neurophysiol, 43: 83-93

KUWAHARA H, HIGASHI H, MIZUKI Y, MATSUNARI S, TANAKA M, INANAGA K
1988
Automatic real-time analysis of human sleep stages by interval histogram methods.
Electroenceph Clin Neurophysiol, 70: 220-229

LARSEN LH, PRINZ PN, MOE KE
1992
Quantitative analysis of the EEG during tonic REM sleep - methodology.
Electroenceph Clin Neurophysiol, 83: 24-35

LEISMAN G, ASHKENAZI M
1980
Aetiological factors in dyslexia: IV. Cerebral functionally equivalent.
Neuroscience, 11: 157-64

LEMOS MS, FISCH BJ
1991
The weighted reference montage.
Electroenceph Clin Neurophysiol, 79: 361-370

LOPES DA SILVA FH, VAN LIEROP TH, SCHRIJVER CF, STORM VAN LEEUWEN
1973
Organization of thalamic and cortical alpha rhythms: spectra and coherences.
Electroenceph Clin Neurophysiol, 35: 627-639

MATHIS P, SCHEFFNER D, BENNINGER C, LIPINSKI C, STOLZIS L
1980
Changes in the background activity of the electroencephalogram according to age.
Electroenceph Clin Neurophysiol, 49: 626-635

NAGATA K, GROSS C, KINDT G, GEIER J, ADEY G
1985
Topographic electroencephalographic study with power ratio index mapping in patients with malignant brain tumours.
Neurosurgery, 17: 613-19

NAGATA K, TAGAWA K, HIROI S, NARA M, SHISHIDO F, UEMURA K
1988
Quantitative EEG and positron emission tomography in brain ischemia.
pp 239-249 In: Functional Brain Imaging, Pfurtscheller G, Lopes da Silva DA (eds), Toronto: Hans Huber

NAGATA K, TAGAWA K, SHISHIDO F, UEMURA K
1986
Topographical EEG correlates of cerebral blood flow and oxygen consumption in patients with neurophysiological disorders.
pp 357-370 In: Topographic Mapping of Brain Electrical Activity, Duffy (ed), Boston: Butterworths

NAGATA K, YUNOKI K, ARAKI G, MIZUKAMI M
1984
Topographical electroencephalographic study of transient ischemic attacks.
Electroenceph Clin Neurophysiol, 58: 291-301

NAKAMURA M, NISHIDA S, NESHIGE R, SHIBASAKI H
1985
Quantitative analysis of 'organization' by feature extraction of the EEG power spectrum.
Electroenceph Clin Neurophysiol, 60: 84-89

NUNEZ PL
1988
Methods to estimate spatial properties of dynamic cortical source activity.
pp 3-10 In: Functional Brain Imaging, Pfurtscheller G, Lopes da Silva DA (eds), Toronto: Hans Huber

NUWER MR, JORDAN SE, AHN SS
1987a
Quantitative EEG is abnormal more often than routine EEG in mild stroke.
Neurology, 37: 369

NUWER MR, JORDAN SE, AHN SS
1987b
Evaluation of stroke using EEG frequency analysis and topographic mapping.
Neurology, 37: 1153-1159

NUWER MR
1988a
Quantitative EEG: I. Techniques and problems of frequency analysis and topographical mapping.
J Clin Neurophysiol, 5: 1-43

NUWER MR
1988b
Quantitative EEG: II. Frequency analysis and topographical mapping in clinical settings.
J Clin Neurophysiol, 5: 45-85

OKEN BS, CHIAPPA KH
1988
Short-term variability in EEG frequency analysis.
Electroenceph Clin Neurophysiol, 69: 191-198

ONOFRJ M, BAZZANO S, MALATESTA G, FULGENTE T
1991
Mapped distribution of pattern reversal VEPs to central field and lateral half-field stimuli of different spatial frequencies.
Electroenceph Clin Neurophysiol, 80: 167-180

OPPENHEIM AV, SCHAFER RW
1975
Digital Signal Processing.
New Jersey: Prentice-Hall

PENTTILA M, PARTANEN JV, SOININEN H, RIEKKINEN PJ
1985
Quantitative analysis of occipital EEG in different stages of Alzheimer's disease.
Electroenceph Clin Neurophysiol, 60: 1-6

PERRIN F, PERNIER J, BERTRAND O, GIARD MH, ECHALLIER JF
1987
Mapping of scalp potentials by spline interpolation.
Electroenceph Clin Neurophysiol, 66: 75-81

PETSCHE H, RAPPELSBERGER P, POCKBERGER H
1988
Sex differences in the ongoing EEG: Probability mapping at rest and during cognitive tasks.
pp 161-169 In: Functional Brain Imaging, Pfurtscheller G, Lopes da Silva DA (eds), Toronto: Hans Huber

PFURTSCHELLER G
1977
Graphical display and statistical evaluation of event-related desynchronization (ERD).
Electroenceph Clin Neurophysiol, 43: 757-760

PFURTSCHELLER G
1980
Central beta rhythm during sensorimotor activities in man.
Electroenceph Clin Neurophysiol, 51: 253-264

PFURTSCHELLER G
1986
Event-related desynchronization mapping : visualization of cortical activation patterns.
pp 99-112 In: Topographic Mapping of Brain Electrical Activity, Duffy (ed), Boston: Butterworths

PFURTSCHELLER G
1988
Mapping of event-related desynchronization and type of derivation.
Electroenceph Clin Neurophysiol, 70: 190-193

PFURTSCHELLER G
1989a
Functional topography during sensorimotor activation studied with event-related desynchronization mapping.
J Clin Neurophysiol, 6: 75-84

PFURTSCHELLER G
1989b
EEG mapping: Current status and future prospects.
Medical Progress through Technology, 14: 89-97

PFURTSCHELLER G, ARANIBAR A
1977
Event-related cortical desynchronization detected by power measurements of scalp EEG.
Electroenceph Clin Neurophysiol, 42: 817-826

PFURTSCHELLER G, ARANIBAR A
1979
Evaluation of event-related desynchronization (ERD) preceding and following voluntary self-paced movement.
Electroenceph Clin Neurophysiol, 46: 138-146

PFURTSCHELLER G, BERGHOLD A
1989
Patterns of cortical activation during planning of voluntary movement.
Electroenceph Clin Neurophysiol, 72: 250-258

PFURTSCHELLER G, HARING G
1972
The use of an EEG autoregressive model for the time-saving calculation of spectral power density distribution with a digital computer.
Electroenceph Clin Neurophysiol, 33: 113-115

PFURTSCHELLER G, FLOTZINGER D, MOHL W, PELTORANTA M
1992
Prediction of the side of hand movements from single-trial multi-channel EEG data using neural networks.
Electroenceph Clin Neurophysiol, 82: 313-315

PFURSTCHELLEER G, KLIMESCH W
1990
Topographical display and interpretation of event-related desynchronization during a visual-verbal task.
Brain Topography, 3: 85-93

PFURTSCHELLER G, STEFFAN J, MARESCH H
1988
ERD Mapping and functional topography : Temporal and spatial aspects.
pp 117-30 In: Functional Brain Imaging, Pfurtscheller G, Lopes da Silva DA (eds), Toronto: Hans Huber

PINKERTON F, WATSON DR, McCLELLAND RJ
1989
A neurophysiological study of children with reading, writing and spelling differences.
Dev. Med. Child Neurol, 31: 1-32

ROLAND PE, WIDEN L
1988
Quantitative measurement of brain metabolism during physiological stimulation.
pp 213-228 In: Functional Brain Imaging, Pfurtscheller G, Lopes da Silva DA (eds), Toronto: Hans Huber

RUMSEY JM, COPPOLA R, DENCKLA MB, HAMBURGER SD, KRUESI MJP
1989
EEG spectra in severely dyslexic men: rest and word and design recognition.
Electroenceph Clin Neurophysiol, 73: 30-40

SAINO K, STENBERG D, KESKIMAKI I, MUURONEN A, KASTE M
1983
Visual and spectral EEG analysis in the evaluation of the outcome in patients with ischemic brain infarction.
Electroenceph Clin Neurophysiol, 56: 117-24

SALINSKY MC, OKEN BS, MOREHEAD L
1991
Test-retest reliability in EEG frequency analysis.
Electroenceph Clin Neurophysiol, 79: 382-392

SALTZBERG B, BURCH NR, MCLENNAN MA, CORELL EG
1957
A new approach to signal analysis in electroencephalography.
IRE Trans Med Electron, 8: 24-30

SAMSON-DOLLFUS D, TSOURIA Z, BERTOLDI I, DREANO E, DORIS J
1986
EEG modifications during visual and motor reactions observed by beta, alpha, and theta quantification and topographical mapping.
pp 169-193 In: Topographic Mapping of Brain Electrical Activity, Duffy (ed), Boston: Butterworths

SCHOPPENHORST M, BRAUER F, FREUD G, KUBICKI S
1980
The significance of coherence estimates in determining central alpha and mu activities.
Electroenceph Clin Neurophysiol, 46: 138-146

SKLAR B, HANLY J, SIMMONS WW
1972
An EEG experiment aimed towards identifying dyslexic children.
Nature, 240: 414-416

SKLAR B, HANLY J, SIMMONS WW
1973
A computer analysis of EEG spectral signatures from normal and dyslexic children.
IEEE Tran. Biomed. Eng, 20: 20-26

SOININEN H, PARTANEN J, HELKALA EL, LAAKSO M, RIEKKINEN PJ
1989
Longitudinal EEG spectral analysis in early stage of Alzheimer's disease.
Electroenceph Clin Neurophysiol, 72: 290-297

SOUFFLET L, TOUSSAINT M, LUTHRINGER R, GRESSER J, MINOT R, MACHER JP
1991
A statistical evaluation of the main interpolation methods applied to 3-dimensional EEG mapping.
Electroenceph Clin Neurophysiol, 79: 393-402

STEER RW
1989
Anti-aliasing filters reduce errors in A/D convertors.
EDN, 34:, 171-185

STORM VAN LEEUWEN W, WIENEKE G, SPOELSTRA P, VERSTEEG H
1978
Lack of bilateral coherence of mu rhythm.
Electroenceph Clin Neurophysiol, 44: 140-146

TATSUNO J
1988
Pattern differences in two-dimensional EEG maps during mental calculation.
pp 193-198 In: Functional Brain Imaging, Pfurtscheller G, Lopes da Silva DA (eds), Toronto: Hans Huber

VAN DER MEIJ W, VAN HUFFELEN AC, WIENEKE GH, WILLEMSE J
1992
Sequential EEG mapping may differentiate "epileptic" from "non-epileptic rolandic spikes.
Electroenceph Clin Neurophysiol, 82: 408-414

VAN DER RIJT CCD, SCHALM SW, DE GROOT G, DE VLIEGER M
1984
Objective measurement of hepatic encephalopathy by means of automated EEG analysis.
Electroenceph Clin Neurophysiol, 57: 423-6

VAUGHAN HG, COSTA LD, RITTER W
1968
Topography of the human motor potential.
Electroenceph Clin Neurophysiol, 25: 1-10

WALTER WG
1943
An improved low frequency analyzer.
Electronic Eng, 16: 236-40

WALTER WG, SHIPTON HW
1951
A new toposcopic display system.
Electroenceph Clin Neurophysiol, 3: 281-92

SELECTED BIBLIOGRAPHY

DUFFY FH (ed)
Topographic Mapping of Brain Electrical Activity.
Boston: Butterworths

KOZELKA JW, PEDLEY TA
1990
Beta and mu rhythms.
J Clin Neurophysiol, 7: 191-207

LOPES DA SILVA FH
1987
EEG analysis: theory and practice.
In: Electroencephalography: basic principles, clinical applications and related fields, Niedermeyer, Lopes da Silva (eds), Baltimore: Urban and Schwartzenburg

MARKAND ON
1990
Alpha rhythms.
J Clin Neurophysiol, 7: 163-189

NUWER MR
1990
The development of EEG brain mapping.
J Clin Neurophysiol, 7: 459-471

PFURTSCHELLER G
1992
Event-related synchronization (ERS): an electrophysiological correlate of cortical areas at rest.
Electroenceph Clin Neurophysiol, 83: 62-69

PFURTSCHELLER G, FLOTZINGER D, MOHL W, PELTORANTA M
1992
Prediction of the side of hand movements from single-trial multichannel EEG data using neural networks.
Electroenceph Clin Neurophysiol, 82: 313-315

PFURTSCHELLER G, LOPES DA SILVA FH (eds)
1988
Functional Brain Imaging.
Toronto: Hans Huber

APPENDIX A

FOURIER ANALYSIS THEORY

The Fourier Series

The basis of the Fourier series is that a complex periodic waveform can be expanded into the sum of an infinite series of harmonically-related sinusoidal waves which constitute an orthogonal set. If we have a periodic signal x(t) with a period equal to T, then x(t) may be represented by the trigonometric series

$$x(t) = A_0 + \sum_{n=1}^{\infty} A_n \cos(n2\pi f_1 t) + \sum_{n=1}^{\infty} B_n \sin(n2\pi f_1 t)$$

where $f_1 = \frac{1}{T}$ is the fundamental harmonic frequency and A_n and B_n are the Fourier series coefficients. f_1 has a period equal to that of the signal x(t). Frequency $2f_1$ is called the 'second harmonic', $3f_1$ is the 'third harmonic, and so on.

The exponential Fourier series can be derived from the trigonometric series by using Euler's identity:

$$e^{j\theta} = \cos(\theta) + j\sin(\theta)$$

giving

$$x(t) = \sum_{n=-\infty}^{\infty} C_n e^{jn2\pi f_1 t}$$

The coefficients C_n for a given periodic signal are generally complex, but can be written in terms of their magnitude and phase i.e.

$$C_n = |C_n| \, e^{\phi_n}$$

where $|C_n|$ represents the magnitude and ϕ_n the phase for the m th harmonic. $|C_n|$ and ϕ_n are related to A_n and B_n by:

$$C_n = \sqrt{A_n^2 + B_n^2}$$

$$\phi_n = \arctan\left(\frac{B_n}{A_n}\right)$$

The spectrum of a periodic signal consists of a number of discrete frequencies and is known

as a 'line' spectrum. Usually both magnitude and phase spectra are given to fully describe the signal in the frequency domain.

Although the analysis of periodic signals gives results which can be of great practical interest, the majority of signals are not of this type, and the analysis of signals which are aperiodic leads us to the Fourier transform.

The Fourier Transform

In order to define the spectrum of a nonperiodic signal, we may think of the nonperiodic signal as arising from a periodic signal in which the period increases without limit. As the period T tends towards infinity, f_1 tends towards zero and the harmonics become extremely closely spaced. In the limit, we are left with a continuous spectrum as illustrated in Figure 1.

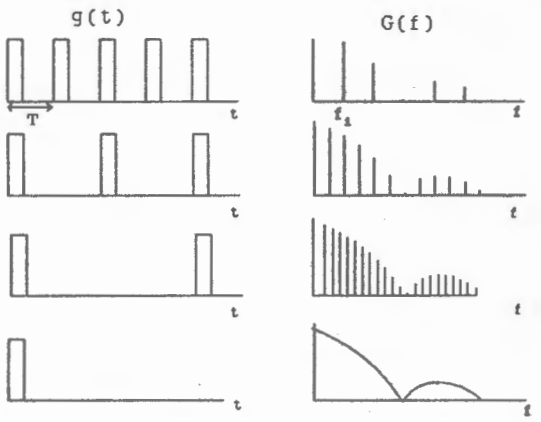

Figure 1: Derivation of the Fourier transform of a non-periodic signal from the Fourier series of a periodic signal. (Reproduced from Challis and Kitney, 1991).

In this case, the Fourier transform X(f) of a signal x(t) is defined as:

$$X(f) = \int_{-\infty}^{\infty} x(t)\, e^{-j2\pi ft}\, dt \qquad (1)$$

X(f) tells us how the energy of the waveform x(t) is continuously distributed in the frequency range between f = $\pm\ \infty$.

The inverse Fourier transform is defined as :

$$x(t) = \frac{1}{2\pi} \int_{-\infty}^{\infty} X(f)\, e^{j2\pi ft} df \qquad (2)$$

Equations 1 and 2 are collectively called the Fourier integral transform pair.

The periodic and aperiodic signals which we have discussed so far have been continuous in time. However, processing of signals is often implemented using digital computers, and since it is not possible to feed continuous signals into a digital computer, these signals must be represented as a set of numerical values at discrete instants in time. Such signals are called discrete or sampled-data signals.

Sampled-Data Signals

A sampled data signal can be considered as arising from sampling a continuous-time signal x(t) at periodic intervals of time T. Thus a discrete or sampled-data signal is just a sequence of real or complex numbers.

Mathematically, sampling a continuous signal x(t) is equivalent to multiplying it by a train of equally-spaced unit Dirac or impulse functions $\delta(t)$ (i.e the comb function) as shown in the left-hand side of Figure 2. In this figure, the signal g(t) seen in (a) is multiplied by the comb function (b) to give the resultant sampled-data signal g(nT) seen in (c). Since the sampled-data signal is obtained by multiplication of the continuous signal and the Dirac pulse train in the time domain, its spectrum may be found by convolving their respective spectra in the frequency domain.

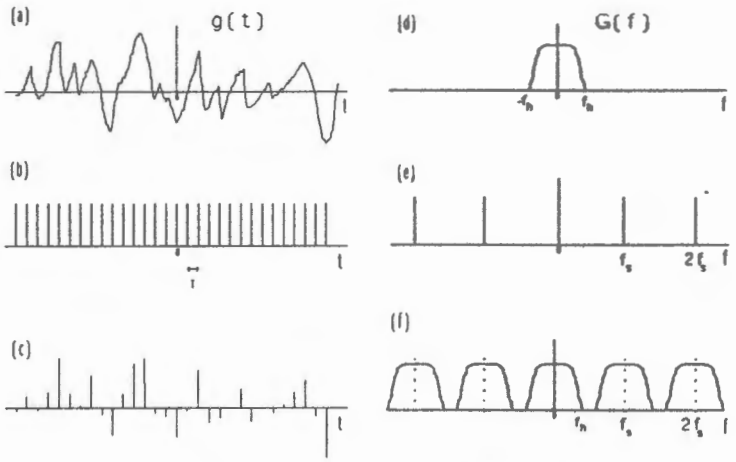

Figure 2 : Multiplication in the time domain and convolution in the frequency domain with the comb function to produce a sampled-data signal.

The right-hand side of Figure 2 shows the spectra of the time signals. The spectrum of the impulse train is itself an impulse train, the spacing between successive harmonics in the frequency domain being inversely related to the spacing in the time domain (i.e $f_s = 1/T$) as shown in Figure 2e. Now the original spectrum of the continuous signal G(f) (Figure 2d) is convolved with this impulse train (Figure 2e) resulting in the spectrum of the sampled-data signal as shown in Figure 2f. This shows that the spectrum of a sampled signal is a repeated

version of the underlying continuous signal's spectrum; the spectrum being repeated at multiples of the sampling frequency f_s, where $f_s = 1/T$.

The above results provide information as to the minimum sampling rate required for sampling the continuous signal. Figure 2d shows that the spectrum of the continuous signal contains frequency components in the range $\pm f_h$ (i.e. the highest frequency component in the signal x(t) is f_h). Sampling this signal causes the spectrum to repeat every f_s Hz. It is therefore clear that if f_h is greater than $f_s/2$, then there will be an overlap between adjacent repetitions of G(f) as shown in Figure 3. This is known as aliasing and results in high frequency components being 'folded-down' into the lower frequency portion of the spectrum, resulting in aliasing errors.

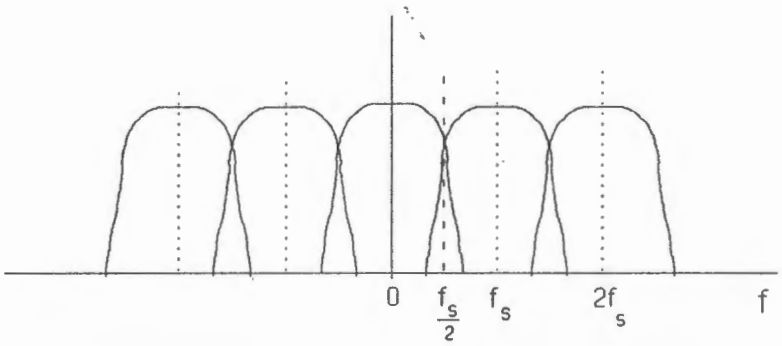

Figure 3 : Frequency folding (aliasing) due to too low a sampling rate. (Adapted from Steer, 1989).

The sampling theorem states that a to avoid aliasing, continuous signal must be sampled at a rate of at least twice the highest frequency component in the signal (i.e $f_s \geq 2f_h$). In practice, an anti-aliasing filter is normally used to band-limit the signal to be sampled to $0 \leq f \geq f_a$, where f_a is the highest frequency of interest in the signal. A sampling rate $f_s \geq 2f_a$ is then required to prevent aliasing. Since there are practical limitations to implementing a filter with an infinitely sharp roll-off, the sampling rate is normally chosen to be somewhat greater than $2f_a$.

The Discrete Fourier Transform

Equations 1 and 2 can be re-written for the case when the time domain signal is discrete. The Fourier transform then become:

$$X(f) = \sum_{n=-\infty}^{\infty} x(nT)\, e^{-j2\pi fnT} \qquad (3)$$

$$x(nT) = T\int_{-\frac{1}{2T}}^{\frac{1}{2T}} X(f)e^{j2\pi fnT}df \qquad (4)$$

Equation 3 is referred to as the discrete-time Fourier transform, and although the time domain signal x(nT) is discrete, the frequency spectrum is continuous. The spectrum is also periodic with a frequency $f_S = 1/T$ corresponding to the sampling frequency as discussed above. However, if we are using a digital computer, we can only deal with values of the spectrum at discrete frequencies, thus effectively sampling in the frequency domain. This leads to the discrete Fourier transform (DFT), where both the time and frequency variables are discrete. The Fourier transform pair is now given by:

$$X(k) = \frac{1}{N}\sum_{n=0}^{N-1} x(n)e^{-j\frac{2\pi kn}{N}} \qquad k=0,1,...,N-1 \qquad (5)$$

$$x(n) = \sum_{k=0}^{N-1} G(k)e^{j\frac{2\pi kn}{N}} \qquad n=0,1,...,N-1 \qquad (6)$$

Defining

$$W_N = e^{-j\frac{2\pi}{N}}$$

then Equation 5 can be written as:

$$X(k) = \frac{1}{N}\sum_{n=0}^{N-1} x(n)W_N^{nk} \qquad k=0,1,...,N-1 \qquad (7)$$

and expressing Equation 7 as an array of equations gives:

$$\begin{aligned}
X(0) &= x(0)W^0+x(1)W^0+x(2)W^0+...+x(N-1)W^0 \\
X(1) &= x(0)W^0+x(1)W^1+x(2)W^2+...+x(N-1)W^{N-1} \\
X(2) &= x(0)W^0+x(1)W^2+x(2)W^4+...+x(N-1)W^{2(N-1)} \\
&\vdots \\
X(N-1) &= x(0)W^0+x(1)W^{N-1}+x(2)W^{2(N-1)}+...+x(N-1)W^{(N-1)^2}
\end{aligned} \qquad (8)$$

It can be seen from Equations 8, that the computation of any one particular spectral

component requires about N complex multiplications and about N complex additions. Since X(k) must be calculated for N different values of k, the direct computation of the DFT requires about N^2 complex multiplications and N^2 complex additions. For most practical cases, this number can be very large, resulting in a prohibitively long computation time. Fortunately, redundancy in the discrete Fourier transform allows for algorithms that permit the implementation of the discrete Fourier transform with considerable savings in computational time, the basis of which is the fast Fourier transform or FFT algorithm developed by Cooly and Tukey in 1965.

The Fast Fourier Transform

Most approaches to improving the efficiency of the computation of the DFT exploit the symmetry and periodicity of the exponential W_N^{kn} , i.e.

(i) $W_N^{k(N-n)} = (W_N^{kn})^*$ where * denotes the complex conjugate

(ii) $W_N^{kn} = W_N^{k(n+N)} = W_N^{(k+N)n}$

Computational algorithms that exploit both these properties were known long before the era of high-speed digital computation. At that time, algorithms with computation proportional to N log N rather than N^2 were described, but the distinction was not of any great importance for the small values of N that were feasible for hand computation. The possibility of greatly reduced computation was generally overlooked until about 1965, when Cooley and Tukey published an article for the computation of the discrete Fourier transform. This led to the discovery of a number of computational algorithms which have come to be known as fast Fourier transform, or simply FFT, algorithms. Collectively, the entire set of such algorithms is often loosely referred to as "the FFT".

The fundamental principle that all these algorithms are based upon is that of decomposing the computation of the discrete Fourier transform of a sequence length N into successively smaller discrete Fourier transforms. The manner in which this is implemented leads to a variety of algorithms, all with comparable improvements in computational speed. There are two basic classes of FFT algorithms. The first, called **decimation-in-time**, derives its name

from the fact that the sequence x(n) is decomposed into successively smaller subsequences. In the second class of algorithms, the sequence of discrete Fourier transform coefficients X(k) is decomposed into smaller subsequences, hence the name **decimation-in-frequency**.

Decimation-in-Time FFT Algorithm

This algorithm makes use of the symmetry and periodicity of the complex exponential W_N^{nk} and decomposes the sequence x(n) into successively smaller subsequences. The principle of decimation-in-time is most conveniently illustrated by considering the special case of N an integer power of 2, i.e.

$$N = 2^v$$

Since N is an even integer, we can consider computing X(k) by separating x(n) into two N/2-point sequences consisting of the even-numbered points in x(n) and the odd-numbered points in x(n). With X(k) given by

$$X(k) = \sum_{n=0}^{N-1} x(n) W_N^{nk} \qquad k=0,1,2,\ldots,N-1$$

and separating x(n) into its even and odd numbered points we obtain

$$X(k) = \sum_{n \text{ even}} x(n) W_N^{nk} + \sum_{n \text{ odd}} x(n) W_N^{nk}$$

or with the substitution of variables n = 2r for n even and n = 2r + 1 for n odd,

$$X(k) = \sum_{r=0}^{(N/2)-1} x(2r) W_N^{2rk} + \sum_{r=0}^{(N/2)-1} x(2r+1) W_N^{(2r+1)k} \tag{9}$$

$$= \sum_{r=o}^{(N/2)-1} x(2r)(W_N^2)^{rk} + W_N^k \sum_{r=0}^{(N/2)-1} x(2r+1)(W_N^2)^{rk}$$

But $W_N^2 = W_{N/2}$ since

$$W_N^2 = e^{-2j(2\pi/N)} = e^{-j2\pi/(N/2)} = W_{N/2}$$

Consequently Equation 9 can be written as:

$$X(k) = \sum_{r=0}^{(N/2)-1} x(2r) W_{N/2}^{rk} + W_N^k \sum_{r=0}^{(N/2)-1} x(2r+1) W_{N/2}^{rk} \qquad (10)$$

$$= G(k) + W_N^k H(k)$$

Each of the sums in Equation 10 is recognized as an N/2-point DFT, the first sum being the N/2-point DFT of the even numbered points and the second being the N/2-point DFT of the odd numbered points of the original sequence. Although the index k ranges over N values, k = 0, 1,..., N-1, each of the sums need only be computed for k between 0 and (N/2)-1, since G(k) and H(k) are each periodic in k with period N/2. After the two DFTs corresponding to the two sums in Equation 10 are computed, they are then combined to yield the N-point DFT, X(k). Figure 4 indicates the computation involved in computing X(k) according to Equation 10 for an eight-point sequence, i.e. for N = 8.

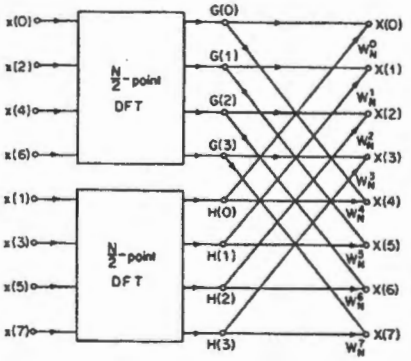

Figure 4 : Flow graph of decimation-in-time decomposition of an N-point DFT computation into two N/2-point DFT computations. (Reproduced from Oppenheim and Schafer, 1975).

Thus we note that two four-point DFTs are computed, with G(k) designating the four-point DFT of the even-numbered points and H(k) the DFT of the odd-numbered points. X(0) is obtained by multiplying H(0) by W_N^0 and adding the result to G(0). For X(4) we would want to multiply H(4) by W_N^4 and add the result to G(4). However, since G(k) and H(k) are both periodic in k with period 4 (i.e. N/2), H(4) = H(0) and G(4) = G(0). Thus X(4) is obtained by multiplying H(0) by W_N^4 and adding the result to G(0).

Equation 10 corresponds to breaking the original N-point computation into two-N/2 point computations. If N/2 is even, as it always is when N is equal to a power of 2, then we can consider computing each of the N/2-point DFTs in Equation 10 by breaking each of the sums in Equation 10 into two N/4-point DFTs, which would then be combined to yield the N/2-

point DFTs. This is shown in Figure 5. Inserting the computation indicated in Figure 5 into the flow graph of Figure 4, we obtain the complete flow graph of Figure 6. Note that we have used the fact that $W_{N/2} = W_N^2$.

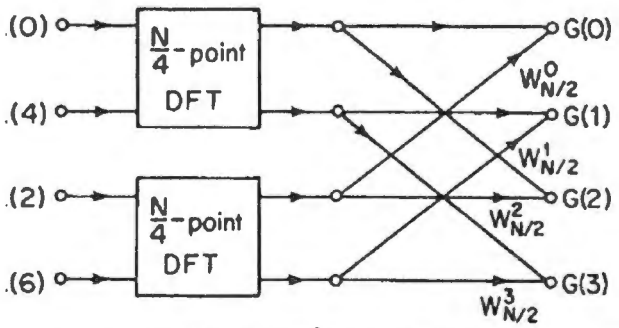

Figure 5 : Flow graph of the decimation-in-time decomposition of an N/2-point computation into 2 N/4-point DFT computations. (Reproduced from Oppenheim and Schafer, 1975).

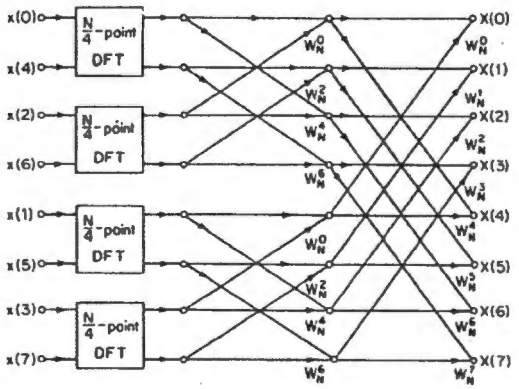

Figure 6 : Result of combining Figure 5 with Figure 4. (Reproduced from Oppenheim and Schafer, 1975).

Thus for the eight-point DFT that has been used as an illustration, the computation has been reduced to a computation of two-point DFTs. The two-point DFT of, for example x(0) and x(4), is depicted in Figure 7. This computation illustrates the basic element of the FFT, the butterfly. With the computation of Figure 7 inserted into the flow graph of Figure 6, we obtain the complete flow graph for the computation of the eight-point DFT as shown in Figure 8.

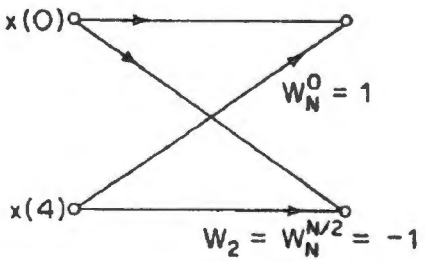

Figure 7 : Flow graph of a two-point DFT. (Reproduced from Oppenheim and Schafer, 1975).

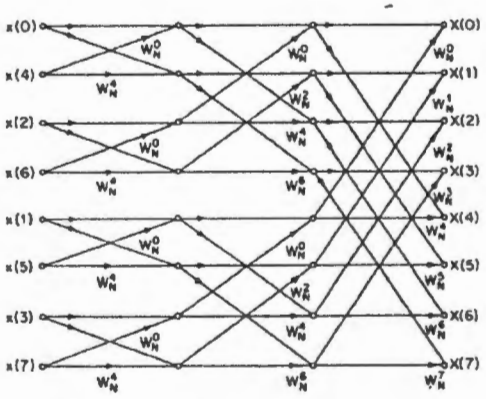

Figure 8 : Flow graph of complete decimation-in-time decomposition of an eight-point DFT computation. (Reproduced from Oppenheim and Schafer, 1975).

For the more general case with N a power of 2 greater than 3, we would continue to decompose the N/4-point transforms into N/8-point transforms, and continue until left with only two point transforms. In general, this requires ν stages of computation, where $\nu = \log_2 N$. Each stage of computation is just a number of butterfly operations, the outputs of one stage forming the inputs to the next stage. The general butterfly operation is shown in Figure 9 and the equations for the decimation in time butterfly are

$$\text{output(upper)} = \text{input(upper)} + W * \text{input(lower)}$$
$$\text{output(lower)} = \text{input(upper)} - W * \text{input(lower)}$$

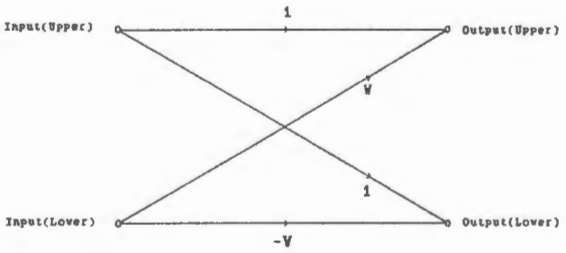

Figure 9 : Flow graph for decimation-in-time single butterfly.

Since there are $\log_2 N$ stages, we have a total of $N \log_2 N$ complex multiplications and additions as compared with N^2 complex multiplications and additions required for the straight implementation of the DFT. For a 1024 point DFT, this is a saving factor of about 150.

Decimation-in-Frequency FFT Algorithm

The decimation-in-time FFT algorithms were all based upon the decomposition of the DFT computation by forming smaller and smaller subsequences of the input sequence x(n). Alternatively, we can consider dividing the output sequence, X(k), into smaller and smaller subsequences in the same manner.

The flow graph for the eight point DFT computation using decimation-in-frequency decomposition is shown in Figure 10.

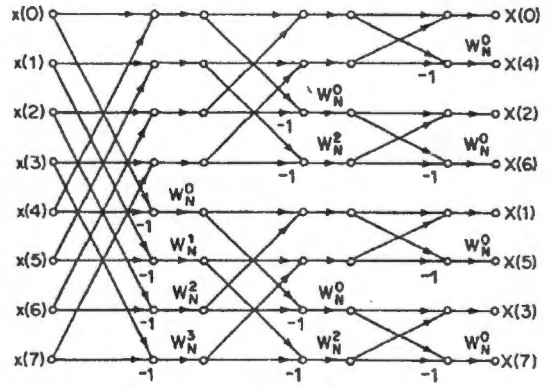

Figure 10 : Flow graph of complete decimation-in-frequency decomposition of an eight-point DFT computation. (Reproduced from Oppenheim and Schafer, 1975).

The flow graph for a single butterfly operation for the decimation-in-frequency FFT computation differs from that for the decimation-in-time FFT computation and is shown in Figure 11. The corresponding equations are

output(upper) = input(upper) + input(lower)

output(lower) = [input(upper) - input(lower)] * W

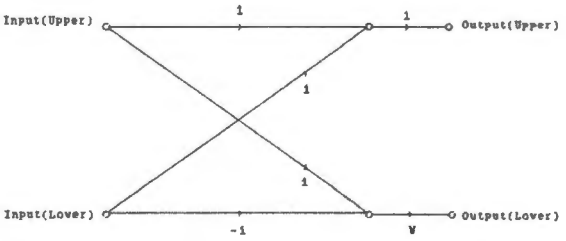

Figure 11 : Flow graph for decimation-in-frequency single butterfly.

Again, there are N $\log_2$N complex multiplications and additions as with the decimation-in-time algorithm.

In-place vs Natural Input-output Algorithm

In-place algorithms are the most economical in terms of memory space since the outputs of any given butterfly are placed in the storage location from which the inputs were taken. With in-place algorithms, either the output spectrum X(k) appears in unnatural order, or the input data must be rearranged prior to the first stage of butterfly operations.

Natural input-output algorithms require more memory in order to maintain the natural order of the input and output.

Optimization of FFT for Real Input Sequences

The FFT in general deals with complex input sequences x(n). However, often the input sequence is strictly real, and there are two ways to take advantage of the full power of the FFT while processing strictly real input sequences.

The first method is called trigonometric recombination. This method accepts any real input sequence and processes it using an FFT of half the size normally required for a complex sequence. This results in nearly a factor of two speed-up in the computation. The second method, called the double sequence FFT, accepts two real sequences of length N and process them using a single N-point complex FFT. This is primarily useful in real-time systems where continuous data is being transformed.

Problems Associated with the FFT

Two problems associated with the FFT are leakage and the picket-fence effect.

Spectral Leakage

The FFT of a set of sampled data is not the true FFT of the process from which the data was obtained. This is because the process is continuous, whereas the data represent a realisation which is truncated at its beginning and end. The data, which represents a length of T seconds of the signal, is obtained by multiplying all the sampled values in the interval T by unity, while all the values outside this interval are multiplied by zero. This is equivalent to multiplying or windowing the signal by a rectangular pulse or window, of width T and height unity. In this case, the sampled data values u(n) are given by the product of the data values x(n), and the window function values w(n) :

$$u(n) = x(n)w(n)$$

The time domain product is equivalent to a convolution in the frequency domain. Thus the resultant spectrum in the frequency domain, U(k), will be the convolution of the 'true' spectrum, X(k), with the spectrum of the window function, W(k). The rectangular window discussed above has a spectrum of the form sin(x)/x shown in Figure 12a. It consists of a main lobe and an infinite number of side lobes. The spectrum of a single sine-wave component of the signal comprises of two impulses. However, convolution of this 'true'

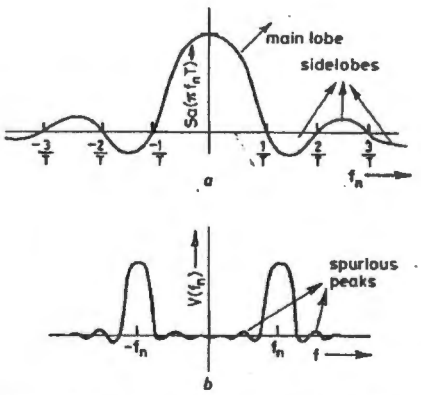

Figure 12 : a) Spectrum of the rectangular window and b) resultant convolution with the spectrum of a single sine-wave. (Reproduced from Jervis et al, 1989).

spectrum with the spectrum of the window function results in the computed spectrum shown in Figure 12b. The effect of the rectangular window has been to introduce spurious peaks into the computed spectrum due to the effects of the side lobes.

Table 1 : Main lobe width versus side lobe suppression for various window functions. N is length of window. (Adapted from Oppenheim and Schafer, 1975).

Window	Peak Amplitude of Side lobe (dB)	TransitionWidth of Main lobe
Rectangular	-13	$4\pi/N$
Bartlett	-25	$8\pi/N$
Hanning	-31	$8\pi/N$
Hamming	-41	$8\pi/N$
Blackman	-57	$12\pi/N$

This will be true of each frequency component of the signal, and so the spectrum will be

distorted due to the addition and subtraction of the large number of window main lobes and side lobes. The effect may be to introduce spurious peaks, or to conceal true peaks in the spectrum, the phenomenon being known as spectral leakage.

A solution to the problem of spectral leakage is to reduce the side lobe effect by multiplying the original data by a suitably shaped window. Suitable windows have a value of 1 at the mid-data point and are tapered to 0 at points n = 0 and N-1. However, reduction in the height of the side lobes is at the expense of a wider main lobe. Many different window functions exist; Table I lists some of these window functions, giving a measure of the side lobe suppression versus the transition width of the main lobe.

Picket-fence Effect

If the physically occurring signal component is at a frequency which lies between two adjacent harmonic frequencies in the spectrum, then it cannot be properly represented. Its energy will be shared between the neighbouring harmonics, and the nearby spectral amplitudes will be distorted. This is known as the picket fence effect.

A solution lies in arranging for the harmonics to be more closely spaced by using augmenting zeros, i.e zero padding the original sequence x(n) prior to transforming the sequence. Zero padding is also useful to ensure that the input sequence x(n) is a power of 2 (i.e $N = 2^m$) as the FFT algorithm usually requires that there are 2^m input datum points (radix-2 FFT).

APPENDIX B

NON-PARAMETRIC SPECTRAL ESTIMATION

Non-parametric spectral estimation is the classical spectral estimation technique which makes use of the Fourier transform to estimate the power spectral density (PSD) of a signal.

The Wiener-Khintchine theorem states that the power spectral density of a random signal is the Fourier transform of the autocorrelation function of the signal :

$$S_{xx} = \int_{-\infty}^{\infty} R_{xx}(\tau)\, e^{-j2\pi f\tau} d\tau$$

where $R_{xx}(\tau)$ is the autocorrelation function given by :

$$R_{xx}(\tau) = E[x(t)x(t+\tau)]$$

Spectral estimators which use the Fourier transform typically fall into one of two categories; the direct or Blackman-Tukey method and the indirect or Periodogram method.

Blackman-Tukey Method

The Blackman-Tukey method is simply an implementation of the Weiner-Khintchine theorem; the autocorrelation is estimated, and the power spectrum is estimated by calculating the Fourier transform of the autocorrelation. This technique tends to produce a noisy spectral estimate; however, a smoothed estimate can be obtained by multiplying R_{xx} by a window function, usually called a lag window. The window primarily reduces spectral leakage (as described in Appendix A) and therefore improves the estimate.

Periodogram Method

The periodogram method operates directly on the raw data, x(t), to transform it to the frequency domain and produces the estimate. The periodogram is defined as :

$$P_{xx} = \frac{1}{N} |X(f)|^2$$

with X(f) the Fourier transform of the input signal x(t). In the discrete case, the periodogram is calculated as :

$$P_{xx}(k) = \frac{1}{N} |X(k)|^2 \qquad k = 1,2,\ldots,N-1$$

The FFT is used to transform the sampled-data signal x(n) to the frequency domain and the absolute value is calculated as :

$$|X(k)| = \sqrt{(X_r(k))^2+(X_i(k))^2}$$

where $X_r(k)$ and $X_i(k)$ are the real and imaginary parts of the k th spectral component.

The periodogram P_{xx} is an estimate of the power spectral density S_{xx}. This estimate can be improved in two ways. Firstly, the input signal x(t) can be multiplied by a window function prior to being transformed, and secondly, consecutive periodograms can be averaged to give an improved estimate of the power spectrum. Multiplication by a window function reduces spectral leakage as explained (in Appendix A), and leads to an improved estimate of the PSD.

Averaging the Periodogram

The time domain data recording is broken up into a number of equal length segments (epochs) and the periodogram of each is calculated. The periodogram of the whole recording is then calculated as the average of all the segmental periodograms. This method is also known as the Bartlett procedure.

The data sequence x(n), $0 \le n \le N-1$, is divided into K segments of M samples each so that $N = KM$; i.e we form the segments

$$x^{(i)}(n) = x(n+iM-M) \qquad 0 \le n \le M-1, \quad 1 \le i \le K$$

Now for each segment of length M, the periodogram is calculated, and then the K periodograms are averaged to give the spectrum estimate. This method gives an improved estimate of the spectrum; the greater the number of periodograms averaged (i.e. the greater K) the better the estimate of the spectrum. However, for a fixed record length N, as the number of periodograms averaged increases, the length of each individual periodogram (M) decreases, and thus the spectrum resolution decreases. Thus there is a tradeoff between improvement of the spectrum estimate and spectral resolution.

Welch introduced a modification of the Bartlett procedure. The data record is again sectioned into $K = N/M$ segments of M samples as was the case in the Bartlett procedure. However, in this case, a window function w(n) is applied directly to the data segments before computation and averaging of periodograms. The Welch method also allows for the overlapping of segments.

APPENDIX C

PARAMETRIC SPECTRAL ESTIMATION

The parametric spectral estimation approach is a three step procedure: (1) a specific model is selected, (2) the model parameters are estimated from the measured data, and (3) the spectral estimate is obtained from the model parameters.

A very effective parametric model is that of the transfer function. The sampled signal (the sequence), x(n), is assumed to be the output of a linear system driven by an (inaccessible) input sequence, u(n). The sequence x(n) is thus given as the solution to the difference equation

$$x(k) = -\sum_{i=1}^{p} a_i x(k-i) + \sum_{i=0}^{q} b_i u(k-i) \qquad (1)$$

and transferring Equation 1 into the z domain, we get

$$X(z) = \frac{B(z^{-1})}{A(z^{-1})} U(z)$$

This model is known as the ARMA model or pole-zero model. In Equation 1, the current (k th) sample of the sequence is expressed as a linear combination of the past p sequence samples and (q + 1) input samples. Hence the models here are also known as linear prediction models. Figure 1 depicts the ARMA model in the z and time domain.

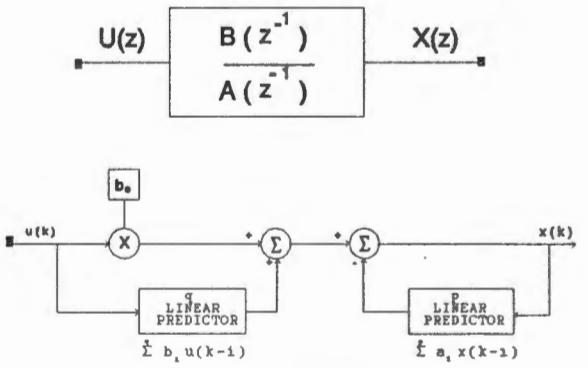

Figure 1 : Autoregressive moving average (ARMA) model. (Reproduced from Cohen, 1986).

Two other models are commonly used: the autoregressive (AR) model and the moving average (MA). The AR model is an all-pole model given by assuming $B(z^{-1}) = G$ (a

constant)

$$X(z) = \frac{G}{A(z^{-1})} U(z)$$

$$x(k) = -\sum_{i=1}^{p} a_i x(k-i) + Gu(k)$$

while the MA, all-zero model, is derived from the ARMA model by assuming $A(z^{-1}) = 1$

$$X(z) = B(z^{-1}) U(z)$$

$$x(k) = \sum_{i=0}^{q} b_i u(k-i)$$

Figure 2 shows, schematically, the AR and MA models in the z and time domains. In all of these models, the parameters G, $A = \{a_1, a_2, a_3, \ldots, a_p\}$, and $B = \{b_0, b_1, b_2, \ldots, b_q\}$ are the system parameters.

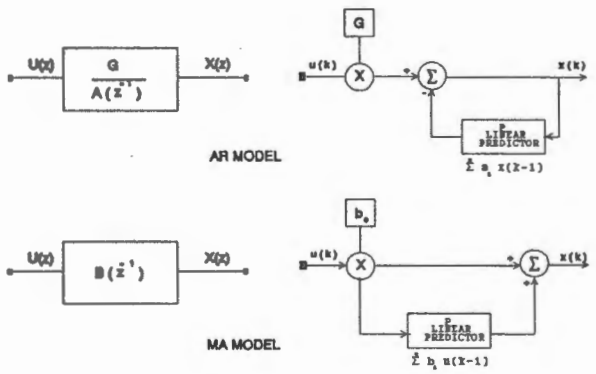

Figure 2 : Autoregressive (AR) and moving average (MA) models. (Reproduced from Cohen, 1986).

The sequence x(n) is therefore represented in a reduced form by system parameters. Since the input is inaccessible, well-known algorithms for system identification cannot be directly applied. The common approach has been to assume an input with a white spectrum (i.e. white noise, impulse). An algorithm commonly used for estimation of the AR parameters, assuming a white noise input, is based on the least squares method and leads to the solving of the Yule-Walker equations to obtain estimates of the system parameters. An efficient recursive procedure (the Durbin algorithm) has been developed to solve these equations.

One of the important decisions that has to be made when modelling data is that of estimating the order of the model. If the order is too high, spurious detail in the spectra may result,

whereas too low an order yields rather smooth spectra. Akaike (1981) has described a method for estimating the order of AR models using a maximum-likelihood approach.

The power spectral density of the sequence x(n), is then calculated by taking the Fourier transform of the system parameters; eg. for an AR model:

$$P_{xx}(f) = \frac{G^2}{\left|1+\sum_{i=0}^{p} a_i e^{-j2\pi fiT}\right|^2}$$

APPENDIX D

MATHEMATICAL FORMULATION OF SOURCE DERIVATION

The radial current component leaving or entering the scalp can be determined by means of the Laplace operator as

$$i_{xy} = -\frac{1}{r} \cdot \left(\frac{\partial^2}{\partial x^2} + \frac{\partial^2}{\partial y^2}\right) V_{xy}$$

where r is a constant having the dimension of resistance and being related to the conductivity of the actual medium and V_{xy} is the potential at point (x,y) on the scalp. The negative sign indicates that the current is assumed to be directed outward from the interior of the volume (i.e. the head).

The current may also be represented as a voltage, having a direction perpendicular to the surface and acting over a resistance of value r;

$$V_{source} = i_{xy} \cdot r = -\left(\frac{\partial^2}{\partial x^2} + \frac{\partial^2}{\partial y^2}\right) V_{xy}$$

Although the Laplace operator in its general form is based on a knowledge of the continuous potential distribution, it can also be represented by a central difference operator, based on a limited number of samples. The second order derivatives are then approximated by means of finite differences:

$$V_{source} \approx -\left(\frac{d^2}{dx^2} + \frac{d^2}{dy^2}\right) V_{xy} \qquad (1)$$

In an EEG recording, the continuous potential distribution on the scalp is sampled at each of the electrode sites on the scalp. Thus to calculate a voltage V_{source} which represents the radial current component at a particular point, one can use these samples.

For the source derivation, the points at which the source voltage is required, is at each of the electrode sites. To calculate the source voltage at any one electrode site, one can thus use the potentials at the other electrodes sites. The minimum configuration of electrode positions for calculating the source voltage at an electrode site (i.e for calculating the Laplacian operator on the potential at this electrode) is shown in Figure 1. From this figure it can be seen that the Laplace operator on the potential at a particular electrode can be calculated by using the potentials at the four surrounding electrodes.

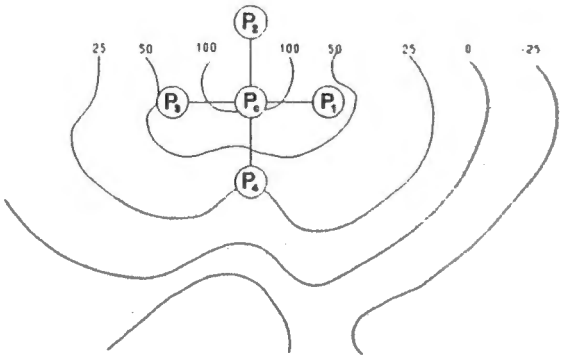

Figure 1 : Minimum configuration of electrodes for 5-point central difference operator. (Reproduced form Hjorth, 1975).

It is assumed that the four electrodes lie on two perpendicular lines as shown in Figure 1 and if one makes the assumption that the distance between samples is equal (i.e. inter-electrode distances are equal) then the operator of Equation 1 simplifies to the sum of second order difference:

$$V_{source} = -(d_x^2+d_y^2)\, V_{xy} \qquad (2)$$

If we were to calculate the radial current voltage V_{source} at electrode P_c in Figure 1, and assuming the potentials at electrodes (P_c, P_1, P_2, P_3, P_4) are (V_c, V_1, V_2, V_3, V_4) respectively, then the second order differences in Equation 2 are

$$d_x^2(V_{xy}) = (V_1-V_c)-(V_c-V_3)$$

and

$$d_y^2(V_{xy}) = (V_2-V_c)-(V_c-V_4)$$

Substituting these into Equation 2 yields the final result

$$V_{source} = (V_c-V_1)+(V_c-V_2)+(V_c-V_3)+(V_c-V_4)$$

constituting a superposition of four "radial" bipolar derivations around the centre point.

Applying the preceding conclusions, the source activity at an electrode in the 10-20 system (see Figure 3-12), for example C_3, may be expressed as

$$C_{3source} = \frac{(C_3-C_z)+(C_3-F_3)+(C_3-T_3)+(C_3-P_3)}{4} \qquad (3)$$

signifying the arithmetic sum of the signals from the bipolar derivations C_3 - C_Z, C_3 - F_3, etc; where C_3 refers to the voltage recorded at electrode C_3 etc. Each bipolar derivation is

multiplied by the normalised distance between the two electrodes. Since equal inter-electrode distances are assumed, the normalised distances for all four bipolar derivations is 1/4, and thus the division by 4 in Equation 3.

Expanding Equation 3 gives :

$$C_{3source} = C_3 - \frac{(C_z+F_3+T_3+P_3)}{4} \qquad (4)$$

from which it is seen that the source potential at a particular electrode is calculated as the difference between the potential at that electrode and the local average of the 4 surrounding electrodes.

This type of composite derivation, referred to as a 5-point operator, can be formulated directly for 9 of the 19 electrode positions used in the 10-20 system (See Figure 3.12). For the remaining 10 electrodes, forming a terminating circle at the edge of the electrode system, 5-point operators cannot be formulated since only three of the four "radial" bipolar derivations are available for superposition (i.e the electrodes on the edge of the scalp do not have 4 surrounding electrodes for calculation of the local average). A superposition of only two bipolar derivations from the edge-line, thus forming a 3-point operator, may therefore replace a 5-point operator.

In the 10-20 electrode placement system, electrode directions are not perpendicular and so the use of the source derivation only approximates the Laplacian operator. Also, Equation 4 assumes that the inter-electrode distances are equal which is not the case in the 10-20 system. The general equation for calculation of the source voltage is thus:

$$C_{3source} = C_3 - (d_1*C_z+d_2*F_3+d_3*T_3+d_4*P_3) \qquad (5)$$

where d_1 = normalized distance from C_3 to C_Z etc.

APPENDIX E

SCHEMATIC CIRCUIT DIAGRAM FOR PRE-PROCESSOR UNIT

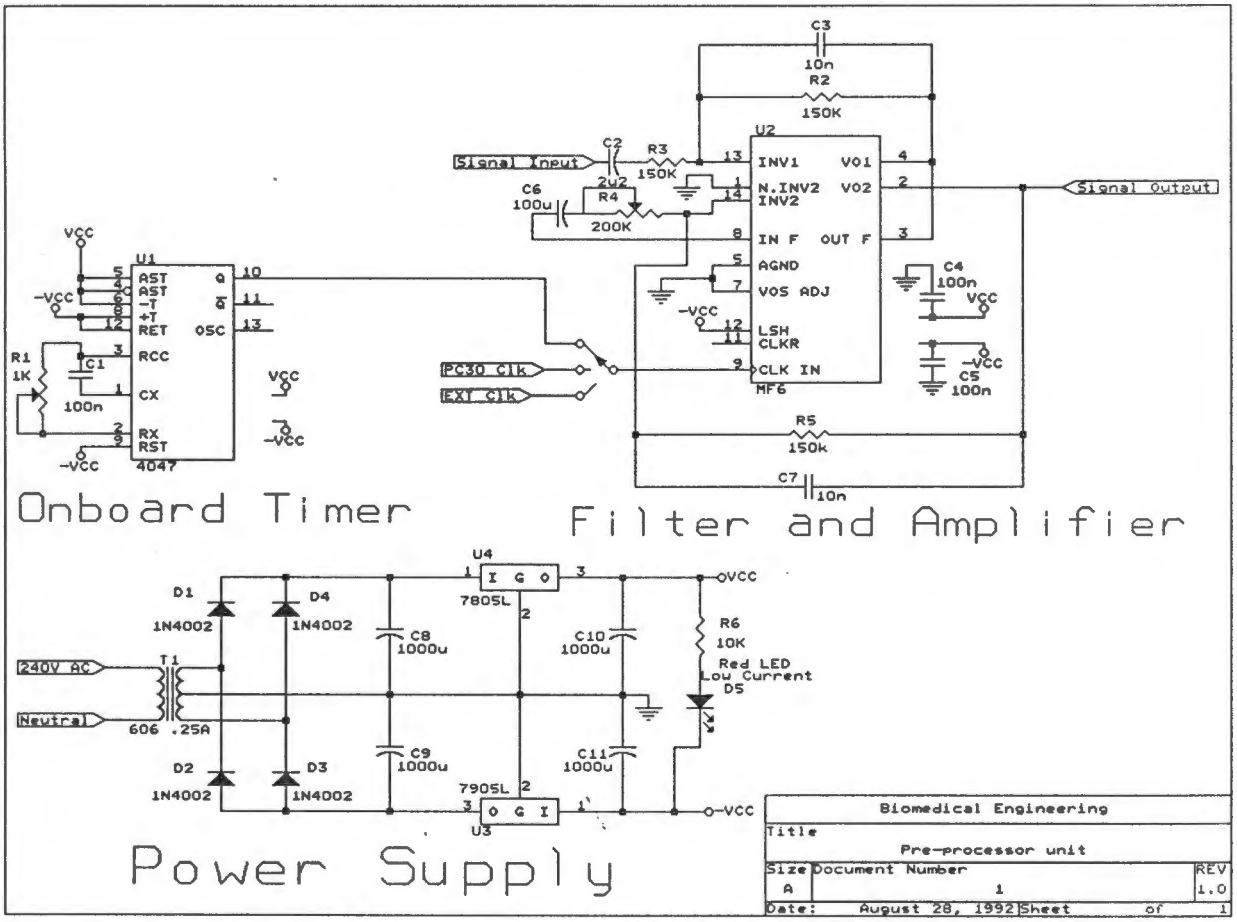

APPENDIX F

PC-30D ANALOG AND DIGITAL I/O BOARD

A block diagram of the PC-30D board (Eagle Electric, Cape Town) is shown in Figure 1. The block diagram highlights the major elements contained on the board, and their interrelationships.

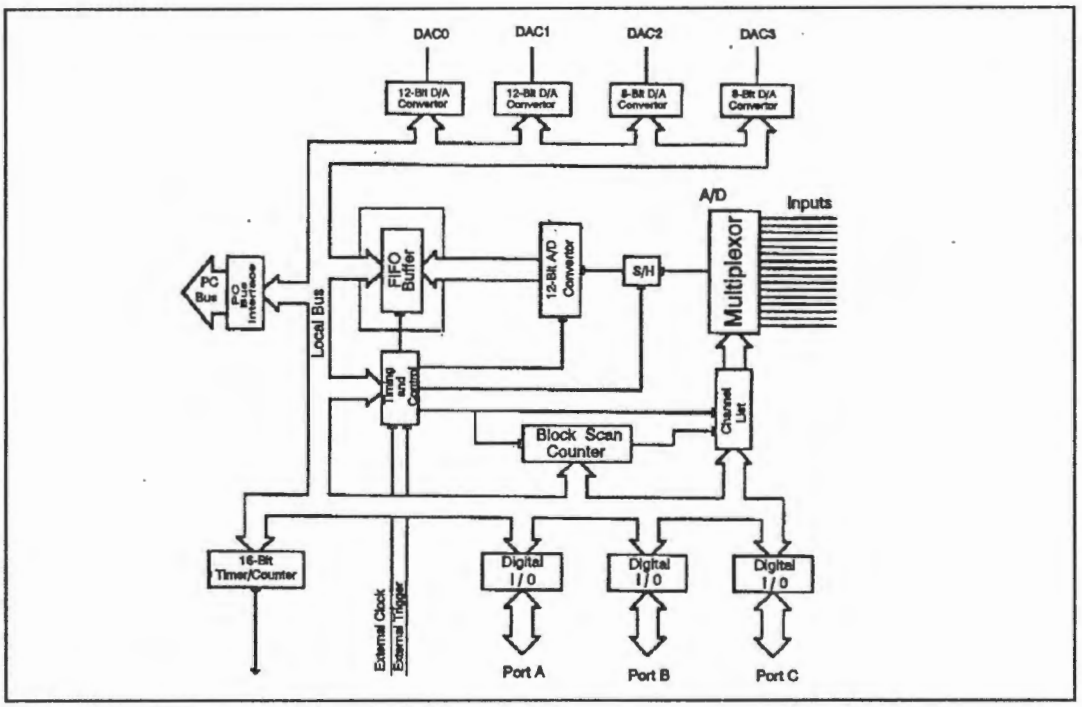

Figure 1 : Block diagram of PC30D Analog and Digital I/O Board.

The board consists of four subsystems, viz. the A/D, the timing and control, the D/A and the digital I/O. The board communicates with the host PC via the bus interface.

1. The A/D Subsystem

The A/D section allows for 16 single-ended analog inputs, and can be configured for unipolar (input range 0 to 10 V) or bipolar (input range $\pm$ 10 V or $\pm$ 5 V) operation. Resolution is 12 bits, and for unipolar inputs the output is straight binary, while for bipolar inputs, the output is offset binary.

The ADC may be operated in either single conversion or continuous conversion mode. In single conversion mode, the board performs a single conversion on the selected input channel and stops on completion of this conversion. In continuous conversion mode, conversions are

performed at a set rate. This rate is set by programming the PC-30's internal timer or an external clock source.

The PC-30 contains logic which allows any sequence of channels, up to a sequence length of 31, to be selected and sampled under hardware control. This allows full throughput to be achieved even when converting multiple input channels.

A/D conversions may be monitored by either polled I/O, DMA or interrupts. In polled I/O mode, the software continuously polls the board's status register to check for completion of the current A/D conversion. DMA (Direct Memory Access) is used to transfer data directly from the A/D subsystem to memory in the host computer. In interrupt mode, the board automatically generates a hardware interrupt on completion of each conversion.

Key Specifications

- ADC resolution : 12 bits
- Nonlinearity : Less than $\pm$ 0.75 LSB
- ADC full scale input ranges : 0 to +10 V and $\pm$ 5 V
- Number ADC inputs : 16 single-ended
- ADC throughput rate : 200 kHz

The A/D subsystem contains several separate components (Figure 1) :

- The input multiplexer.

  The multiplexer selects one of sixteen single ended input channels. This channel is selected by a channel address, obtained from the channel list.

- The channel list

  The channel list contains a list of channels to be converted. This may be up to 31 channels in length. After the conversion of one channel, the next channel in the channel list is selected under hardware control. When the end of the

channel list is reached, the ADC loops back to the first channel in the list.

· The sample and hold unit

The sample and hold unit holds the selected input channel steady for the duration of the ADC's conversion process.

· The ADC

The ADC performs the actual analog to digital conversion. An A/D conversion is begun by an A/D strobe. This is generated by the timing and control section, described later.

· The FIFO buffer

The FIFO (First In First Out) buffer is a temporary store for the converted results. The FIFO stores data while the host computer is performing other tasks, such as memory refresh, and also stores data while the CPU changes memory buffers during DMA operation. Changing memory buffers allows the PC-30D to perform DMA into the entire memory space of the host computer without a break. The FIFO buffer can store up to 16 samples.

A/D Triggering Mode

The PC-30 can operate in one of two modes. These are block mode and normal mode.

In normal mode, for each A/D strobe, one A/D conversion is performed. This is illustrated in Figure 2.

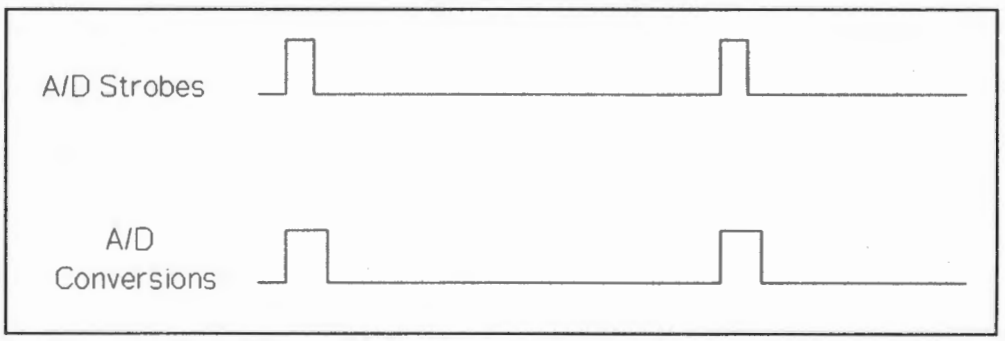

Figure 2 : Normal mode A/D operation

In block trigger mode, for each A/D strobe, as many A/D conversions as are programmed into the block counter are performed. Block mode operation is illustrated in Figure 3 for a block count of 3. Block mode operation occurs at maximum throughput, and hence allows a group of channels to be sampled almost simultaneously. For example, 16 channels can be sampled within 80 μsec.

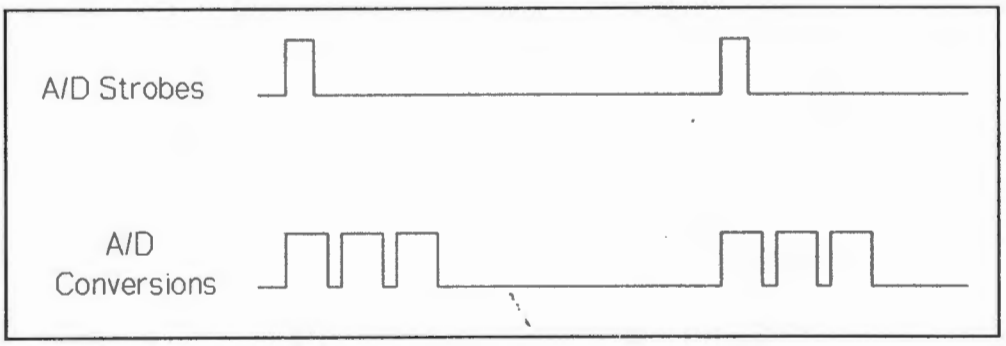

Figure 3 : Block mode A/D operation

DMA Data Transfer

Data from the FIFO buffer can be transferred to the host PC's memory either via single channel or dual channel DMA transfer.

(i) Single channel DMA transfer

The host PC's DMA hardware is first set up with the address of the memory into which the samples are to be put, and the number of samples to be obtained. The board is then initialized, and sampling started. When the ADC's FIFO buffer contains data, a DMA cycle is initiated. This DMA cycle reads the data from the ADC's buffer, and stores it in the PC's memory, without the PC's CPU taking any action. This process repeats until the required number of samples have been read.

(ii) Dual channel DMA transfer

The size of the memory block that the DMA hardware of the IBM compatible computer can write to, is limited to 64 Kbytes. Once this block has been filled, DMA transfers continue to the address at the top of the block, overwriting data which has already been written to this block. Dual DMA solves this problem by using two DMA channels, and splitting the area of memory that the samples are to be transferred to, into many 64 Kbyte blocks.

The address of the first block is then programmed into the first channel of the DMA controller, the address of the second block into the second DMA channel, and sampling is initiated. The PC30 then begins to transfer samples into memory via the first DMA channel. When the DMA controller reaches the end of the first block, it generates a TC (terminal cycle) signal. The PC30 uses this to change to the second DMA channel. Samples are now transferred via the second DMA channel to the second block of memory. Once the routine detects the end of block condition, it programs the address of the next block into the first channel of the DMA controller. When the second channel of DMA reaches the end of its block, DMA swops back to the first channel. This process continues, with DMA channels continuously being swopped, until the required number of samples have been read.

2. Timing and Control Subsystem

The timing and control subsystem is responsible for the generation of A/D strobes, and also contains an uncommitted counter/timer which can be used for signal generation, or as a frequency counter. A/D strobes cause the ADC to begin a conversion (or multiple conversions if in block trigger mode). A simplified block diagram of this section is shown in Figure 4.

A/D strobes may be selected under program control to be either hardware or software strobes.

i) Software strobes. These are generated by a write operation to a control register. They hence allow a single conversion to be started under program control.

ii) Hardware strobes. The source of the hardware strobes is jumper selected from one of two sources:

   a) The external clock. This is a TTL level signal; conversions are started on the positive edges of this signal.

   b) The internal clock. This is derived from a crystal controlled oscillator, which operates at 2 MHz. The 2 MHz signal is then divided down by a prescaler and clock divider; values are programmed into the prescalar and clock divider registers to divide down the 2 MHz crystal frequency to the required sampling frequency.

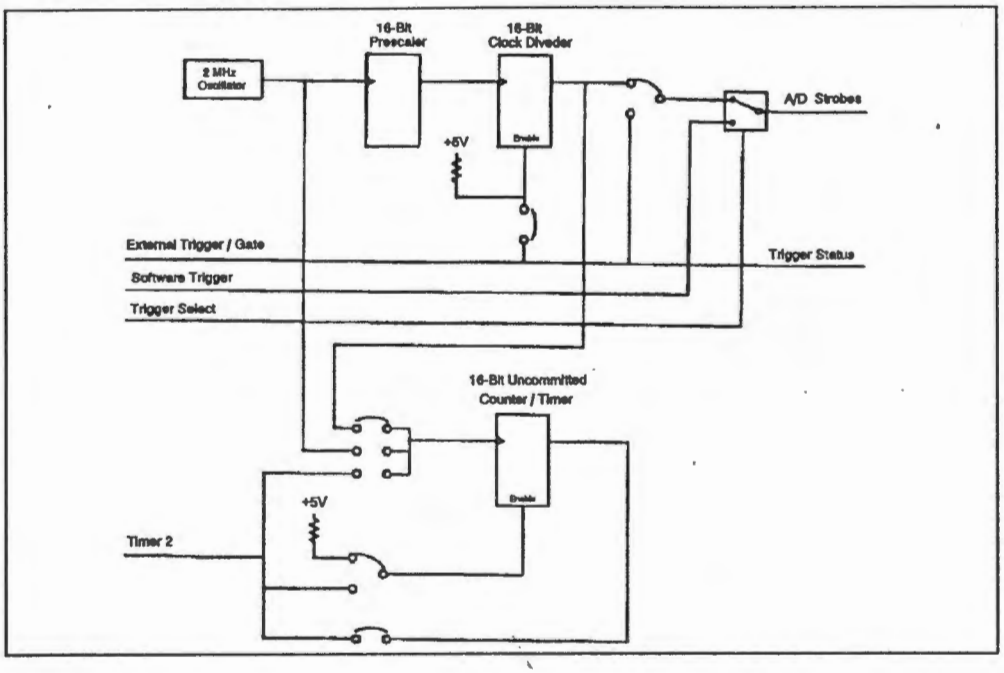

Figure 4 : Block diagram of timing and control subsection.

The uncommitted counter/timer can be configured to count either

i) pulses from the 2 MHz master oscillator,

ii) pulses from the output of the clock divider, or

iii) pulses from an external source.

This allows the counter to be used for measuring frequency, or for generating a frequency.

3. D/A Subsystem

The D/A subsystem consists of two 12-bit and two 8-bit DAC. The four DAC's are independent of one another and can operate at a throughput of 130 kHz. Output ranges are independently configurable as 0 to +10 V unipolar or $\pm$ 10 V bipolar.

4. Digital I/O Subsystem

The digital I/O subsystem is an interface for the transfer of digital data from (to) the PC bus to (from) one or more peripheral devices connected to the PC-30. The digital I/O portion of

the PC-30 emulates a 8255 PPI (Programmable Peripheral Interface). There are three bidirectional eight bit digital I/O ports, which can each be used in a variety of operating modes.

The three ports are divided into two groups, group A (consisting of port A and the upper half of port C) and group B (consisting of port B and the lower half of port C). Each of these groups can be individually configured in one of three operating modes.

The three basic modes of operation are :

- Mode 0 : Basic I/O
- Mode 1 : Strobed I/O
- Mode 2 : Bidirectional bus operations

Mode 0 (Basic Input/Output)

With mode 0 operation, the ports are divided into two 8-bit ports (A and B) and two 4-bit ports (upper and lower halves of port C). These ports can be individually programmed as either inputs or outputs and provide simple I/O operations.

Mode 1 (Strobed Input/Output)

With mode 1 operation, the ports are divided into two groups, each consisting of one 8-bit port and one 4-bit port. The 4-bit port is used for control and status of the 8-bit port, while the 8-bit port may be programmed as either input or output. Input and output operations are latched and this mode of operation provides I/O operations with simple handshake protocols.

Mode 2 (Strobed Bidirectional Input/Output)

With mode 2, there is one 8-bit bidirectional port and one 5-bit control port. The 5-bit port is used for control and status of the 8-bit port. Input and output operations are latched and this mode provides a means for bidirectional I/O operations on a single 8-bit port.

5. Bus Interface

The bus interface is responsible for three functions:

i) The decoding of the board's base address. The board's base address is set by a DIP switch.

ii) The generation of interrupts. Interrupts can be generated under one of three jumper selectable conditions:

a) The end of each A/D conversion.

b) The end of a DMA block.

c) On each pulse from the uncommitted counter/timer.

The board can be configured to use one of the following hardware interrupt levels: 2, 3, 5, 7, 10, 11, 12, 14 or 15

iii) The generation of DMA signals. The board can be configured to support single DMA channels 5, 6 or 7 or dual DMA channels 5 and 6 or channels 6 and 7.

APPENDIX G

OPERATION OF HARDWARE INTERRUPTS IN THE PC

Hardware interrupts are a mechanism which allow the normal flow of a program to be interrupted at any time, so that some other task can be performed before returning to the program at the point of interruption. Hardware interrupts are generated by sending an interrupt request signal to the CPU. The PC AT, 386 and 486 support 16 hardware interrupts (IRQ0 - IRQ15).

When an interrupt occurs, the interrupt vector table is indexed. The first 1024 bytes of memory are reserved for the interrupt vector table, this table being set up by MS-DOS. The interrupt vector table contains a list of addresses of the locations of each of the interrupt handlers, each address being 4 bytes. Since there are 1024 bytes in the table, and each interrupt address is 4 bytes, a total of 256 interrupts are supported. Of these, 16 are the hardware interrupts (IRQ0 - IRQ15).

The interrupt handlers contain the code which must be executed to service the interrupt. When a specific hardware interrupt occurs, normal program flow is interrupted and vectored to the address stored at the indexed location in the vector table. This then results in the interrupt handler code being executed and the interrupt being serviced. On completion of execution of the interrupt handler, program flow returns to the location in the program that was being executed when the interrupt occurred.

Most of the hardware interrupts are used for specific system functions in the PC. For example, IRQ0 is used for the system timer and IRQ1 is the keyboard scan code interrupt. When MS-DOS is loaded, it loads the addresses of these specific interrupt service routines into the correct index positions in the interrupt vector table. Now, when a specific hardware interrupt occurs, for example IRQ1, program flow is interrupted and vectored to one of these specific interrupt service handlers, the address of this service handler being obtained by indexing the interrupt vector table. In this example, an IRQ1 interrupt is generated every time a key on the keyboard is pressed. This interrupt causes the execution of the keyboard interrupt service routine which contains the code for reading the keyboard and storing the key in the keyboard buffer.

It is possible to take over the control of any of the interrupts so that a specific interrupt service handler written to perform some function, will be executed when a specific hardware

interrupt occurs. To do this, the address of the new interrupt service handler must be loaded into the interrupt vector table at the correct index location, overwriting the old system interrupt handler address. Now when this interrupt occurs, program flow will be vectored to this new interrupt handler which can perform the required function. It is important to save the address of the old system interrupt handler so that this can be reloaded into the interrupt table once control of the interrupt is relinquished.

APPENDIX H

DIGITAL FILTER DESIGN AND IMPLEMENTATION

A filter is normally a linear, time invariant system as depicted by Figure 1. In the case of a digital filter, the input u(k), the output y(k) and the impulse response of the filter h(k), are sampled-data signals. The output of the filter is given by the linear convolution of the input signal and impulse response of the filter.

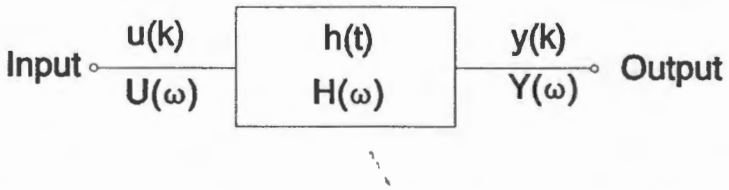

Figure 1 : Linear system in the time and frequency domain.

The general transfer function of a digital filter is

$$H(z) = \frac{Y(z)}{U(z)} = \frac{b_o + b_1 z^{-1} + \cdots + b_n z^{-n}}{1 + a_1 z^{-1} + \cdots + a_n z^{-n}} \qquad (1)$$

and this is equivalent to the standard difference equation

$$y(k) = \sum_{i=0}^{n} b_i u(k-i) - \sum_{i=1}^{n} a_i y(k-i) \qquad (2)$$

There are two primary classes of digital filters. If in Equation 1 and Equation 2, $a_i = 0$ for $i = 1, 2, 3, \ldots, n$, the filter is a finite-impulse response (FIR) filter. Otherwise, the filter is an infinite-impulse response (IIR) filter.

FIR Filter

For an FIR filter, the output sequence, y(k), is determined from past values of the input sequence u(k), as seen from the standard difference equation with $a_i = 0$, i.e.

$$y(k) = \sum_{i=0}^{n} b_i u(k-i) \qquad (3)$$

The impulse response sequence h(k) of the FIR filter is $h(k) = \{b_0, b_1, b_2, \ldots, b_n\}$, with the b_i being known as the filter coefficients.

FIR filters have the following properties:

1. A linear phase response is easily obtainable. Linear phase filters are distortion-free since the linear phase implies a pure time delay.

2. Stability of the filter is guaranteed.

3. Finite register effects are of less consequence than in IIR filters.

4. For sharp cutoff frequencies, the number of filter taps N (i.e the filter length) is large, implying a large computational burden.

IIR Filter

For an IIR filter, the output of the filter not only depends on the past values of the input, but also on past values of the output of the filter, as seen from the standard difference equation (see Equation 2).

The phase response of the IIR filter is usually non-linear. The number of filter taps required to meet a required filter specification is normally less than that for an FIR filter, thereby easing the computational burden of the filter.

Design of Filters

The design of a digital filter involves finding the impulse response h(k) (i.e. the filter coefficients a_i and b_i) which meet the design specifications. There are many different methods for the design of FIR and IIR filters. Some of the more popular methods are listed below. Many excellent texts are available which discuss these different methods (Candy, 1988; Oppenheim and Schafer, 1975). Computer-based filter design packages are available. Most of these allow the choice of a variety of different design methods. It is important to have an understanding of the procedures involved behind each of the design methods in order to select the appropriate one, rather than just blindly selecting any design method.

IIR Design

The traditional approach to the design of IIR digital filters involves the transformation of an analog filter into a digital filter meeting the prescribed specifications. One such approach involves finding a difference equation, with the associated H(z), that yields an output sequence close to the samples of the analog output signal. This is termed the **impulse invariant** method. Another approach is to transform the analog filter, by means of the bilinear transformation, into the Z domain yielding a digital filter, H(z). This method is known as the **bilinear transformation** method.

FIR Design

The most straightforward approach to FIR filter design is to obtain a finite-length response by truncating an infinite-duration impulse response sequence. This is known as the **window** method. In this case, the finite-impulse response for the filter can be represented as the product of the desired infinite impulse response and a window function. The design procedure involves selecting the appropriate window function. The trade-off between different window functions is similar to that described in Appendix A. In the frequency domain, this trade-off is between width of the main lobe and height of the side lobes. In filter design, this translates to a trade-off between steepness of roll-off of the filter and ripple in the stopband, this ripple dictating the maximum attenuation in the stopband. The narrower the side lobe of the window function, the steeper the roll-off of the filter, at the expense of a large ripple in the stopband.

Another method of FIR filter design is the **frequency sampling** method. This method is based on the approximation of a function by a sum of sinc (sin(x)/x) functions. With this method, the filter is specified in terms of sample points of one period of the desired frequency response of the filter. An iterative procedure is then used to fit a function to this desired frequency response, such that the function differs from the desired response by the smallest maximum stopband approximation error.

A third method of FIR filter design, called the **Parks-McClellan** algorithm, uses equiripple approximation to the desired frequency response.

Implementation of Filters

One method is a **recursive algorithm** which implements the linear convolution of the input signal and the impulse response of the filter. For an FIR filter, this would then involve convolving the input sequence $u(k) = \{u_0, u_1, \ldots, u_n\}$ with the filter coefficients $\{a_0, a_1, a_2, \ldots, a_N\}$. If the length of the filter is large (i.e. if N is very large), then this approach involves a high computational burden.

To ease this computational burden, the filter can be implemented using a 'fast convolution'. Since convolution in the time domain is equivalent to multiplication in the frequency domain, the convolution of the two sequences (input and impulse response) can be implemented by computing their discrete Fourier transform, multiplying, and computing the inverse discrete Fourier transform. The highly efficient FFT algorithm for calculation of the Fourier transform makes this method of implementation computationally efficient.

However, the multiplication of discrete Fourier transforms corresponds to a circular convolution of the sequences. To obtain a linear convolution of the sequences, we must ensure that the circular convolution has the effect of a linear convolution. If we consider two N-point sequences $x_1(n)$ and $x_2(n)$, and let $x_3(n)$ denote their linear convolution, it is straightforward to verify that $x_3(n)$ is of length 2N-1, ie. it can have at most 2N-1 non-zero points. If it is to be obtained by multiplying the discrete Fourier transforms of $x_1(n)$ and $x_2(n)$, then each of these discrete Fourier transforms, $X_1(k)$ and $X_2(k)$, must also be computed on the basis of 2N-1 points to ensure that the inverse Fourier transform of the result, $x_3(n)$, will be the linear convolution of the two sequences. If the N-point DFT's were taken, multiplied and the inverse DFT taken, then the result would correspond to circular and not a linear convolution.

Thus to implement the FIR filter using **'fast convolution'**, the n-point input signal u(k) and the N-point impulse response h(k) (i.e. the N filter coefficients), must each be zero-padded to at least length (N+n-1), the FFT for each of the zero-padded sequences computed, the FFT results multiplied together, and the inverse FFT computed to give the filter output, y(k).